UNIVERSITÀ DI PADOVA  FACOLTÀ DI INGEGNERIA

Dipartimento di Ingegneria dell'Informazione

Scuola di Dottorato di Ricerca in Ingegneria dell'Informazione
Indirizzo: Bioingegneria

CICLO XXI

ON-LINE FILTERING ALGORITHMS FOR CONTINUOUS GLUCOSE MONITORING

Direttore della Scuola: Ch.mo Prof. Matteo Bertocco

Supervisore: Ch.mo Prof. Claudio Cobelli

Dottorando: Ing. Andrea Facchinetti

Gennaio 2009

Contents

Sommario **IX**

Summary **XIII**

1 Continuous Glucose Monitoring **1**
1.1 Diabetes & Self Monitoring Blood Glucose (SMBG) 2
1.2 Continuous Glucose Monitoring (CGM) Devices 3
1.2.1 Minimally-Invasive Devices 4
1.2.2 Non-Invasive Devices 5
1.3 Two Popular CGM Devices 6
1.3.1 Abbott FreeStyle Navigator™ 6
1.3.2 Menarini GlucoDay® 9
1.4 Pros and Cons of CGM Devices 10
1.5 Open Problems in CGM Devices 11
1.5.1 Physiological Aspects 11
1.5.2 Calibration 12
1.5.3 Filtering 14
1.5.4 Prediction 15
1.6 Aim of the Work and Outline 16

2 CGM Time Series Denoising: State of the Art **19**
2.1 Noise in CGM Data: Origin and Characteristics 20
2.2 On-Line Filtering: Problem Statement 22
2.3 Filters Embedded in Current Commercial CGM devices 23
2.4 The Moving-Average Approach 23
2.5 Moving-Average: Limitations & Challenges 24

3 The New Stochastic Approach for Filtering **27**
3.1 The Kalman Filter 28
3.1.1 Kalman Filter Features 28
3.1.2 The Discrete KF Implementation 28

3.2 *A Priori* Model for $u(t)$ 30
3.2.1 The Models 30
3.2.2 The Stochastic Context and the Regularization Method 32
3.2.3 CV-Based Method for Choosing the Optimal m 34
3.2.4 The State-Space Model for $u(t)$ 35
3.3 Q and R Estimation Procedure 36
3.4 Implementation 37
3.4.1 Burn-In Interval Approach 37
3.4.2 Sliding Window Approach 38
3.5 Computationally Efficient Algorithm 38
3.5.1 Diagonalization 38
3.5.2 Explicit formula for $q(\gamma)$ 40

4 Assessment on Simulation Studies **41**
4.1 The Choice of Optimal Model Order m 42
4.1.1 The Simulated Dataset 42
4.1.2 Implementation and Results 42
4.2 Coping with Inter-Individual SNR Variability 48
4.3 Coping with Intra-Individual SNR Variability 54
4.4 Coping with Sensor-to-Sensor Variability 58
4.5 Discussion 61

5 Assessment on Real Data **63**
5.1 Evaluation Criteria 64
5.2 The Glucoday® Dataset 64
5.2.1 General Overview of the Results 64
5.2.2 Representative Subjects 68
5.3 The FreeStyle Navigator™ Dataset 78
5.3.1 General Overview of the Results 78
5.3.2 Representative Subjects 81
5.4 Discussion 87

Conclusions **89**

Bibliography **91**

List of Figures

1.1 Two devices for SMBG: Lifescan OneTouch® (left) and Abbott FreeStyle (right) [57, 61]. 2
1.2 Comparison between real glycemia (blue profile) and SMBG measurements (red dots). The green area highlights the range of normality. 3
1.3 FreeStyle Navigator™ sensor [57]. 7
1.4 FreeStyle Navigator™ transmitter [57]. 7
1.5 FreeStyle Navigator™ receiver [57]. 8
1.6 Schematic diagram of the Wired Enzyme™ sensing layer, showing redox polymer, incorporated enzyme (GOx), and path of electron flow from glucose to the working electrode. The detail on the right shows the actual structure of the redox polymer [16, 17]. 9
1.7 The Menarini GlucoDay® device [63]. 10
1.8 Schematic representation of the GlucoDay® apparatus and the microdialysis fiber [33]. 10
1.9 The two-compartment model for describing the plasma-to-ISF dynamics [39] 12
1.10 Portion of a representative subject in which both plasma (red stars) and ISF (blue line) glucose were simultaneously measured [53]. 13
1.11 Portion of a representative subject in which plasma (red stars) and ISF (blue line) glucose where measured in parallel [53]. . . 14
1.12 CGM representative subjects. Top: FreeStyle Navigator™ time series [53]. Bottom: GlucoDay® time series [33]. 15
1.13 Original CGM data (blue line) vs 30-minutes ahead in time predicted profile (red line) by using Auto-regressive models. Top: FreeStyle Navigator™ subject. Bottom: GlucoDay® subject [45]. 16

2.1 Two Glucoday® noisy signals. *Top:* high SNR with some huge spikes. *Bottom:* low SNR with medium-intensity spikes. 21
2.2 Two FreeStyle Navigator™ noisy signals. *Top:* high SNR. *Bottom:* low SNR. 21
2.3 Detail of SMA, LMA and EMA assessment on Glucoday® and FreeStyle Navigator™ representative time series (top and bottom panels, respectively). 25

3.1 Representative glycemic profile obtained with blood plasma measurements sampled every 5 minutes for about 2 days [60]. . 30
3.2 Realizations of a white noise process and its single and double integrations (top, middle and bottom panels, respectively) . . 31

4.1 Simulated subject #1. Detail of hours from 28 to 32. Noisy (blue) and filtered (red) time series. In each panel the filtered profile has been obtained applying *a priori* model for $u(t)$ of order m equal to the value reported on the title of the panel itself. 43
4.2 Simulated subject #1 with noise variance $\sigma^2 = 2\ mg^2/dl^2$. For each 6-hour window $V_m(\hat{\gamma})$, for $m = 1, 2, 3, 4$, has been reported (blue star). The minimum value is highlighted by using a red circle. 45
4.3 Simulated subject #1 with noise variance $\sigma^2 = 16\ mg^2/dl^2$. For each 6-hour window $V_m(\hat{\gamma})$, for $m = 1, 2, 3, 4$, has been reported (blue star). The minimum value is highlighted by using a red circle. 46
4.4 Simulated subject #1 with noise variance $\sigma^2 = 64\ mg^2/dl^2$. For each 6-hour window $V_m(\hat{\gamma})$, for $m = 1, 2, 3, 4$, has been reported (blue star). The minimum value is highlighted by using a red circle. 47
4.5 Top: simulated CGM (blue) with $\sigma^2 = 4\ mg^2/dl^2$ vs KF (red) time series. The gray box is the burn-in interval, in which $\hat{\sigma}^2 = 3.7\ mg^2/dl^2$ has been estimated. Middle: noise-free CGM (blue) vs KF (red) time series. Bottom: details of top and middle panels (left and right boxes, respectively. 50
4.6 Top: simulated CGM (blue) with $\sigma^2 = 16\ mg^2/dl^2$ vs KF (red) time series. The gray box is the burn-in interval, in which $\hat{\sigma}^2 = 14.1\ mg^2/dl^2$ has been estimated. Middle: noise-free CGM (blue) vs KF (red) time series. Bottom: details of top and middle panels (left and right boxes, respectively. . . . 51

4.7 Top: simulated CGM (blue) with $\sigma^2 = 64\ mg^2/dl^2$ vs KF (red) time series. The gray box is the burn-in interval, in which $\hat{\sigma}^2 = 62.2\ mg^2/dl^2$ has been estimated. Middle: noise-free CGM (blue) vs KF (red) time series. Bottom: details of top and middle panels (left and right boxes, respectively. . . . 52

4.8 Detail concerning the burn-in interval of the simulations of Figures 4.5-4.7. Left: noisy (blue) vs bayesian non-casual estimates $\hat{u}(t)$ (red) time series. Right: noise-free CGM (blue) vs bayesian non-causal estimates $\hat{u}(t)$ (red) profiles. Left boxes report original and estimated σ^2 values. 53

4.9 Simulated CGM profile #1. Top: simulated CGM (blue) vs KF (red) time series. Gray boxes highlight three intervals in which σ^2 has been estimated (the estimated value is also reported). Middle: noise-free CGM (blue) vs KF (red) time series. Bottom: true (blue) vs estimated (red) measurement noise variance σ^2. 55

4.10 Simulated CGM profile #2. Top: simulated CGM (blue) vs KF (red) time series. Gray boxes highlight three intervals in which σ^2 has been estimated (the estimated value is also reported). Middle: noise-free CGM (blue) vs KF (red) time series. Bottom: true (blue) vs estimated (red) measurement noise variance σ^2. 56

4.11 Simulated CGM profile #3. Top: simulated CGM (blue) vs KF (red) time series. Gray boxes highlight three intervals in which σ^2 has been estimated (the estimated value is also reported). Middle: noise-free CGM (blue) vs KF (red) time series. Bottom: true (blue) vs estimated (red) measurement noise variance σ^2. 57

4.12 Simulated CGM profile #3 with time sampling period $T_s = 3$ *min*. Top: simulated CGM (blue) vs KF (red) time series. Gray boxes highlight three in intervals in which σ^2 has been estimated (the estimated value is also reported). Middle: noise-free CGM (blue) vs KF (red) time series. Bottom: True (blue) vs estimated (red) measurement noise variance σ^2. 59

4.13 Simulated CGM profile #2 with time sampling period $T_s = 5$ *min*. Top: simulated CGM (blue) vs KF (red) time series. Gray boxes highlight three in intervals in which σ^2 has been estimated (the estimated value is also reported). Middle: noise-free CGM (blue) vs KF (red) time series. Bottom: True (blue) vs estimated (red) measurement noise variance σ^2. 60

5.1 Menarini Glucoday® time series #19 and #7 (top and bottom panels, respectively) taken from dataset used in [33]. 65
5.2 Menarini Glucoday® subject #5. Top: original CGM (blue), the EMA (red) and NF (green) time series. The gray shaded area highlights the 6-hour burn-in window used for initialize NF parameters. Middle: two 6-hour details. Bottom: the $\hat{\sigma}^2$ estimate obtained using the ML-based procedure. 71
5.3 Menarini Glucoday® subject #9. Top: original CGM (blue), the EMA (red) and NF (green) time series. The gray shaded area highlights the 6-hour burn-in window used for initialize NF parameters. Middle: two 6-hour details. Bottom: the $\hat{\sigma}^2$ estimate obtained using the ML-based procedure. 73
5.4 Menarini Glucoday® subject #13. Top: original CGM (blue), the EMA (red) and NF (green) time series. The gray shaded area highlights the 6-hour burn-in window used for initialize NF parameters. Middle: two 6-hour details. Bottom: the $\hat{\sigma}^2$ estimate obtained using the ML-based procedure. 75
5.5 Menarini Glucoday® subject #14. Top: original CGM (blue), the EMA (red) and NF (green) time series. The gray shaded area highlights the 6-hour burn-in window used for initialize NF parameters. Middle: two 6-hour details. Bottom: the $\hat{\sigma}^2$ estimate obtained using the ML-based procedure. 77
5.6 Abbott FreeStyle Navigator™ time series #6 and #8 (top and bottom panels, respectively) taken from dataset used in [53]. 78
5.7 Abbott FreeStyle Navigator™ subject #4. Top: original CGM (blue), the EMA (red) and NF (green) time series. The gray shaded area highlights the 6-hour burn-in window used for initialize NF parameters. Middle: two 2-hour details. Bottom: the $\hat{\sigma}^2$ estimate obtained using the ML-based procedure. . . . 84
5.8 Abbott FreeStyle Navigator™ subject #14. Top: original CGM (blue), the EMA (red) and NF (green) time series. The gray shaded area highlights the 6-hour burn-in window used for initialize NF parameters. Middle: two 2-hour details. Bottom: the $\hat{\sigma}^2$ estimate obtained using the ML-based procedure. . . . 86

List of Tables

4.1 Optimal model order m for each simulated subject and for each level of noise variance σ^2. 44

5.1 Menarini Glucoday® dataset: T and SRG summary results for both EMA and NF. 67
5.2 Menarini Glucoday® dataset: $\hat{\sigma}^2$ and $\hat{\lambda}^2$ mean and standard deviation (sd) values estimated by the ML-based procedure. . 69
5.3 Abbott FreeStyle Navigator$^{\text{TM}}$ dataset: T and SRG summary results for both EMA and NF. 80
5.4 Abbott FreeStyle Navigator$^{\text{TM}}$ dataset: $\hat{\sigma}^2$ and $\hat{\lambda}^2$ mean and standard deviation (sd) values estimated by the ML-based procedure. 82

Sommario

Il diabete è una malattia cronica caratterizzata dell'impossibilità da parte del pancreas di produrre insulina (diabete di Tipo-1) o dal malfunzionamento sia nella secrezione insulinica che nell'azione che essa svolge (diabete di Tipo-2). Come risultato, nel soggetto diabetico il livello glicemico nel sangue può oltrepassare il range di normalità, portando a diverse complicazioni sia a breve che lungo termine. Dal punto di vista quantitativo, il diabete sta assumendo proporzioni di tipo epidemico, con una stima di oltre 220 milioni di individui in tutto il mondo affetti da questa patologia (1 adulto ogni 20, il 95% dei quali è affetto da diabete di Tipo-2), numero che le previsioni indicano crescere a 366 milioni entro il 2030.

La terapia convenzionale per il suo trattamento è basata su iniezioni sottocutanee di insulina, le cui dosi sono calcolate ed aggiustate mediante automonitoraggio della glicemia (Self Monitoring Blood Glucose, SMBG), che consiste in 3-4 misurazioni pungi-dito al giorno. Purtroppo, il SMBG non è in grado di identificare tutte le escursioni glicemiche al di fuori del range di normalità che si possono verificare durante la vita quotidiana.

Per questo motivo, all'inizio del XXI secolo sono stati sviluppati dei nuovi dispositivi che consentono di effettuare il monitoraggio (quasi) in continuo (ovvero una misurazione ogni 1-5 minuti) della concentrazione glicemica, comunemente chiamato Continuous Glucose Monitoring (CGM).

Come verrà introdotto nel *Capitolo 1*, i dispositivi CGM posso essere considerati, potenzialmente, uno efficace strumento per il miglioramento della terapia del diabete. Per prima cosa, essi consentono di individuare un numero maggiore di episodi pericolosi, quali eventi di ipo e iperglicemia, rispetto al convenzionale SMBG, sfruttando informazioni a tempo continuo sul livello glicemico. Secondo, essi consentono di effettuare un'analisi retrospettiva dell'andamento glicemico stesso, analisi che può risultare estremamente utile nella gestione della terapia del paziente, per esempio nell'aggiustarne la dieta o le dosi di insulina. Terzo, un altro miglioramento significativo è rappresentato dal fatto che molti dispositivi CGM incorporano al loro interno un meccanismo che consente di generare allarmi sonori e visivi quando la

concentrazione glicemica oltrepassa le soglie del range di normalità. Infine, la grossa quantità di informazioni prodotta da questi dispositivi può essere sfruttata per prevenire (piuttosto che semplicemente individuare) episodi di ipo e iperglicemia, per esempio generando un allarme con 20-30 minuti di preavviso. In ogni caso, per poter sfruttare al meglio tutti questi vantaggi, è necessario che alcuni aspetti chiave dei sensori CGM vengano notevolmente migliorati.

Un aspetto critico, che necessita di essere affrontato e risolto, è quello relativo al miglioramento in tempo reale (*on-line enhancement*) del Rapporto Segnale-Rumore (Signal-to-Noise Ratio, SNR) dei profili CGM. Infatti, i dati CGM sono inevitabilmente corrotti da un rumore di misura e, per poter migliorare la generazione di allarmi e la predizione del livello glicemico, questa componente rumorosa deve essere ridotta, per es. utilizzando dei filtri causali. Fino ad ora, il problema di trovare una strategia ottima per il filtraggio on-line dei dati CGM non è stato ancora trattato in modo soddisfacente né dalle case produttrici di sensori né da ricercatori.

L'obiettivo di questo lavoro è quello di proporre una nuova procedura di filtraggio, sviluppata in un contesto stocastico, per migliorare la qualità delle serie temporali CGM e le informazioni in esse contenute. In particolare, mostreremo come la nuova procedura sia in grado di affrontare con successo la variabilità inter- ed intra-individuale del SNR, e quella da sensore a sensore, presente nei dati CGM, portando ad un miglioramento significativo nella qualità dei dati forniti in output dal sensore.

Nel *Capitolo 2* vedremo come un metodo di filtraggio di tipo deterministico, per es. il filtro a Media Mobile (Moving-Average, MA), che attualmente è il filtro più utilizzato all'interno dei dispositivi CGM, consenta di migliorare la qualità dei dati CGM. Tuttavia, il miglioramento prodotto risulta essere subottimo, in quanto tale approccio non è in grado di adattarsi alla variabilità inter- ed intra-individuale del SNR, e quella da sensore a sensore, presente nei dati CGM.

Per migliorare la qualità dei dati CGM, tenendo in considerazione la loro variabilità, abbiamo sviluppato un nuovo approccio di filtraggio di tipo stocastico, che verrà descritto in dettaglio nel *Capitolo 3*. La caratteristica chiave di questo nuovo approccio, implementato mediante il Filtro di Kalman (Kalman Filter, KF), è legata al fatto che esso incorpora un modello *a priori* sulla regolarità del segnale glicemico. Questo modello è caratterizzato da un parametro che può essere stimato in *real-time* mediante una procedura automatica basata su un criterio di Massima Verosimiglianza (Maximum Likelihood, ML) dei dati.

Le prestazioni della nuova procedura di filtraggio stocastico sono state testate prima di tutto su dati simulati (*Capitolo 4*). Una procedura basata

sul criterio di Cross Validation (CV) è stata utilizzata per individuare il miglior modello *a priori* per descrivere la regolarità del segnale glicemico. Successivamente, le capacità del filtro di adattarsi alla variabilità inter- ed intra-individuale del SNR, e quella da sensore a sensore, presente nei dati CGM, sono state illustrate in dettaglio.

Successivamente, il nuovo filtro è stato applicato su dati reali (*Capitolo 5*), ovvero su un dataset Glucoday® (Menarini) e su uno FreeStyle Navigator™ (Abbott), composti rispettivamente da 24 e 20 serie temporali CGM. Le prestazioni del nuovo filtro sono state confrontate con il filtro MA, usando come indici di confronto il ritardo introdotto dal filtro e la sua capacità di regolarizzare il segnale.

I risultati ottenuti sui due dataset mostrano come il nuovo filtro sia correttamente in grado di adattarsi alla variabilità inter- ed intra-individuale del SNR, e quella da sensore a sensore, presente nei dati CGM, introducendo un ritardo minore di quello prodotto dai filtri deterministici e riducendo in maniera soddisfacente la componente rumorosa, adeguando la regolarizzazione del segnale in base alle caratteristiche del profilo CGM.

Summary

Diabetes is a chronic disease characterized by the inefficiency of the pancreas to produce insulin (Type-1 diabetes), or by malfunctions in both insulin secretion and action (Type-2 diabetes). As a result, in a diabetic subject the plasma glycemic level exceeds the normal range, with several long and short term complications. Diabetes is taking on epidemic proportions with over 220 million individuals affected by this disease worldwide (1 over 20 adults, 95% of whom have Type-2 diabetes), a number which is expected to grow to 366 million by the year 2030.

The conventional diabetes therapy is usually based on subcutaneous insulin injections, the doses of which are determined on the basis of the Self Monitoring of Blood Glucose (SMBG), which consists in 3-4 finger stick measurements per day. However, SMBG is not able to track all glycemic excursions outside the normal range that happen during daily life.

For this reason, at the beginning of the 21st century new sensors have been developed which allow a quasi-continuous monitoring of blood glucose concentration (e.g. a measurement every 1 to 5 minutes), the so-called Continuous Glucose Monitoring (CGM). As discussed in *Chapter 1*, CGM devices are potentially an efficient tool for improving the diabetes management. First, they allow to detect more critical episodes, e.g. hypo and hyperglycemic events, than conventional SMBG thanks to the exploitation of the continuous-time information about the glycemic level. Second, they allow to perform a retrospective analysis of glucose profile, which could be very useful in the management of patient's therapy, e.g. in the adjustment of the diet and the insulin dosage. Third, another significant improvement is represented by the embedding in many of the CGM systems of a tool able to generate visual and acoustic alerts when glucose concentration exceeds the normal-range thresholds. In the end, the huge amount of information coming from CGM devices could be managed to prevent (rather than simply detect) hypo and hyperglycemic events before they occur, e.g. by generating an alert, say, 20-30 min ahead of time. However, in order to usefully exploit all these advantages, some key features in CGM devices need to be significantly

improved.

One important and critical aspect that needs to be faced is the *on-line enhancement* of the Signal-to-Noise Ratio (SNR) of CGM profiles. In fact, CGM data are unavoidably affected by measurement error and, in order to improve e.g. the alert generation and future glucose level prediction, the noise component needs to be reduced, e.g. by using causal filters. So far, the problem of finding an optimal strategy for on-line filtering CGM data has not been yet satisfactorily treated, neither from industries nor from researchers.

The aim of this work is to propose a new on-line stochastically-based filtering procedure to improve the quality and the information of CGM time series. In particular, we will prove that the new stochastically-based filtering procedure is able to cope with to inter-individual SNR, intra-individual SNR, and sensor-to-sensor variability of CGM data, significantly improving CGM device output.

Deterministic approaches for filtering, e.g. the Moving-Average (MA), which is currently the most common and diffused filter methodology embedded in CGM devices, allow to improve the quality of CGM data. However, as discussed in *Chapter 2*, the enhancement produced is expected to be suboptimal, because MA filters do not adapt the regularization they introduce to inter-individual SNR, intra-individual SNR, and sensor-to-sensor variability of CGM data.

To improve the enhancement of CGM data taking into account inter-individual SNR, intra-individual SNR, and sensor-to-sensor variability, we developed a new stochastically-based filtering procedure, which is described in detail in *Chapter 3*. The core key of this new approach, implemented through the Kalman Filter (KF), lies in the exploitation of an *a priori* model of glucose signal smoothness. This model incorporates a parameter which can be estimated in *real-time* by a fully-automated Maximum Likelihood (ML)-based procedure.

Performance of the new stochastic filtering procedure is first tested on a simulated dataset (*Chapter 4*). A Cross Validation (CV)-based procedure has been used to find the optimal *a priori* model of the signal smoothness. Then, the ability of the filter to cope with inter-individual SNR, intra-individual SNR, and sensor-to-sensor variability of CGM data have been demonstrated.

Then, the new filter has been then applied on real data, i.e. a Menarini Glucoday® and a Abbott FreeStyle Navigator™ datasets of 24 and 20 CGM time series, respectively (*Chapter 5*). A comparison with performance of the MA approach has been performed, using as criteria for the comparison the delay introduced by the filter together with its smoothing ability.

Results on the two real datasets show that the new filter is able to correctly cope with inter-individual SNR, intra-individual SNR, and sensor-to-

sensor variability of CGM data, introducing less delay than deterministic filters and performing a satisfactory denoising, adequately tuning the smoothing to the characteristics of the CGM profile.

Chapter 1

Continuous Glucose Monitoring

Diabetes Mellitus is a disease characterized by the inability of the pancreas to produce sufficient amounts of insulin to maintain the glucose level in the normal range (Type-1 diabetes), which is usually set between 70 and 180 mg/dl, or by malfunctions in both insulin secretion and action (Type-2 diabetes). To cover this deficiency, people with diabetes are treated with subcutaneous insulin injection treatment. To determine the dose for their insulin injections, patients have to frequently monitor their blood glucose concentration by means of Self Monitoring Blood Glucose (SMBG) therapy (i.e. 3-4 finger stick measurements per day). In the last few years new sensors have been developed which allow Continuous Glucose Monitoring (CGM), e.g. a glucose measurement is obtained every e.g. 5 minutes, and for several days. These devices significantly improve diabetes management detecting more critical episodes (i.e. hypo and hyperglycemia) rather than conventional SMBG.

In this chapter Diabetes and related complications, SMBG and devices for CGM will be briefly introduced and described.

1.1 Diabetes & Self Monitoring Blood Glucose (SMBG)

Glucose is the most important fuel for human beings and its level in the blood is precisely controlled by insulin by a negative feedback system. In diabetic patients, the body does not secrete insulin (Type-1 diabetes) or derangements in both insulin secretion and action (Type-2 diabetes) occur. Diabetes is taking on epidemic proportions with over 220 million individuals affected by this disease worldwide (1 over 20 adults, 95% of whom have Type-2 diabetes), a number which is expected to grow to 366 million by the year 2030 [65].

Maintaining glucose levels in the normal range is essential for preventing diabetes related complications, including microvascular complications like nephropathy leading to renal insufficiency, retinopathy leading to blindness, and neuropathy leading to foot ulcer or amputation as well as macrovascular complications such as heart infarction and cerebral infarction with their associated mortality [65].

Diabetes conventional therapy is mainly based on insulin and drug administration, diet, and physical exercise. Insulin therapy is vital for patients affected by Type-1 diabetes, essential for blood glucose control and prevention of complications in many Type-2 diabetic patients and extremely valuable for non diabetic patients in critical situations that impair physiological glucose homeostasis like intensive care. However, in spite of continuous improvements in insulin preparations (insulin analogs), insulin delivery tools (user-friendly insulin pens, wearable pumps) insulin therapy remains one of the most difficult therapies. In fact, bringing glucose levels to target using insulin therapy is limited by the occurrence of hypoglycaemic episodes, i.e. too low glucose values, due to the narrow therapeutic range of insulin [22]. In the conventional therapy, the insulin dosage management is usually tuned according to some capillary blood glucose measurements taken 3-4 times a day. This kind of glycemic control is called Self Monitoring Blood Glucose

Figure 1.1: *Two devices for SMBG: Lifescan OneTouch® (left) and Abbott FreeStyle (right) [57, 61].*

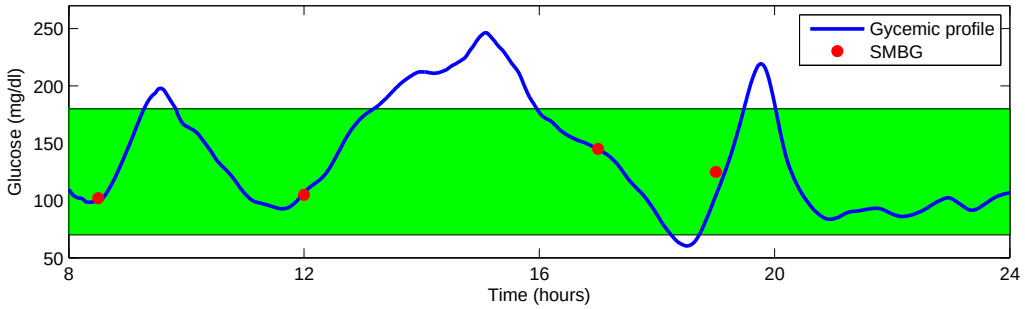

Figure 1.2: *Comparison between real glycemia (blue profile) and SMBG measurements (red dots). The green area highlights the range of normality.*

(SMBG). SMBG is a point-in-time blood glucose test [25] which provides discrete, highly accurate data about current blood glucose levels. Figure 1.1 shows two devices for SMBG.

However, these few samples per days are not sufficient to follow all glycemic variability and to detect critical glycemic episodes that occurs all day long, e.g. post-prandial hyperglycemia and hypoglycemia due to an extra-dosage of insulin. An example of this inefficiency is reported in Figure 1.2. The highlighted green area represents the range in which the ideal glycemia must be contained. The four SMBG measurements (red dots) preformed in this example are all contained in the range and apparently do not evidence critical episodes. However the true glycemic profile (blue line) shows one hypoglycemic and three hyperglycemic episodes that SMBG has not been able to catch. This SMBG inability to track all glycemic excursions outside the normal range, led at the beginning of the 21st century to the development of new devices that allow a quasi-continuous measurement of blood glucose concentration, the so-called Continuous Glucose Monitoring (CGM) systems.

1.2 Continuous Glucose Monitoring (CGM) Devices

As previously explained, conventional SMBG does not necessary detect all hypo and hyperglycemic events occurring during the whole day. As a consequence, pharmaceutical industries started to invest economic and human facilities for the development of Continuous Glucose Monitoring (CGM) systems. These kind of devices measure the glucose concentration very frequently, e.g. every 1 to 5 minutes, and for several days (up to 7). The potential improvement in the management of diabetes therapy due to these new sys-

tems is rather evident [20, 24]. The analysis of these multiple readings not only facilitates retrospective identification of glucose trends, but these trends can also be predictive of the glucose level in the immediate future, leading to a more effective therapeutic intervention and providing more information for planning daily insulin dosages.

As the development of new technological devices concerns, also CGM systems present some critical aspects than need to be studied and faced to improve their efficiency. Even if all the pro and cons of CGM devices will be treated in Section 1.4, here we can anticipate that the major weakness of CGM systems is that their readings result fairly accurate. This is the most important reason why the U.S. Food and Drug Administration (FDA) decided not to consider them as substitute of conventional SMBG. As it will be described in details later, this inaccuracy is principally related to the fact that CGM systems do not directly measure the glucose concentration in the blood.

Many prototypes of CGM devices (most of them have been approved and commercialized) have been developed in the last few years. From a technological point of view, they can the mainly divided into two different categories: minimally-invasive and non-invasive devices.

1.2.1 Minimally-Invasive Devices

The minimally-invasive technologies are so-called because the measurement sensor does not directly measure the glucose concentration in the blood, but in the interstitial fluid, where a part of the sensor itself is implanted. Minimally-invasive CGM systems usually consist of two components:

- a wearable device, composed by a needle-based (or microdialysis-based) subcutaneous measurement sensor plus a transmitter, which provides real-time measurements;

- a pocket device, composed by a receiver, a memory (to store data) and a display to visualize the measurements received from the sensor.

In some of the systems the communication between the sensor and the monitoring part is wireless. The portability of this kind of system is clear and the size is relatively small, which means that it can be easily worn on the body without obstructing the mobility of the person. In general the measurement given by the sensor is an estimate of the blood glucose concentration. In fact, the sensor measures a raw signal (usually a current in mV or mA) produced by chemical reaction (usually a glucose oxidase-based), which is proportional to the glucose concentration of the site in which the biosensor is implanted.

In the case of minimally-invasive devices the site is the interstitial fluid. This raw signal is then converted into a glucose level through a calibration procedure, different for device to device, which usually needs one or more SMBG measurements.

The most important and used minimally-invasive devices are:

- CGMS® System Gold™ (Medtronic MiniMed, northridge, CA), which received the FDA approval in March 2001 [62];
- Guardian® Real-Time (Medtronic MiniMed, northridge, CA), which received the FDA approval in June 2005 [64];
- GlucoDay® (Menarini Diagnostics, Florence, Italy), which received the CE mark in Europe (no FDA approval has been asked for) [63];
- STS-7™ (Dexcom, San Diego, CA), which received the FDA approval in June 2007 [58];
- FreeStyle Navigator™ (Abbott Laboratories, Alameda, CA), which received the FDA approval in March 2008 [57].

The two devices, FreeStyle Navigator™ and GlucoDay®, which have been used for providing the data of this thesis, will be deeply described in Section 1.3.

1.2.2 Non-Invasive Devices

Non-invasive CGM devices are obviously the most attractive user concept for blood glucose measurement. They have been under development for many years by numerous researchers, but it will still take several years before such a systems providing accurate and precise data will reach the market place. Compared to minimally-invasive devices, all of which perform the glucose measurement in the interstitial fluid, these systems use different number of transcutaneous methods to measure glucose: reverse iontophoresis, measurements of dermal characteristics such as photoacoustics, radio frequency impedance and refractive index, and occlusion spectroscopy.

In the following some of the most interesting non-invasive CGM prototypes are listed and briefly described:

- The GlucoWatch G2 Biographer (Cygnus, Inc., Redwood City, CA) received the FDA approval in 2001 [47]. Although its process is often described as reverse iontophoresis, it actually measures bulk flow of glucose across a membrane. The device utilizes an electrical charge to

pull sodium and chloride out of the patient's skin; glucose is passively pulled along with the water of hydration of the salts. The extracted solution is then oxidized and measured for glucose content. This product has been retired from the market in 2006 because a lot of skin irritation cases due to its usage have been experienced.

- The Aprise (Glucon Inc., Boulder, CO) device uses an interesting methodology called photoacoustics [55]. A laser light is applied to the skin above a blood vessel, causing a small but rapid increase in temperature in the blood vessel and making a soft popping sound. The device "listens" to the pop and determines glucose levels from the acoustic characteristics of the sound. Unlike the other systems, which measure interstitial glucose, the Aprise actually measures blood glucose. The device is not yet approved by the FDA and is not for sale in the US.

- The NBM (OrSense Ltd., Nes Ziona, Israel) device is based on occlusion spectroscopy [2]. The measurement is performed using an annular probe, which is positioned on the finger's root. The probe contains light sources and detectors operating in the red/near-infrared (RNIR) spectral region and pneumatic cuffs that produce oversystolic pressure to occlude blood flow. The technology is based on the direct effect of glucose on the scattering properties of the organ. Glucose decreases the mismatch in refractive index between scatterers and their surrounding media, leading to a smaller scattering coefficient and, consequently, a shorter optical path. As a result, with the growing concentration of glucose, fewer photons are absorbed and the light intensity increases. The NBM devices is a prototype and neither CE nor FDA approval have been still asked for it.

1.3 Two Popular CGM Devices

In this section the two minimally-invasive CGM devices, the Abbott FreeStyle Navigator™ and the Menarini GlucoDay®, which have been used for providing data for this thesis, will be briefly described.

1.3.1 Abbott FreeStyle Navigator™

The FreeStyle Navigator™ produced by Abbot Diabetes Care is a subcutaneous electrochemical sensor which operates up to 5 days implanted at the site in the body. It is composed by:

- a sensor (Figure 1.3), which is placed on the back of your upper arm or your abdomen, and is held there with a special adhesive. A tiny filament 5mm long as thin as several strands of hair goes just under the skin;

Figure 1.3: *FreeStyle Navigator^{TM} sensor [57].*

- a transmitter (Figure 1.4), which is attached to the sensor and sends glucose readings to the wireless receiver up to 10 feet away;

Figure 1.4: *FreeStyle Navigator^{TM} transmitter [57].*

- a receiver (Figure 1.5), which is like a little computer. It stores all glucose readings, for up to 60 days, and it gives an accurate picture of what your glucose is doing.

The glucose measurement is based on a Wired-Enzyme$^{\text{TM}}$ sensing technology [16], very similar to the conventional electrochemical glucose-oxidase technology already used e.g. by the Minimed CGMS Gold. The original glucose-oxidase measurement principle is based on the generation of hydrogen peroxide via the enzyme glucose oxidase [8]:

$$\begin{aligned} \text{glucose} + O_2 &\xrightarrow{\text{glucose oxidase}} H_2O_2 + \text{gluconic acid} \\ H_2O_2 &\xrightarrow{\sim 700\text{mV}} O_2 + 2H^+ + 2e^- \end{aligned} \tag{1.1}$$

Figure 1.5: *FreeStyle Navigator^{TM} receiver [57].*

An ammeter detects the current generated due to the oxidation of hydrogen peroxide at the working electrode. The major limitation of this technology is related to the chemical reaction itself, which requires an oxygen for each glucose molecule. In contrast, Wired Enzyme technology used by FreeStyle Navigator^{TM} works at lower potential (+40mV) using an osmium (Os)-based moderator molecule specifically designed. The sensing element is a redox active gel, consisting of Os-based mediator molecules attached to a polymeric backbone film and glucose oxidase (GOx) enzyme molecules. In this way the oxygen can compete for electrons with the Os-based mediator molecules, reducing the oxygen dependency and minimizing the sensitivity *in vivo* oxygen variations and good linearity at high glucose concentrations. Figure 1.6 reports a schematic diagram of the Wired-Enzyme^{TM} layer and a detail of the structure of the redox polymer.

The electrical signal produced by the chemical reaction is then transformed into glucose level by a calibration procedure based on SMBG measurements, which are required after 10, 12, 24 and 72 hours after the sensor has been implanted [17].

In order to evaluate the performance of the FreeStyle Navigator^{TM}, the accuracy of the measurement has been tested comparing the readings both to blood glucose reference values [27] and to other CGM devices [9, 28]. In all these studies the FreeStyle Navigator^{TM} readings resulted very accurate (98.4% of correct measurements using FDA criteria [9]), especially in hypoglycemia zone [28]).

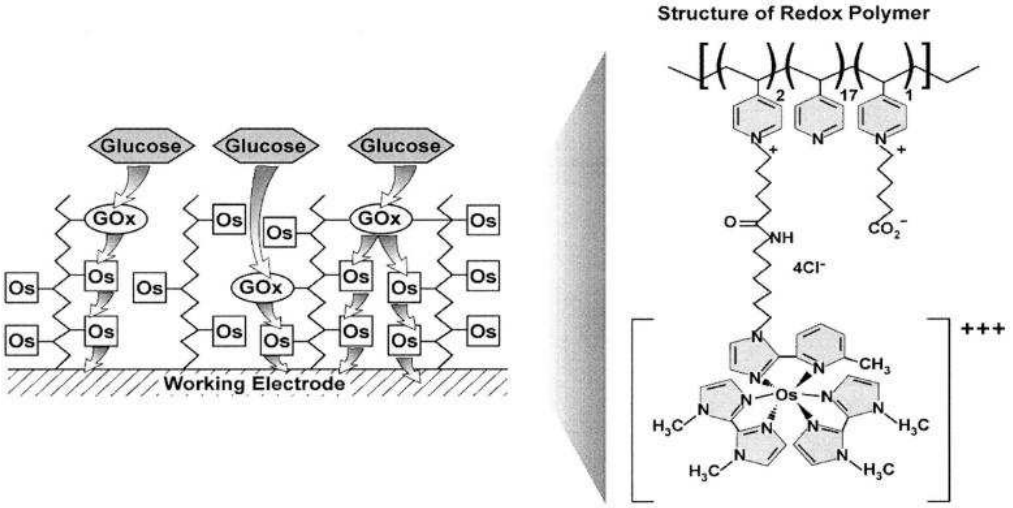

Figure 1.6: *Schematic diagram of the Wired Enzyme^{TM} sensing layer, showing redox polymer, incorporated enzyme (GOx), and path of electron flow from glucose to the working electrode. The detail on the right shows the actual structure of the redox polymer [16, 17].*

1.3.2 Menarini GlucoDay®

The GlucoDay® device from Menarini Diagnostics, illustrated in Figure 1.7, is the only minimally-invasive CGM system which doesn't use any implantable sensor, but it is based on a microdialysis technique.

A microdialysis tube is inserted into the abdominal wall and connects a micropump to a biosensor. A schematic representation of the GlucoDay® apparatus is reported in Figure 1.8.

The micropump pumps a perfusion solution through the tube; as the fluid flows through the tube under the patient's skin it picks up glucose through the dialysis membrane and is transported to the biosensor and is there measured for glucose content. The glucose measurement is performed every second, but the device is set to measure an average value every 3 minutes. GlucoDay® can be used in real-time and, as a consequence, it is provided with a calibration procedure that is usually performed 2 hours after the microdialysis tube has been inserted using a capillary finger stick measurement.

As for the other CGM devices, the accuracy of GlucoDay® readings has been tested. Different studies can be found in literature [29, 33, 54, 28]. The most recent one, which performed a comparison of GlucoDay® readings with blood glucose reference values, reports a global accuracy of 96.2%, with a particular elevated percentage of accuracy in the hypoglycemic range [28].

Figure 1.7: *The Menarini GlucoDay® device [63].*

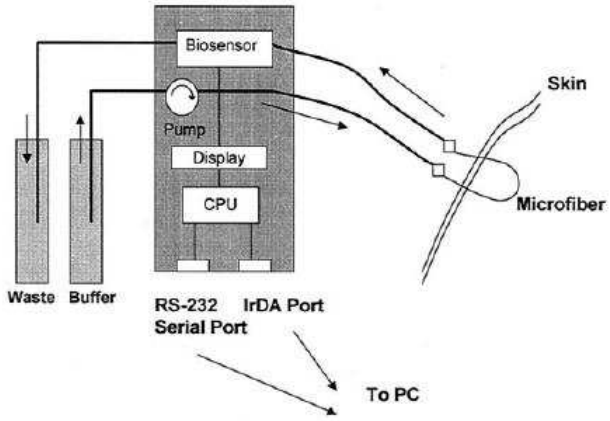

Figure 1.8: *Schematic representation of the GlucoDay® apparatus and the microdialysis fiber [33].*

1.4 Pros and Cons of CGM Devices

We have seen that CGM devices have the great advantage to return to both clinicians and diabetic patients a more complete information about the glycemic profile rather than SMBG. The possibility to have real-time information about the glycemic level and its trend results very useful in the management of patient's therapy, e.g. in the adjustment of the diet and the insulin dosage. Another significant improvement in diabetes management is

also represented by the embedding in many of the CGM system of a tool able to generate visual and acoustic alerts when glucose concentration exceeds the normal range thresholds. Furthermore, the huge amount of information coming from CGM devices could also be used to trying to prevent (rather than simply detect) hypo and hyperglycemic events before they occur [7], e.g. by generating an alert, say, 20-30 min ahead of time.

The portability of these devices and the possibility to receive an alarm when some fixed glycemic thresholds have been crossed, allow the diabetic patient to become more self-sufficient in the management of both therapy and critical events, e.g. post-prandial hyperglycemia and nocturnal hypoglycemia. On the other side, the more information is available the more the diabetic needs to be trained to correctly use it. It is also important to remind that, nowadays, none of the CGM devices has been approved to substitute SMBG as reference in both control and management of the therapy. This fact is principally due to the lack of accuracy of CGM readings [20], accuracy which is crucial point in the correct working of such a devices. Errors in both measurement and calibration make these sensors useless. In the end, the economic aspect cannot be neglected. As many other technological devices, CGM systems result rather expansive. For example, the price of a CGM system goes from a minimum of $800 for the devices plus $60 for a 7-days sensor in the case of the STS-7™, to a maximum of $1339 for the device and $35 for a 3-days sensors if one chooses to use the Guardian® Real-Time [59].

1.5 Open Problems in CGM Devices

The innovation introduced in the management of diabetes therapy by the use of CGM systems has been significantly worthwhile. But, in order to become more useful, some key CGM features need to be significantly improved. A review on these problems can be found in Sparacino et al. [45].

1.5.1 Physiological Aspects

In order to reduce the invasivity of the readings, minimally-invasive CGM devices use to measure a signal that is proportional to the glucose concentration in the interstitial fluid (ISF) rather than to plasma glucose. Because the glucose metabolism and regulation is based on plasma concentration, the relation which characterizes the dynamics and the communication between the two sites needs to be explored.

Different models for describing the plasma-to-ISF dynamics have been proposed in literature. The most popular, accepted and used is the two-

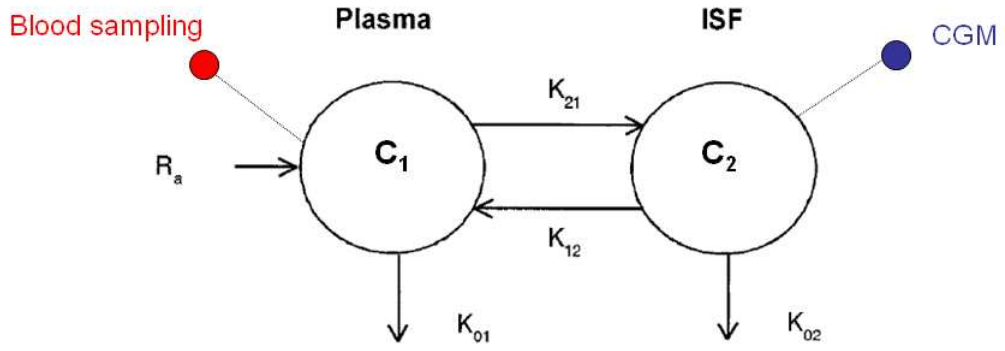

Figure 1.9: *The two-compartment model for describing the plasma-to-ISF dynamics [39]*

compartment model of Rebrin et al. [39], illustrated in Figure 1.9, where the left (C_1) and right (C_2) compartments represent the plasma and interstitial glucose concentrations, respectively, R_A represents the rate of appearance of the glucose, and K_{ij} represents the diffusion constant from compartment j to compartment i (where 0 is the external compartment).
The transfer function of the presented two-compartment model resembles a low-pass filter and it characterized by two parameters, i.e. the *diffusion gradient* (from plasma to ISF) and the *diffusion time constant*. The model has been identified applying it to some dataset in which both CGM and plasma glucose concentrations have been simultaneously measured. Figure 1.10 illustrates a portion of representative subject, taken from one of these dataset [53], in which both plasma (red stars) and ISF (blue line) glucose concentrations were measured in parallel. The distortion introduced by the plasma-to-ISF dynamic is rather evident.
Results show that the diffusion gradient can be considered almost constant, while the diffusion time constant not only seems to be time varying [13] but also the delay due to the diffusion is significantly large (from 8-12 minutes in [38, 46] up to 20 minutes [13]).

These results need to be considered in analyzing other problems, e.g. calibration.

1.5.2 Calibration

The calibration of CGM devices is a key aspect. Most of CGM systems measure an electrical signal which needs to be transformed into glucose level

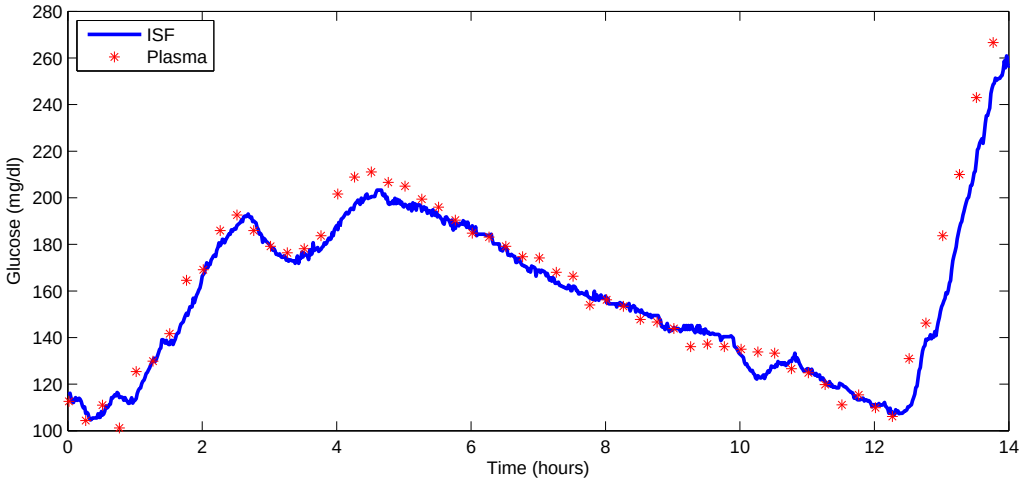

Figure 1.10: *Portion of a representative subject in which both plasma (red stars) and ISF (blue line) glucose were simultaneously measured [53].*

by using finger stick as reference. If the raw signal were directly proportional to blood glucose concentration, the calibration would be precise (neglecting errors in measurements).

In Section 1.5.1 we have seen that the ISF glucose concentration is a distorted version of plasma glucose and that the delay introduced by the dynamic model cannot be neglected. This physiological delay plays a key role in calibration. In fact, during fast changes in the glycemic level, e.g. after a meal, the point-to-point glucose concentration of capillary and ISF could be significantly different (e.g. from 5 to 20 mg/dl). Performing a calibration in these situations could introduce an error in CGM readings and consequently could make the CGM device useless [41]. Not only, due to the deterioration of some of the technological parts of the sensors, the calibration procedure needs to be performed many times during a monitoring (e.g. in the FreeStyle Navigator^{TM} after 10, 12, 24, and 72 hours the sensor has been implanted).

Figure 1.11 shows a portion of data of a representative subject, taken from one of these dataset [53], in which both plasma (red stars) and ISF (blue line) glucose were measured in parallel. Discrepancies between plasma and ISF measurements due to bad calibration are rather evident in time window 16-18, in which CGM readings drastically underestimate the real glycemic values.

The calibration aspect has been partially investigated in the literature [26, 31, 32, 41]. A recent simulation study [15] proposes a new on-line calibration

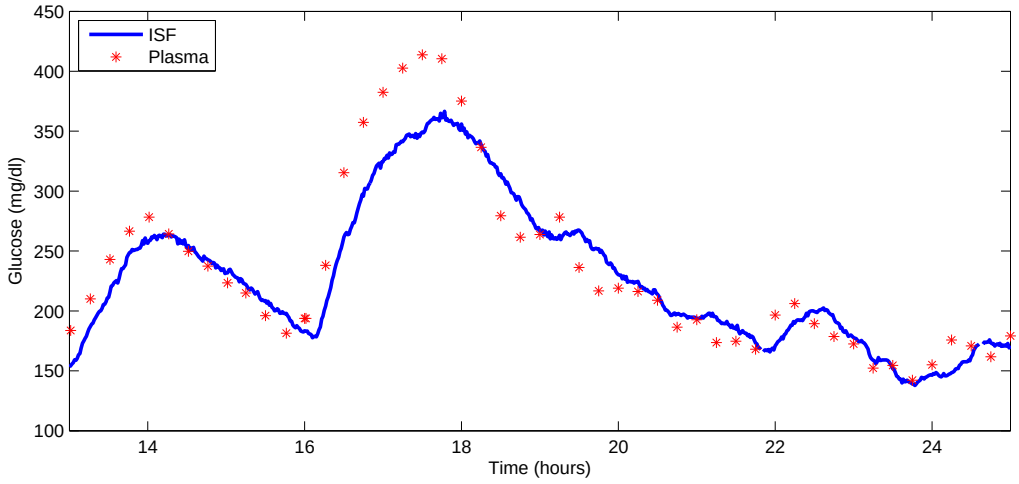

Figure 1.11: *Portion of a representative subject in which plasma (red stars) and ISF (blue line) glucose where measured in parallel [53].*

method based on the two-compartment model of [39] and implemented with the Kalman Filter. This new on-line calibration procedure aims to face the problems of both to find the correct allocation of calibration points and to recover the glycemic profile in presence of deteriorations of the sensor.

Even if calibration and related physiological aspects play a key role, they would not be treated in this thesis. The lack of free datasets and patents limit their investigation.

1.5.3 Filtering

Another important problem concerning with CGM devices is filtering. As every measurement device, CGM data are unavoidably affected by measurement noise. In order to make CGM data useful, e.g. for alert generation and future glucose level prediction, the noise component needs to be reduced, e.g. by using causal filters. Due to the recent development of this devices, the problem of finding an optimal strategy for on-line filtering CGM data has not been yet satisfactory treated neither from industries nor from researchers [26, 30, 36]. Figure 1.12 reports two representative CGM time series collected using two different CGM devices, i.e. the Abbott FreeStyle Navigator™ and the Menarini GlucoDay® (top and bottom panels, respectively).

In both profiles the presence of a noise component overlapped to the true glycemic signal is rather evident. From a visual inspection, this component

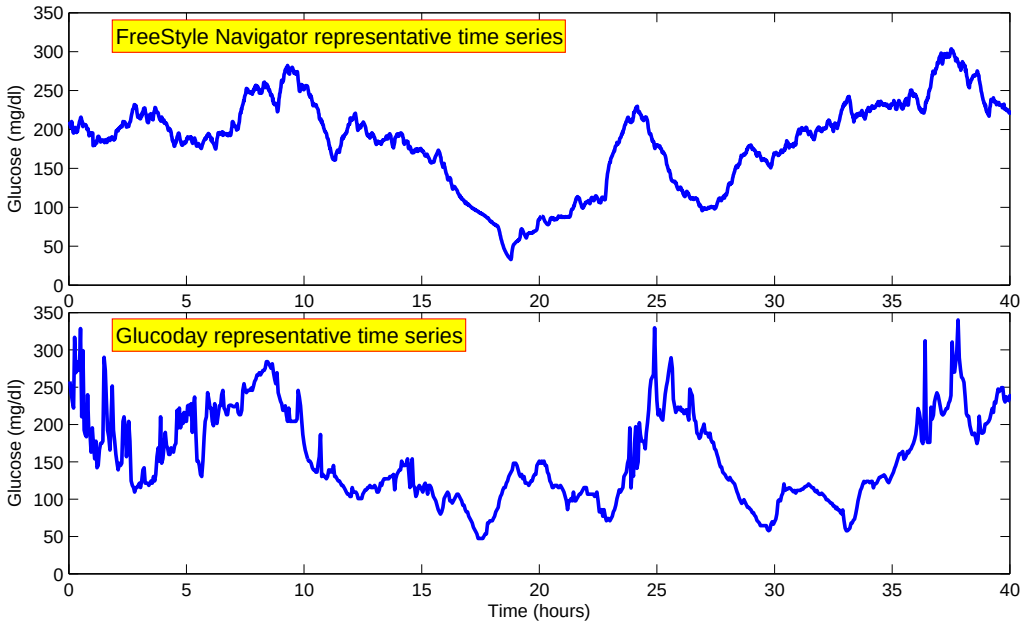

Figure 1.12: *CGM representative subjects. Top: FreeStyle Navigator^{TM} time series [53]. Bottom: GlucoDay® time series [33].*

not only varies from a subject to another, but also inside a single monitoring. An optimal filtering algorithm is needed to improve the quality of CGM data.

In this thesis existing and embedded filtering techniques will be analyzed and a new stochastically-based filtering method to cope with most of the unsolved open problems will be proposed.

1.5.4 Prediction

A natural application in CGM is the prevention of hypo and hyperglycemic events. In fact, the large amount of information given by CGM devices could be used to predict the future glycemic level. Figure 1.13 illustrates two representative subjects in which the 30-minute ahead in time Auto-Regressive Prediction Model of Sparacino et al. [44] has been applied. The blue and red lines represent original CGM and predicted data, respectively.

Some preliminary studies in literature have shown that forecasting is possible [14, 37, 40, 45]. In these works it has been demonstrated that prediction could be very important in order to prevent, rather than detect, critical events, e.g. hypo and hyperglycemia. However, in order to minimize the error propagation, prediction calls for accurate data. As a consequence, the prediction problem could be completely and correctly faced only if the filtering

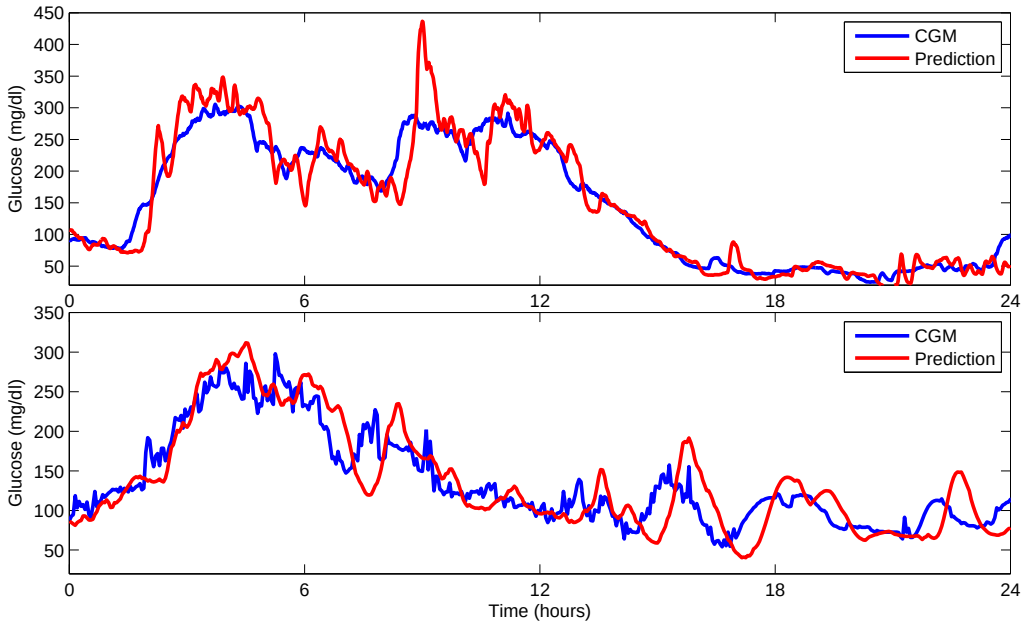

Figure 1.13: *Original CGM data (blue line) vs 30-minutes ahead in time predicted profile (red line) by using Auto-regressive models. Top: FreeStyle Navigator^{TM} subject. Bottom: GlucoDay® subject [45].*

step has been completed.

1.6 Aim of the Work and Outline

In the previous section we have seen the one of the major problems we have to deal with in CGM devices is the noise present on CGM readings. The aim of this work is to propose a new stochastically-based filtering procedure to improve the quality and the information of CGM time series. In particular, we will prove that the new filter is able to cope with inter-individual Signal-to-Noise Ratio (SNR), intra-individual SNR, and sensor-to-sensor variability of CGM data, significantly improving CGM device output.

Chapter 2 is dedicated to the analysis of both the characteristic of the noise component which overlaps the glycemic signal and the filtering algorithm embedded in CGM devices to face it. It will be shown that these deterministic algorithms, e.g. the Moving Average, are not the optimal solution for filtering.

Chapter 3 is the core of this work. The new on-line stochastically-based filtering procedure, implemented through the Kalman Filter (KF), will be

described in details.

Chapter 4 illustrates on simulated datasets first how the *a priori* model that lies behind the new filter has been selected and second that the new filter is able to successfully cope with all the problems detected in Chapter 3, i.e. inter-individual SNR, intra-individual SNR, and sensor-to-sensor variability of CGM data.

Chapter 5 shows results of the application of the new filter on the two real CGM datasets, i.e. the Menarini Glucoday® and the Abbott FreeStyle Navigator™, considered for this work. In this chapter it will be also proved on real datasets that the new filter is able to adequately and satisfactory improve the quality of CGM time series.

Chapter 2

CGM Time Series Denoising: State of the Art

In the previous chapter major advantages in the use of CGM devices have been introduced. We have shown that CGM devices can facilitate the daily management of diabetes, e.g. allowing to detect hypo and hyperglycemic events through the generation of visual or acoustic alerts. However, in order to properly generate hypo and hyperglycemic alerts and to avoid the risk of detecting false and missing true events, the quality of CGM must be evaluated. Analyzing some CGM time series we will show that CGM data are unavoidably affected by random measurement error. To reduce the noise component, the use of real-time filtering methodologies able to enhance the Signal-to-Noise Ratio (SNR) of CGM data is needed.

In this chapter the characteristic of the noise component that overlaps the true glycemic signal is considered and analyzed. In addition, the most used and embedded (in CGM devices) deterministic approach for filtering, the Moving-Average filter, is implemented, and its limitations in following SNR variations, that occurs between sensors, between individuals and also inside a single monitoring, are illustrated.

2.1 Noise in CGM Data: Origin and Characteristics

The noise component that overlap the true glycemic signal in CGM measurements has different origins. For example, in order to reduce the invasivity of the measurement, in Section 1.2.1 we have seen that minimally-invasive CGM devices measure a flux of electrons, result of an electrochemical reaction, that is proportional to the glucose concentration in the interstitial fluid rather than to the blood glucose concentration. This measurement is affected by a random error and consequently the row electric signal so produced (usually in mV or mA) results unavoidably noisy. Moreover, in successive steps, this raw signal is transformed into glucose concentration through a calibration procedure that involves other measurements, e.g. Sensitivity and Temperature of the sensor in Abbott FreeStyle Navigator™, which are affected by measurement error their selves. Another noise source is related to the signal instability after the biosensor has been implanted on the body site. In fact, all sensors require a running period in which the body interacts with the needle/microdialysis tube till a stable point is reached. This time lag may vary between 1 to 10 hours [24]. For this reason the FreeStyle Navigator™ acquires the first data only 10 hours after the sensor has been implanted [53]. Furthermore, in microdialysis-based devices, e.g. the Glucoday®, the microdialysis tube inserted in the adipose tissue needs to be flexible and consequently it is sensible to patient movements, which may cause the occlusion of the tube, leading to the generation of spikes in the signal.

Figure 2.1 and 2.2 show some examples of noisy CGM data. Figure 2.1 reports two representative Glucoday® noisy signals in which spurious spikes created by the occlusion of the microdialysis tube are rather visible.

The top panel shows a CGM profile with a high SNR but with some accentuated spikes around hour 21, while the bottom panel a CGM signal with low SNR but with a lot medium-intensity spikes diffused all over the monitoring.

Figure 2.2 reports two representative profiles obtained using the FreeStyle Navigator™ instead. At a first glance, the two signals do not present so accentuated spikes as the ones observed in Figure 2.1, but it is rather evident the presence of a noise component diffused on the whole profiles.

Previously reported examples are sufficient to highlight the principal characteristics of the noise component affecting CGM data:

- *the presence of spurious spikes*, rather evident in the Glucoday® data (Figure 2.1);

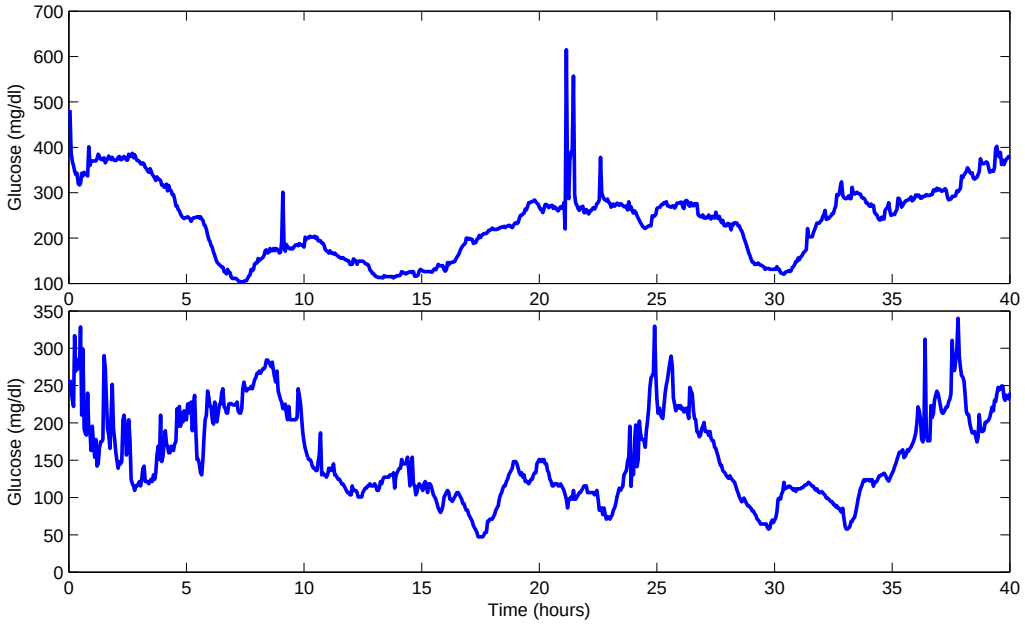

Figure 2.1: *Two Glucoday® noisy signals. Top: high SNR with some huge spikes. Bottom: low SNR with medium-intensity spikes.*

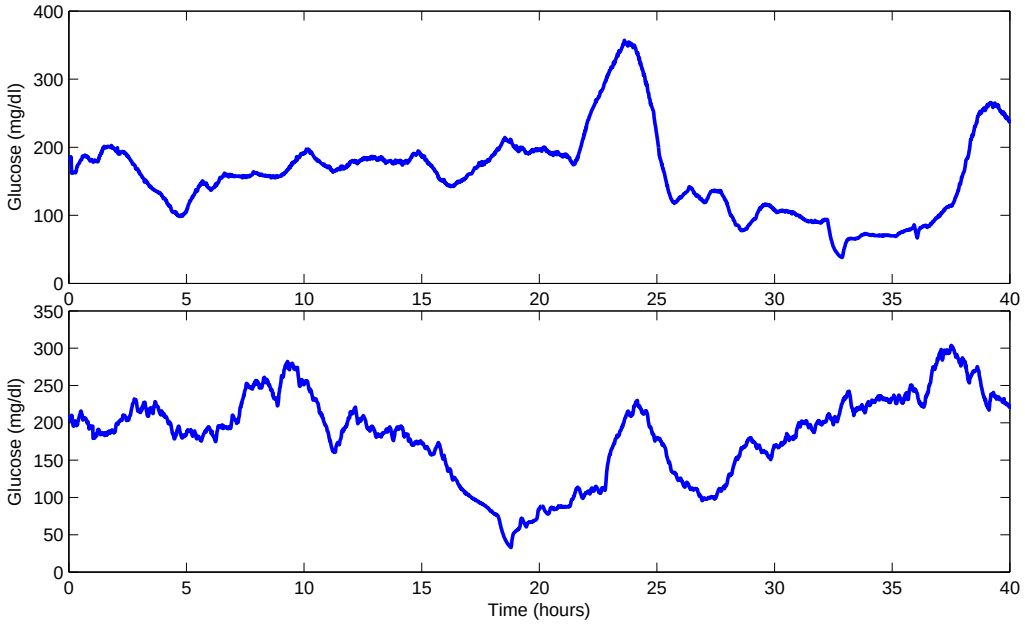

Figure 2.2: *Two FreeStyle Navigator™ noisy signals. Top: high SNR. Bottom: low SNR.*

- *the inter-individual SNR variability*, which can be observed comparing top and bottom panels of both Figure 2.1 and Figure 2.2;

- *the intra-individual SNR variability*, i.e. the SNR is also time-variant inside a single monitoring (bottom panel of Figure 2.1);

- *the SNR variability between different devices*, which is clear by visual comparison between Figure 2.1 and Figure 2.2.

The necessity to enhance the quality of CGM signals is evident. This can be faced by developing digital filters able to cope and solve all previously cited problems.

2.2 On-Line Filtering: Problem Statement

We can start considering the following equation:

$$y(t) = u(t) + v(t) \tag{2.1}$$

where $y(t)$ represents the glucose level measured by the CGM device at time t, $u(t)$ is the true, unknown, glucose level and $v(t)$ is the noise affecting it, which is supposed to be additive. The purpose of filtering is recovering $u(t)$ from $y(t)$. It is well known that, given the expected spectral characteristics of noise, e.g. noise is white, (causal) low-pass filtering represents the most natural candidate to separate signal from noise in on-line applications [3]. However, one major problem in low-pass filtering is that, since signal and noise spectra normally overlap, it is not possible to remove noise $v(t)$ from the measured signal $y(t)$ without distorting the true signal $u(t)$.

The distortion introduced by a filter can be principally divided in two components:

- the *delay* introduced, which affects the estimate $\hat{u}(t)$ obtained after filtering with respect to the true $u(t)$. The more aggressive the filtering, the larger the delay;

- the *regularity* of $\hat{u}(t)$, i.e. how well the noise component has been reduced.

It is easily understood that having a consistently delayed, even if less noisy, version of CGM data could be useless in practice, e.g. for the generation of hypo-alerts. A clinically significant task is thus the establishment of a compromise between regularity of $\hat{u}(t)$ and its delay with respect of the true $u(t)$.

2.3 Filters Embedded in Current Commercial CGM devices

The first step in approaching the SNR enhancement problem is to understand whether or not CGM devices embed on-line filtering algorithms and which types are used. In the literature there are no studies facing this kind of problem, but some information can be extracted from inherent works and CGM devices patents. For example, a prototype of a CGM device, now owned by iSense Corporation [51], has been used in a research study on rats [10], evidencing that, in order to reduce the noise component, a median filter over 11 samples needed to be introduced. The CGMS® Gold embeds a kind of Moving-Average (MA) filter, that works as follow: every minute the sensor returns the arithmetic mean value of the 10-second measurements performed in the previous 1-minute interval (the maximum and the minimum values of this interval have been excluded), then the procedure has been re-applied, i.e. every 5 minutes the arithmetic mean value of the 1-minute measurements performed in the previous 5-minute interval (excluding again the maximum and the minimum values) [34, 38, 46, 48]. Unfortunately, details on filtering strategy used neither by FreeStyle Navigator™ [17] nor by Glucoday® [33] are reported in the studies found in the literature, but both devices seem to use approaches which are very similar to the one implemented in the CGMS® Gold.

From this brief analysis, most of the commercialized CGM devices embed, or seem to embed, a sort of MA filter. In order to understand in which aspects the filtering problem needs to be improved, in Section 2.4 the MA approach will be deeply investigated and some MA filters will be applied to representative profiles of the two dataset used in this thesis. Then, in Section 2.5, the majors weakness of this approach will be discussed, calling for the realization of more sophisticated filtering techniques.

2.4 The Moving-Average Approach

The Moving-Average (MA) is a linear causal filter that is commonly used not only in the CGM field. This kind of filter belong the category of Finite Impulsive Response (FIR) because its impulsive response has a limited duration. Calling back the notation used in eq. 2.1, the classical MA filter performs a weighted average of the last N measured samples, returning an estimate $\hat{u}(t)$ of the real glucose value as follow:

$$\hat{u}(t) = \sum_{k=0}^{N-1} b_k y(n-k) \tag{2.2}$$

where b_k is the weight given to the sample measure exactly k times before current one. All b_k must be defined in order to satisfy the following equation:

$$\sum_{k=0}^{N-1} b_k = 1 \tag{2.3}$$

Different MA filters can be realized choosing different combinations of weights:

- Simple Moving Average (SMA), with arithmetic weights

$$\hat{u}(t) = \frac{1}{N} \sum_{k=0}^{N-1} y(n-k) \tag{2.4}$$

- Linear Moving Average (LMA), with linearly decreasing weights

$$\hat{u}(t) = \frac{2}{N(N-1)} \sum_{k=0}^{N-1} (N-k) y(n-k) \tag{2.5}$$

- Exponential Moving Average (EMA), with exponentially decreasing weights

$$\hat{u}(t) = \frac{1}{\sum_{m=0}^{N-1} \mu^m} \sum_{k=0}^{N-1} \mu^k y(n-k) \tag{2.6}$$

  where μ represents is a real value between 0 and 1 acting as a "forgetting factor" (the higher μ, the higher the memory of past data).

2.5 Moving-Average: Limitations & Challenges

MA have been applied on the two datasets, which consist of 24 time series (2-day long) obtained using the Glucoday® and taken from a larger dataset [33], and 20 time series (4- or 5-day long) obtained with FreeStyle Navigator™ device and taken from the Abbott Accuracy Study [53], respectively. An example of implementation on two representative time series is reported in Figure 2.3.

As evidenced in Figure 2.3, MA-based filtering algorithms has the disadvantage to introduce an elevated delay. Furthermore, the more the smoothing is needed, the higher the delay introduced.

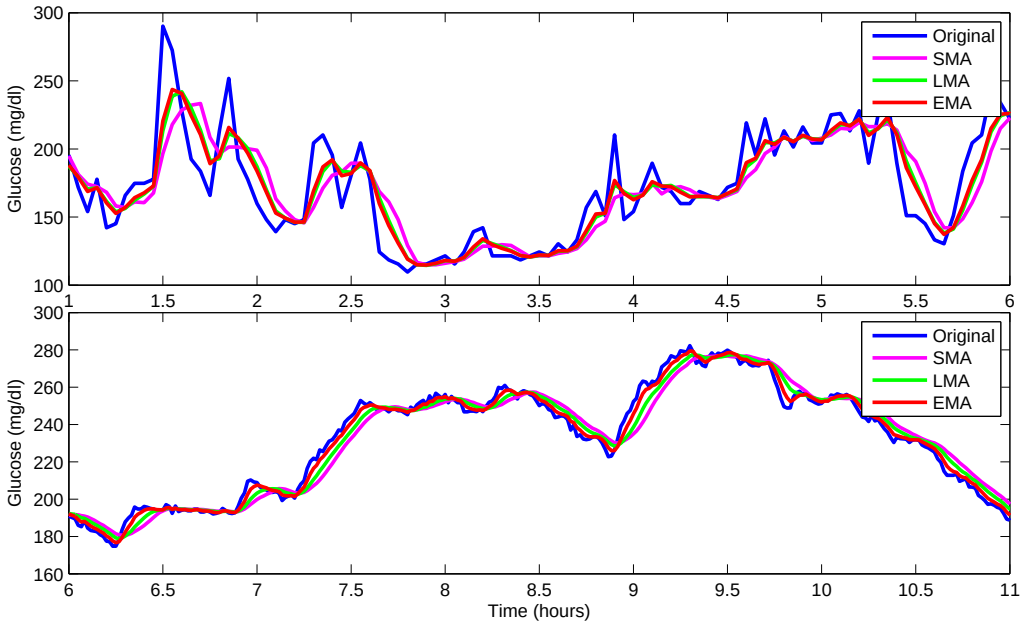

Figure 2.3: *Detail of SMA, LMA and EMA assessment on Glucoday® and FreeStyle Navigator™ representative time series (top and bottom panels, respectively).*

As will be later illustrated in Chapter 5, the delay introduced by MA is greater than 4 minutes in the Glucoday® dataset and 1 minute in the FreeStyle Navigator™ dataset. Furthermore, MA introduces the same delay on time series that have different SNR. This behavior is not correct, because on a CGM profile with high SNR the action of the filter has to be less aggressive than on one with low SNR.

The major problem related to MA filters is that they are not adaptable. Roughly speaking, once MA weights have been chosen, the filter treats any time series in the same way, irrespectively of possible differences of its SNR due to inter-individual SNR, intra-individual SNR, or sensor-to-sensor variability. As a consequence, a MA filter with fixed parameters is suboptimal in denoising CGM data.

In the next chapter, a stochastic approach able to cope with all these problems will be developed.

Chapter 3

The New Stochastic Approach for Filtering

Deterministic approaches for filtering, e.g. the Moving-Average (MA), which is the most common and diffused filter embedded in CGM devices, allow to enhance the Signal-to-Noise Ratio (SNR) of CGM profiles. However, the enhancement produced is expected to be suboptimal. In fact, MA is mostly empiric, especially because it does not use any kind of *a priori* statistical information on neither the regularity of the glycemic profile nor the intensity of the noise component which affects it. For this reason, to improve the enhancement of CGM data and in order to cope with inter-individual SNR, intra individual SNR, and sensor-to-sensor variability, in this chapter a new stochastic approach for filtering is developed.

The core key of this new approach, implemented through the Kalman Filter (KF), lies in the Maximum Likelihood (ML)-based parameter estimation procedure, which is completely automatic and allows to on-line adapt filter parameters each time a new CGM value is measured. The methodology that leads the new proposed filtering approach is illustrated in all its aspects. In the end of the chapter, some tricks to make the filtering algorithm more computationally efficient will be presented.

3.1 The Kalman Filter

3.1.1 Kalman Filter Features

Theoretically, the Kalman Filter (KF) is an estimator for what is called the *linear-quadratic problem*, which is the problem of estimating the instantaneous "state" of a linear dynamic system perturbed by white noise, by using measurements linearly related to the state but corrupted by noise. The resulting estimator is statistically optimal to any quadratic function of estimator error.

Pratically, the KF is certainly one of most commonly used tools in statistical estimation theory. Its most immediate applications have been for the control of complex dynamic systems such as continuous manufacturing processes, aircraft, ships, or spacecraft. In many dynamic systems it is not always possible to measure every variable that you want to control, and the KF provides a means for inferring the missing information from indirect (and noisy) measurements. The KF is also used for predicting the likely course of dynamic systems, such as the flow of rivers during flood, the trajectories of celestial bodies, or the prices of traded commodities [21].

From a practical stand point, it is important to remember that KF is a *computer program*. In fact, it has been called "ideally suited to digital computer implementation" [19], because it uses a *finite representation* of the estimation problem, by a *finite* number of variables. Not only, KF returns a *complete statistical characterization* of an estimation problem, because it propagates the entire *probability distribution* of the variables it is tasked to estimate. In the end, we has to remember that, in order to be solved, the problem needs to be converted into a *State-Space Model*.

3.1.2 The Discrete KF Implementation

The KF addresses the general problem of trying to recursively estimate the state $x \in \mathbb{R}^n$ of a discrete-time controlled process that is governed by the linear stochastic difference equation:

$$x(t) = Ax(t-1) + Gw(t-1) \tag{3.1}$$

where A is the $n \times n$ matrix which relates the state at the previous step $t-1$ to the state at the current step t, G is the $n \times k$ matrix which relates $w(t)$ to the state at the current step t, and the $w(t)$ is vector of dimension k representing the process noise. The measurement $y \in \mathbb{R}^m$ is given by:

$$y(t) = Hx(t) + v(t) \tag{3.2}$$

where the $m \times n$ matrix H relates the state to the measurement, and the random vector $v(t)$ represents the measurement noise. It is important to say that $w(t)$ and $v(t)$ are assumed to be independent (of each other), white, and with gaussian probability distributions:

$$p(w) \sim N(0, Q) \tag{3.3}$$

$$p(v) \sim N(0, R) \tag{3.4}$$

In practice, the *process noise covariance* Q and *measurement noise covariance* R matrices might change with each step or measurement (and this fact could be extremely important in CGM filtering problems).

The KF estimates a process by using a form of feedback control: the filter estimates the process state at some time and then obtains feedback in the form of noisy measurements. As such, the equations for the KF fall into two groups: *time update* equations and *measurement update* equations. Calling with $\hat{x}(t|t-1) = E[x(t|t-1)]$ the *a priori* state estimate at time t given knowledge of the process prior to step t, and $\hat{x}(t|t) = E[x(t|t)]$ the *a posteriori* state estimate at step t given the measurement $y(t)$, one can define the *a priori* and *a posteriori* estimate error covariance matrices as:

$$P_{t|t-1} = E[(x(t) - \hat{x}(t|t-1))(x(t) - \hat{x}(t|t-1))^T] \tag{3.5}$$

$$P_{t|t} = E[(x(t) - \hat{x}(t|t))(x(t) - \hat{x}(t|t))^T] \tag{3.6}$$

respectively. The time update equations:

$$\begin{aligned} \hat{x}(t|t-1) &= A\hat{x}(t-1|t-1) \\ P_{t|t-1} &= AP_{t-1|t-1}A^T + Q \end{aligned} \tag{3.7}$$

are responsible for projecting forward (in time) the current state and error covariance estimates to obtain *a priori* estimates for the next time step, while the measurement equations:

$$\begin{aligned} K_t &= P_{t|t-1}H^T(HP_{t|t-1}H^T + R)^{-1} \\ \hat{x}(t|t) &= \hat{x}(t|t-1) + K_t(y(t) - H\hat{x}(t|t-1)) \\ P_{t|t} &= (I - K_tH)P(t-1|t-1) \end{aligned} \tag{3.8}$$

are responsible for the feedback, i.e. for incorporating a new measurement into the *a priori* estimate to obtain an improved *a posteriori* estimate. The $n \times m$ matrix K_t is called the *Kalman Gain*. It can be demonstrated that this minimizes the *a posteriori* error covariance given by equation 3.6.

More generally, if the *a priori* estimates are not necessary for the purpose of the study and only the *a posteriori* estimates are needed, the two steps can be compressed into:

$$
\begin{aligned}
K_t &= (AP_{t-1|t-1}A^T + Q)H^T(H(AP_{t-1|t-1}A^T + Q)H^T + R)^{-1} \\
\hat{x}(t|t) &= A\hat{x}(t-1|t-1) + K_t(y(t) - HA\hat{x}(t-1|t-1)) \\
P_{t|t} &= (I - K_tH)(AP_{t-1|t-1}A^T + Q)
\end{aligned}
\tag{3.9}
$$

In order to use the KF to denoise CGM data, two points need to be solved:

- the *a priori* model which best describes the real glycemic profile $u(t)$ is needed, in order to transform it into state-space model;

- a complete description of the process noise covariance Q and measurement noise covariance R matrices is required.

3.2 *A Priori* Model for $u(t)$

The first problem is to specify an *a priori* model describing the real, but unknown, glycemic profile $u(t)$. In this section some candidate models for describing the unknown signal $u(t)$ will be presented. Then, the Cross Validation (CV)-based methodology will be used to choose the optimal model.

3.2.1 The Models

Considering physiological information and observing high-frequently sampled plasma glucose concentration time series, the real glycemic profile can be considered as a smooth signal.

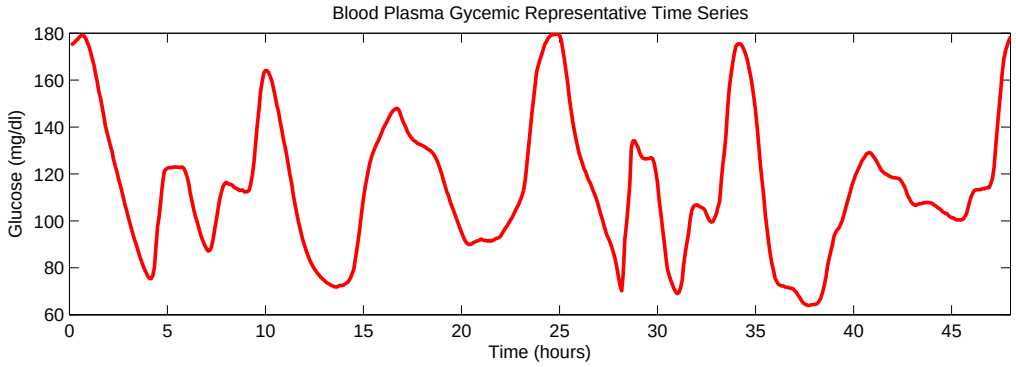

Figure 3.1: *Representative glycemic profile obtained with blood plasma measurements sampled every 5 minutes for about 2 days [60].*

Figure 3.1 reports a representative glycemic profile obtained with blood plasma measurements sampled every 5 minutes for about 2 days [60]. A simple but versatile way to model such a signal is to describe it as the realization of the multiple integration of a white noise process [11]. The choice of the number of integrators play a key role in the description of the signal. In order to understand this aspect, some simulated time series are reported in Figure 3.2. The top panel shows a realization of a white noise process, while middle and bottom panels its single and double discrete integrations, respectively.

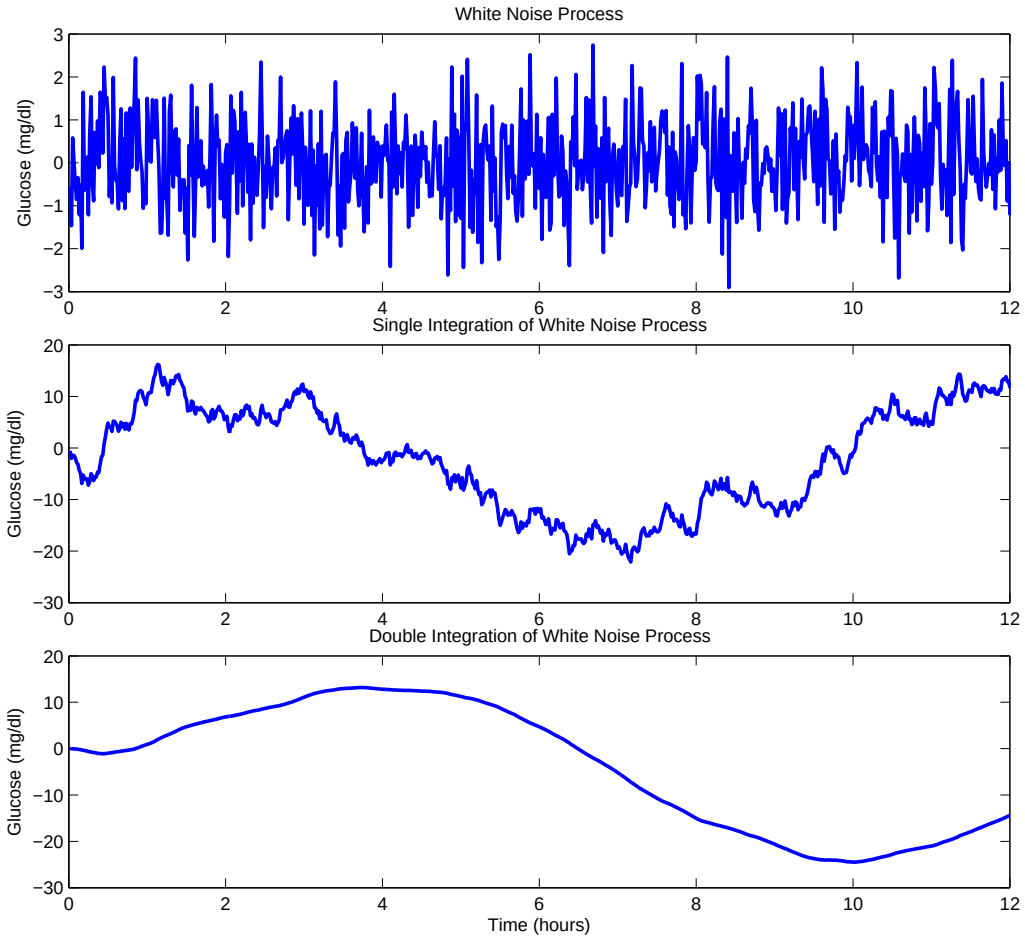

Figure 3.2: *Realizations of a white noise process and its single and double integrations (top, middle and bottom panels, respectively)*

.

Do not minding to the units reported on the y axis, which directly depends on the amplitude of the variance of the white noise process used to create the

profiles, but simply looking at the structure of the time series, the highest the number of integrators, the more regular the profile. From a mathematical point of view, starting from a zero mean gaussian noise process $w(t)$ with variance equal to λ^2, $u(t)$ processes with one, two, and three integrators can be obtained as follow (also the name that is usually given to them is reported):

- the single integration of a white noise process (the so-called random walk model)

$$\begin{array}{c} u(t) = u(t-1) + w(t), \\ t = 1, \ldots, N, \quad u(0) = 0 \end{array} \tag{3.10}$$

- the double integration of a white noise process (the so-called integrated random walk model)

$$\begin{array}{c} u(t) = 2u(t-1) - u(t-2) + w(t) \\ t = 1, \ldots, N, \quad u(-1) = u(0) = 0 \end{array} \tag{3.11}$$

- the triple integration of a white noise process (the so-called double-integrated random walk model)

$$\begin{array}{c} u(t) = 3u(t-1) - 3u(t-2) + u(t-3) + w(t), \\ t = 1, \ldots, N, \quad u(-2) = u(-1) = u(0) = 0 \end{array} \tag{3.12}$$

Equations for models with more than 3 integrators can easily obtained iterating the structure here presented.

3.2.2 The Stochastic Context and the Regularization Method

The next step is to find a method that, using a consistent criterion, allows to understand which is the best number of integrators m to be used in modelling the real glycemic profile $u(t)$. Find the optimal model means to find the model which optimally reconstructs $u(t)$ starting from noisy discrete observations $y(t)$. This is a classical smoothing problem, which does not need to be faced in on-line mode, but it can be solved in a *retrospective way* and treated therefore through classical *regularization methods*. As a consequence, the first step is to introduce the problem into a *stochastic context*. Secondly, we need to find which value of m performs the optimal smoothing of the data, by using a consistent criterion for the choice.

Therefore, supposing to work off-line and in a retrospective way, we can start the analysis calling back the notation of equation 2.1 and transforming it into a vectorial form:

$$y = u + v \tag{3.13}$$

where y, u and v are three vectors containing a certain number of measurements, real (unknown) glycemic values and measurement errors, respectively. We can assume, without loss of generality, that v and u are zero-mean random vectors with $\text{Var}[v] = \sigma^2\Sigma_v$, $\text{Var}[u] = \lambda^2\Sigma_u$, where Σ_v and Σ_u are positive define matrices, and σ^2 and λ^2 are positive scalars.

Matrices Σ_v and Σ_u express the prior knowledge of the unknown signals $v(t)$ and $u(t)$. Supposing that the measurement errors are uncorrelated and have the same variance σ^2, then the measurement noise covariance matrix can be written as $\Sigma_v = \sigma^2 I$. Furthermore, supposing not to have precise knowledge on $u(t)$, we can think it as a multiple integration of a white noise process. In this way it is easily seen that its covariance matrix becomes $\Sigma_u = \lambda^2(F^T F)^{-1}$. F is a suitable design matrix:

$$F = (F_{base})^m \tag{3.14}$$

where m represents the m-order derivative penalization of the signal $u(t)$ and F_{base} is a Toeplitz matrix:

$$F_{base} = \begin{bmatrix} 1 & 0 & 0 & \dots & 0 & 0 \\ -1 & 1 & 0 & \dots & 0 & 0 \\ 0 & -1 & 1 & \dots & 0 & 0 \\ \vdots & \vdots & \vdots & \ddots & \vdots & \vdots \\ 0 & \dots & \dots & \dots & -1 & 1 \end{bmatrix} \tag{3.15}$$

which penalizes the first order derivative of the signal. It is quite clear that elevating F_{base} to the m-power means not only to penalize the m-order derivative of the signal, but also that the a priori model on $u(t)$ is the m-th integration of a white noise process.

Using concepts of the regularization theory and using a linear mean-square estimator, given the measurement vector y, our purpose now is to find $\hat{u}$ which minimizes $E[\|u - \hat{u}\|^2]$. The regularization theory says that $\hat{u}^R$ is:

$$\hat{u}^R = \underset{\hat{u}}{\text{argmin}} \left\{ (y - \hat{u})^T (y - \hat{u}) + \gamma \hat{u}^T F^T F \hat{u} \right\} \tag{3.16}$$

where the scalar $\gamma = \sigma^2/\lambda^2 > 0$ is the so-called *regularization parameter*. The first term of the cost function on the right-hand side of equation 3.16

measures the fidelity to the data while the second term weights the roughness of the estimate. The solution of equation 3.16 is:

$$\hat{u}^R = (I + \gamma F^T F)^{-1} y \tag{3.17}$$

The so-found $\hat{u}^R$ is clearly a function of the two parameters m and γ. The CV-Based method proposed in the next section allows to find which values of m returns the optimal $\hat{u}^R$ in terms of predictive mean square error.

3.2.3 CV-Based Method for Choosing the Optimal m

The choice of m, i.e. the number of integrators of the a priori model of $u(t)$, is still an open problem because, to the best of our knowledge, it cannot be easily addressed on firm theoretically basis. As a matter of fact, in the smoothing/regularization literature the choice of m is normally left to the user or handled on empirical bases. The reason is twofold: firstly in the smoothing/regularization problems considered in the literature the signal estimate is not very sensitive to the value of m; secondly, an analytical investigation on how to choose m is difficult. As a consequence, in the smoothing/regularization literature typical choice of m are restricted to $m = 1$ or $m = 2$, depending on the particular problem (the user usually finds a posterior which is the most appropriate value) [43], and choices with more than 3 or 4 integrators are hardly used [50]

The only contributions aimed at theoretically addressing the choice of m are those based on Cross-Validation (CV) or Generalized-Cross-Validation (GCV) reviewed in [18, 49, 50]. The work [49] is the most interesting and from this work we took inspiration for the development of a CV-based method for choosing m.

The method simply resembles the *ordinary cross-validation* implemented with the leave-one-out technique. We first define the function $V_m(\gamma)$. Let $u^{(k)}_{N,m,\gamma}$ be the minimiser of:

$$N^{-1} \sum_{\substack{j=1 \\ j \neq k}}^{N} (u_j - y_j)^2 + \gamma J_m(u) \tag{3.18}$$

where $J_m(u) = u^T F^T F u$ in which the m-order derivative has been penalized. To be note that in 3.18 the k-th point has been left out. Then:

$$u^{(k)}_{N,m,\gamma} - y_k \tag{3.19}$$

is the difference between the k-th point from the remaining data when m and γ are used. If m andγ are a good choice the quantities in 3.19 should be small on average and this can be measured by:

$$V_m(\gamma) = N^{-1} \sum_{k=1}^{N} (u_{N,m,\gamma}^{(k)} - y_j)^2. \tag{3.20}$$

The general idea of the CV-based method is that one would choose m andγ to minimize 3.20.

From a practical point of view, it results very difficult to find both m and γ at the same time. Anyway, because the values that m could assume are very limited (i.e. positive natural numbers), one could suppose to fix m and then to find which value of $\hat{\gamma}$ minimizes the cost function $V_m(\gamma)$. The procedure needs to be repeated for each value of m. Once $V_m(\hat{\gamma})$ has been calculated for each considered m, the optimal m value is the one which returns the minimum $V_m(\hat{\gamma})$ among them. The results of Section 4.1 will show $m = 2$ as optimal value.

One could think that the CV-based procedure could also be used to estimate σ^2 and λ^2, solving in this way the second problem, i.e. the Q and R estimation. This is not true at all. Once m is fixed, the procedure allows to find the γ value which minimizes the cost function $V_m(\gamma)$, but from γ it is not possible to obtain neither to $\hat{\sigma}^2$ nor to $\hat{\lambda}^2$ values. In fact, the procedure works under the hypothesis that σ^2 is given. In our case, both σ^2 and λ^2 are unknown and, as a consequence, from $\gamma = \sigma^2/\lambda^2$ it is not possible to estimate their values. The restriction of knowing σ^2 value is the reason why this procedure has been applied only on simulated datasets (Section 4.1).

3.2.4 The State-Space Model for $u(t)$

Now that m has been set and the *a priori* model for $u(t)$ has been selected, the problem of filtering CGM can be transformed into a state-space model, so that the KF can be applied.

Starting from equation 3.11, two state variables are needed, one for the actual real glucose value and one for the previous value, i.e. $x_1(t) = u(t)$ and $x_2(t) = u(t-1)$, respectively. The equation 3.11 becomes:

$$x(t+1) = Ax(t) + Gw(t) \tag{3.21}$$

where $x(t) = [x_1(t) \quad x_2(t)]^T$ is the state vector at time t, and A and G are given by:

$$A = \begin{bmatrix} 2 & -1 \\ 1 & 0 \end{bmatrix}, G = \begin{bmatrix} 1 \\ 0 \end{bmatrix}. \tag{3.22}$$

The measurement equation 2.1 becomes:

$$y(t) = Hx(t) + v(t) \tag{3.23}$$

with $H = [1 \quad 0]$.

Once that the order of the a priori model on $u(t)$ has been determined, also Q and R assume a precise structure:

$$Q = \begin{bmatrix} \lambda^2 & 0 \\ 0 & 0 \end{bmatrix}, R = \sigma^2 \tag{3.24}$$

but they still remain undetermined.

In fact, till now only the first of two problems set at the end of the Section 3.1.2, i.e. finding the optimal m, as been solved. In the next section the methodology used to face and solve the second problem, i.e. to obtain a complete description of the process noise covariance Q and measurement noise covariance R matrices, which are the only two unknown variables we have still to determine, will be illustrated.

3.3 Q and R Estimation Procedure

The problem of estimating process and measurement error noise covariance matrixes Q and R when they are unknown has been faced in the field of the automatic control design, e.g. in [1, 35, 56]. However, most of these approaches requires to many hypothesis on controllability, observability and stationarity of the model to be satisfied. For this reason, in this work the Q and R estimation is performed in a retrospective way using a stochastically-based smoothing procedure based on Maximum Likelihood (ML) criterion [4, 11, 42].

Calling back equation 3.24, we remind that to estimate Q and R means to estimate λ^2 and σ^2 values, i.e. process and measurement noise variances, respectively.

Approaching the problem of smoothing the data of a predetermined interval in vector y as a linear minimum variance estimation problem, one has to find $\hat{u}^R$ which minimizes the problem of equation 3.16.

When both σ^2 and λ^2 are unknown, the minimization problem of equation 3.16 should be solved for several trial values of $\gamma = \sigma^2/\lambda^2$ until:

$$\frac{WRSS(\gamma)}{n - q(\gamma)} = \gamma \frac{WESS(\gamma)}{q(\gamma)} \tag{3.25}$$

where n is the number of measurements collected in the predetermined interval considered, $WESS(\gamma)$:

$$WESS(\gamma) = \hat{u}^T F^T F \hat{u}, \tag{3.26}$$

is the weighted estimates sum of squares, $WRSS(\gamma)$:

$$WRSS(\gamma) = (y - \hat{u})^T (y - \hat{u}), \tag{3.27}$$

is the weighted residual sum of squares, and $q(\gamma)$:

$$q(\gamma) = trace[I_n + \gamma F^T F]^{-1} \tag{3.28}$$

which is termed *degree of freedom*, with I_n an n-size identity matrix.

The so-found value of γ maximizes the likelihood of the data. As γ is determined, the estimations of σ^2 and λ^2 are given by:

$$\sigma^2 = \frac{WRSS(\gamma)}{n - q(\gamma)} \tag{3.29}$$

and

$$\lambda^2 = \sigma^2 / \gamma. \tag{3.30}$$

3.4 Implementation

Fixed the order of the *a priori* model for $u(t)$, given its state-space model and determined the procedure for estimating the unknown parameters σ^2 and λ^2, we propose here two ways in which the new stochastic filtering procedure can be implemented.

3.4.1 Burn-In Interval Approach

The first way of implementation reminds to the so-called *burn-in interval* approach. An initial window (e.g. 6 hours) of measurements is used to estimate the unknown parameters σ^2 and λ^2 by applying the procedure of Section 3.3. Then the KF with the so-tuned parameters is applied on the rest of the data.

This kind of approach results very useful and computationally cheap when the Signal-to-Noise Ratio (SNR) is supposed to be time invariant for the whole monitoring. However, this particular condition is hardly matched in

CGM data, in which intra-individual SNR variability is rather evident (Section 2.1).

3.4.2 Sliding Window Approach

A second possible way of implementation is based on the so-called *sliding window* approach. An initial window of measurements is still used to estimate the unknown parameters σ^2 and λ^2, but, then, parameter values are re-estimated after a fixed-lag interval (e.g. after 1 day, 6 hours, or, in the extreme case, every time a new measurement is performed).

This kind of approach results very useful when the SNR variability is elevated, because it allows to adapt the filter performance to changes in the noise component. On the other hand, it results computationally expensive for two principal reasons. First, supposing to re-adapt the KF parameters every time a new sample is received (e.g. every 1 minute), we need to store CGM values to use inside the parameter estimation procedure. Second, we need to run this procedure faster than the sampling period, in order to avoid possible delays in the real-time visualization of CGM readings. Because, due to the intra-individual SNR variability, the necessity to re-adapt KF parameters during the same monitoring is necessary, in Section 3.5 we are going to illustrate some tricks to speed up the steps involved in Q and R estimation procedure.

3.5 Computationally Efficient Algorithm

In this section we are going to introduce some tricks to improve the numerical efficiency of algorithms/procedures presented in this chapter.

3.5.1 Diagonalization

In smoothing/regularization algorithms developed in Section 3.3 it is necessary to solve the equation $\hat{u}^R = (I + \gamma F^T F)^{-1} y$, in which the calculation of the inverse matrix requires $O(N^3)$ operations. This step need to be repeated for several values of γ, till the optimal value $\hat{\gamma}$ is reached. The implementation of the algorithm in this way is very inefficient. It is more convenient to perform a preliminary change of coordinates that brings the problem into a diagonal form. In the new coordinates, the determination of γ only requires scalar operations, so that a great saving in computation is achieved. The so-called *diagonalization procedure* [11] can be summarized in the following steps:

- defining $H = F^{-1}$;

- performing a singular value decomposition (SVD) of H, and finding unitary matrices U and V such as $U^T U = V^T V = I$ and $U^T H V = D$, where $D = diag\{d_j\}$, $i = 1, \ldots, N$. The complexity of this step is $O(N^3)$;

- considering the change of coordinates $\xi = U^T y$, $\eta = V^T F u$ and $\varepsilon = U^T v$, equation 3.13 becomes:

$$\xi = D\eta + \varepsilon \tag{3.31}$$

  with $Var[\varepsilon] = \sigma^2 I$ and $Var[\eta] = \lambda^2 I$;

- computing the regularized estimate $\hat{\eta}(\gamma)$ as:

$$\hat{\eta}_i(\gamma) = \frac{d_i}{d_i^2 + \gamma}\xi_i, \quad i = 1, \ldots, N \tag{3.32}$$

  in $O(N)$ operations, using as indexes for the regularization:

$$q(\gamma) = \sum_{i=1}^{N} \frac{d_i^2}{d_i^2 + \gamma} \tag{3.33}$$

$$WESS(\gamma) = \sum_{i=1}^{N} \left(\frac{d_i \xi_i}{d_i^2 + \gamma} \right)^2 \tag{3.34}$$

$$WRSS(\gamma) = \sum_{i=1}^{N} \left(\frac{\gamma \xi_i}{d_i^2 + \gamma} \right)^2 \tag{3.35}$$

- when the optimal value of γ has been found, the input estimate is obtained by $\hat{u}^R = F^{-1} V \hat{\eta}$ in $O(N^2)$ operations.

The most computationally expansive step is the SVD, which requires $O(N^3)$ operations. But SVD has to be perform only once. Each time γ is recalculated, only $O(N)$ operations are required (compared to the $O(N^3)$ of the original algorithm). The efficiency of diagonalization is evident. More details on the diagonalization procedure can be found in [11, 42].

3.5.2 Explicit formula for $q(\gamma)$

In this chapter we have seen that in smoothing algorithms the trade-off between the data fit and the regularity of the estimate is controlled by the smoothing parameter γ. Many criteria for tuning γ, i.e. CV-based in Section 3.2.3 and the ML-based in Section 3.3, require γ to be adjusted iteratively, until the criterion is matched, by evaluating at each step the trace of the so-called influence matrix, yielding to the positive real number $q(\gamma)$. The computation of $q(\gamma)$ is one of the most computer-intensive part of the overall regression algorithm. By using a generic algorithm, this task requires $O(N^3)$ operations, where N is the number of the measurements involved.

A very interesting study of De Nicolao et al. [12] faces the problem of the calculation of $q(\gamma)$ in cubic smoothing spline problems and proposes a closed-form expression of the degree of freedom.

Briefly, letting N the number of data collected with sampling period T, the asymptotic smoothing ratio $s(\gamma)$ is defined as:

$$s(\gamma) \doteq \lim_{N \to +\infty} \frac{q(\gamma)}{N} \tag{3.36}$$

and an explicit formula for its calculation is provided. Then the value for the degree of freedom can be easily obtained by approximation $q(\gamma) = Ns(\gamma)$.

For more details on the formula and on the implementation we remind the reader to [12].

Chapter 4

Assessment on Simulation Studies

In this chapter we will test the new stochastic filtering procedure proposed in Chapter 3 on simulated problems.

In the first part, a simulated dataset will be created and then used for the choice of the optimal model order m, applying the Cross Validation (CV)-based procedure of Section 3.2.3. Then, the ability to cope with inter-individual, intra-individual Signal-to-Noise Ratio (SNR) and sensor-to-sensor variability of CGM data will be tested. In particular, concerning with inter- and intra-individual SNR variability, some CGM time series with both constant and time-varying SNR will be generated and both the ability to correctly estimate the parameters of the filter, using the Q and R estimation procedure presented in Section 3.3, and the performance of the filter, will be stressed. In the end, the simulated dataset will be undersampled to simulate the different frequency sampling and the ability of the new filter to cope with the sensor-to-sensor variability will be tested.

4.1 The Choice of Optimal Model Order m

Before applying the new stochastic filtering procedure proposed in Chapter 3 on real CGM data, it is necessary to understand which is the optimal value of m, i.e. the optimal number of integrators of the *a priori* model for $u(t)$, to be used. The Cross Validation (CV)-based method for choosing the optimal m, proposed in Section 3.2.3, is here applied on simulated CGM time series. Figure 4.1 displays the simulated subject #1, created selecting a noise-free profile and adding a white gaussian noise $N(0, \sigma^2)$ with $\sigma^2 = 16$ mg^2/dl^2 (details on how this profile has been simulated are reported in the Section 4.1.1). In particular, a detail of hours from 28 to 32 has been highlighted, in which both the noisy simulated (blue) and the filtered (red) time series are reported. In each panel the filtered profile has been obtained applying the *burn-in interval* approach filter implementation, with *a priori* model for $u(t)$ whose order m is equal to the value reported on the title of the panel itself (i.e. $m = 1, 2, 3, 4$). From a graphical inspection, results show that only in the case $m = 1$ the SNR is not sufficiently improved. For all the other cases, i.e. $m = 2, 3, 4$, the filtered time series perform very similar smoothing (no apparent differences from one profile to another can be observed). This brief analysis allows to understand that graphical inspection it is not sufficient to suggest the optimal m value for CGM data filtering and demonstrates the importance of determining m by using e.g. The CV-based criterion.

4.1.1 The Simulated Dataset

A total of 18 simulated CGM time series has been created for the choice of optimal value of m as follows:

- 3 real, 2-day long, CGM profiles (not belonging to any of the datasets used in thesis) have been considered;
- each of the profiles of the previous step has been filtered with a low-pass Butterworth filter, in order to remove the noise component;
- an uniform white gaussian noise $N(0, \sigma^2)$ has been added to each noise-free profile. Here 6 different values of σ^2, i.e. $\sigma^2 = 2, 4, 8, 16, 32$, and 64 mg^2/dl^2, have been selected.

4.1.2 Implementation and Results

For each of the 18 simulated time series 8 consecutive 6-hour windows have been considered. In each window the CV-based procedure has been applied

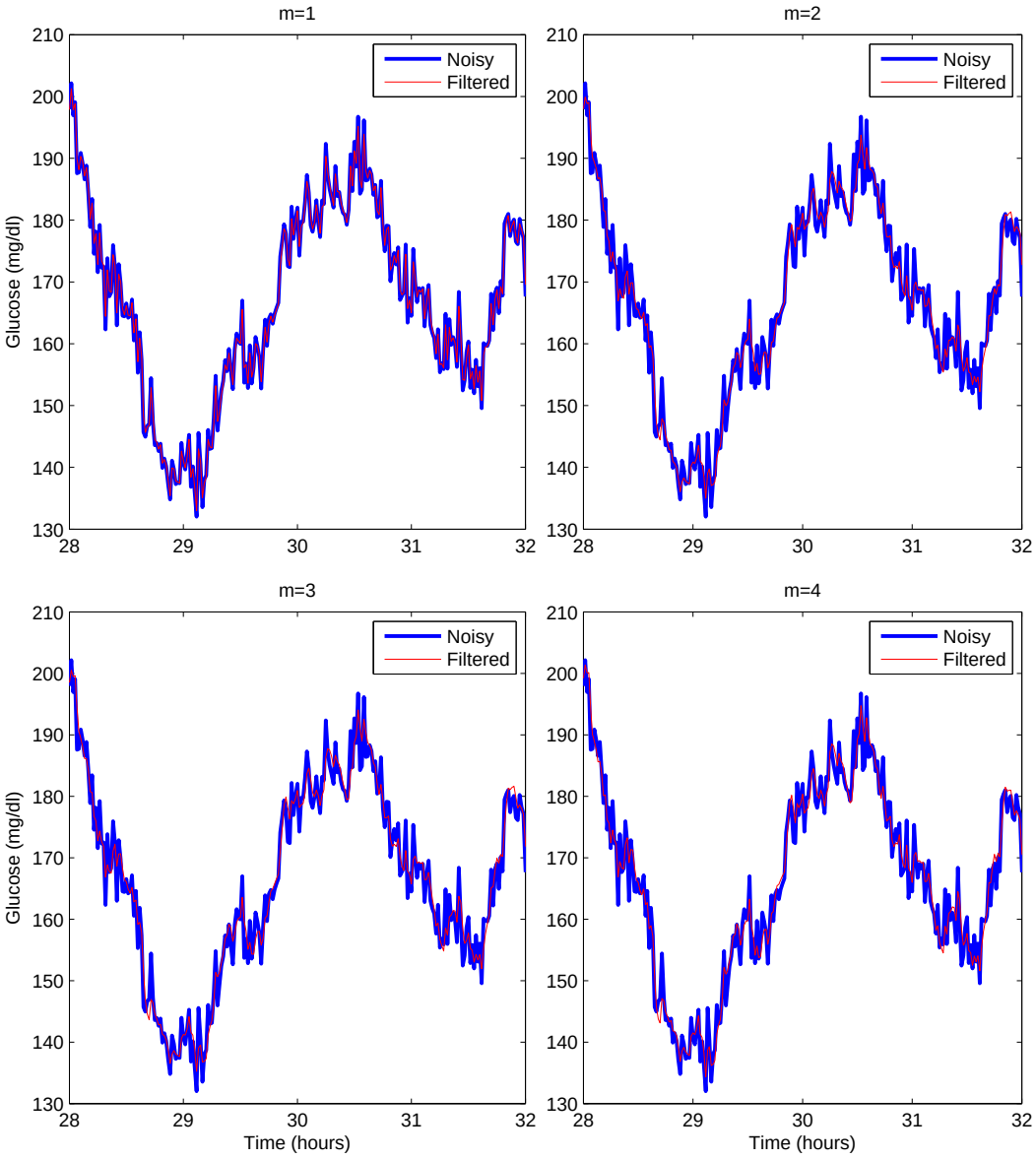

Figure 4.1: *Simulated subject #1. Detail of hours from 28 to 32. Noisy (blue) and filtered (red) time series. In each panel the filtered profile has been obtained applying* a priori *model for* $u(t)$ *of order* m *equal to the value reported on the title of the panel itself.*

and $V_m(\hat{\gamma})$ has been calculated for $m = 1, 2, 3, 4$ (as suggested in the literature [43, 50]).

Figures from 4.2 to 4.4 report the results obtained on the simulated subject #1 for $\sigma^2 = 2, 16$, and 64 mg^2/dl^2, respectively. Each figure illustrates the optimal $V_m(\hat{\gamma})$ (blue star) for each considered m value. For each window, the $V_m(\hat{\gamma})$ returning the minimum value has been highlighted (red circle). The order $m = 2$ results the best for all simulated SNR situations, except for the case of $\sigma^2 = 2$ mg^2/dl^2. Similar results have been obtained also on simulated subjects #2 and #3.

Table 4.1 reports, for each subject and for each value of the noise variance σ^2 used in these simulations, the value of the model order m which resulted the optimal among the selected 6-hour windows (when two numbers are reported, both resulted equally efficient).

Table 4.1: *Optimal model order m for each simulated subject and for each level of noise variance* σ^2.

	Optimal m		
σ^2 (mg/dl)	Subject #1	Subject #2	Subject #3
2	3,4	2	2,3
4	2,3	3	3
8	2,4	2,3	2
16	2	3	2,4
32	2	2	2
64	2	2	2

Looking both at Table 4.1 and Figures from 4.2 to 4.4, $m = 2$ results the optimal choice. This is not surprising. In fact, the integrated random walk model ($m = 2$) is a suitable compromise between the random walk model ($m = 1$), which is optimal for describing more irregular processes, and the double-integrated random walk model ($m = 3$), which, on opposite, results too much regular to correctly represent all the variability present in a glycemic profile. Furthermore, we can also observe that, when the SNR of the time series is elevated, i.e. the noise variance is very low (e.g. with $\sigma^2 = 2$ or 4 mg^2/dl^2), a model with $m = 3$ integrators can perform as well as a model with $m = 2$, because in this situation of high SNR the profile results very smooth and regularity in the *a priori* model is needed. On the other hand, when the SNR becomes lower, i.e. the noise variance increases, the time series becomes more irregular and the integrated random walk ($m = 2$) model results the optimal choice.

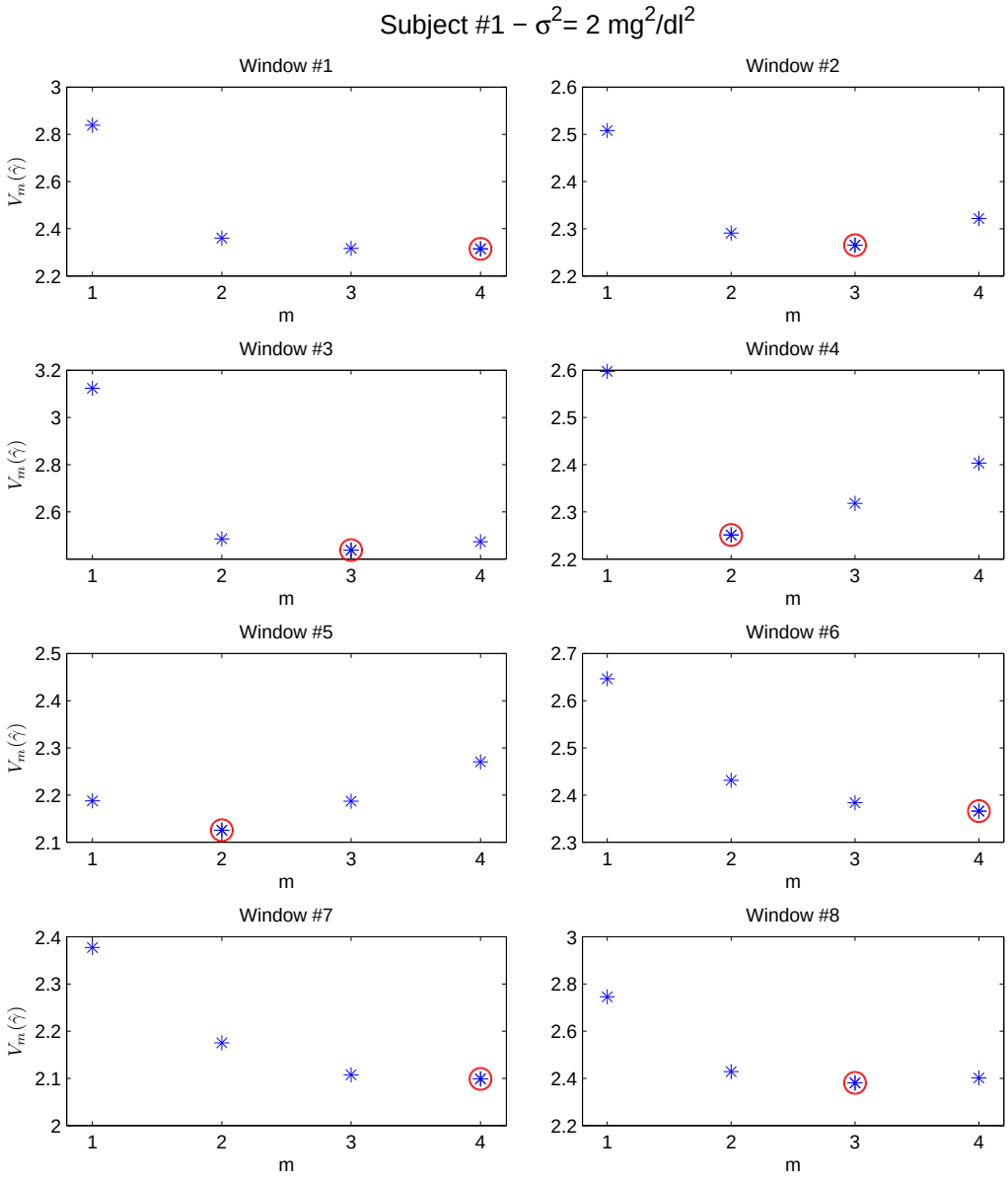

Figure 4.2: *Simulated subject #1 with noise variance* $\sigma^2 = 2\ mg^2/dl^2$. *For each 6-hour window* $V_m(\hat{\gamma})$, *for* $m = 1, 2, 3, 4$, *has been reported (blue star). The minimum value is highlighted by using a red circle.*

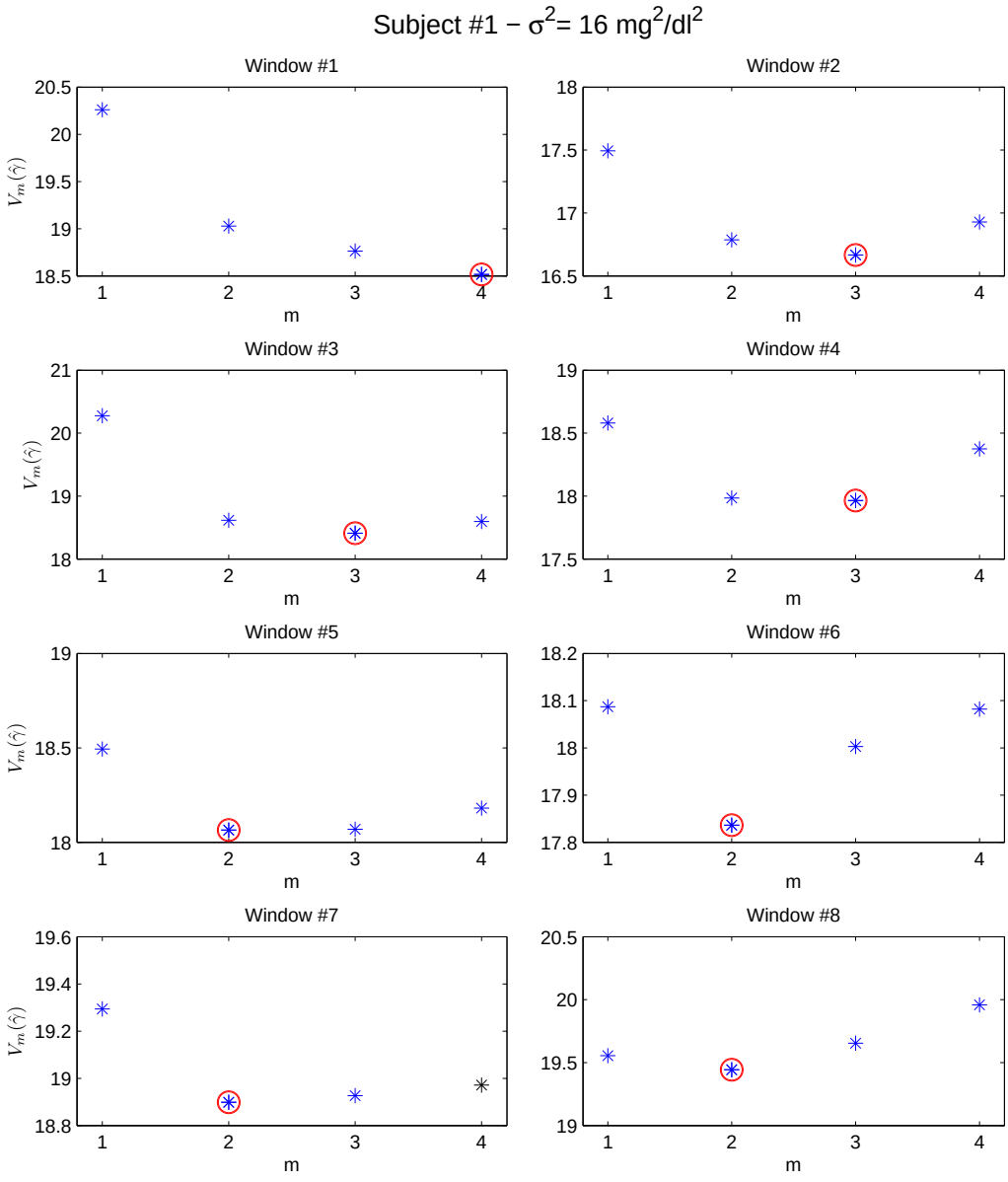

Figure 4.3: *Simulated subject #1 with noise variance* $\sigma^2 = 16\ mg^2/dl^2$. *For each 6-hour window* $V_m(\hat{\gamma})$, *for* $m = 1, 2, 3, 4$, *has been reported (blue star). The minimum value is highlighted by using a red circle.*

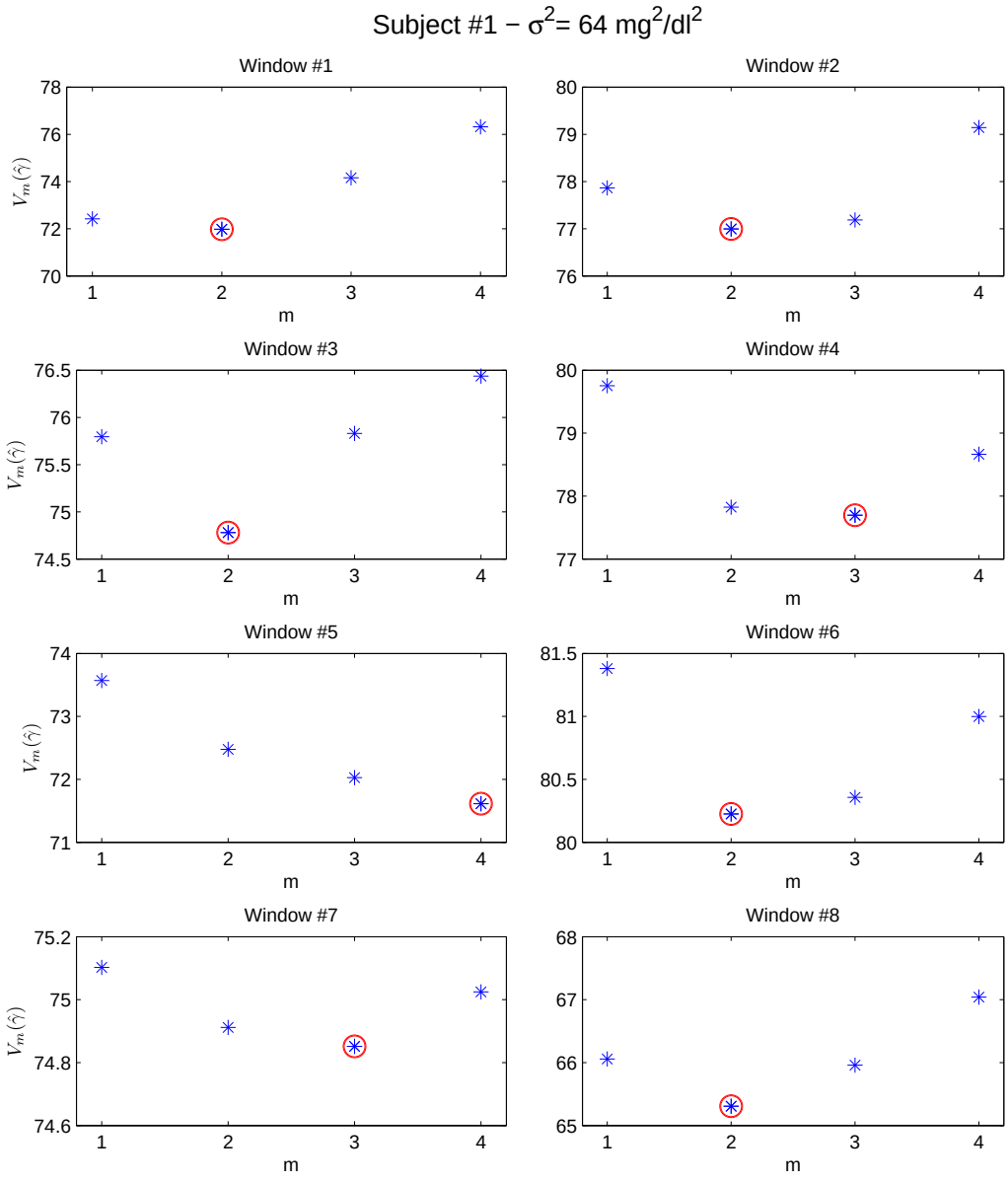

Figure 4.4: *Simulated subject #1 with noise variance* $\sigma^2 = 64\ mg^2/dl^2$. *For each 6-hour window* $V_m(\hat{\gamma})$, *for* $m = 1, 2, 3, 4$, *has been reported (blue star). The minimum value is highlighted by using a red circle.*

4.2 Coping with Inter-Individual SNR Variability

In this section we are going to test the ability of the new stochastic filtering procedure to cope with the inter-individual SNR variability.

For this test, the simulation dataset has been created as follow: 1-minute sampled noise-free CGM profile has been selected and white gaussian noise $N(0, \sigma^2)$, with $\sigma^2 = 4$, 16, and 64 mg^2/dl^2, has been added, creating three simulated CGM profiles with high, medium, and low SNR, respectively. The three time series are visualized with a blue line on the top panels of Figures 4.5, 4.6, and 4.7.

Because in this simulation the SNR remains the same for the whole profile, here the *burn-in interval* approach filter implementation has been used. This means that only the first 6-hour window of data has been used for the estimation of σ^2 and λ^2 values. Then, starting from the end of this window, the KF, with the so-tuned parameters, has been applied to the remaining data, simulating an on-line working situation.

Results are reported in Figures 4.5, 4.6, and 4.7 for the three different SNR values, respectively. The top panel of each Figure reports the comparison between the noisy simulated CGM profile and the filtered one (a detail is represented in the left box of the bottom panel). The middle panel shows a comparison between the noise-free CGM time series and the filtered one (a detail in the right box of the bottom panel). In the top and middle panels, the gray box highlights the data used for the estimation of KF parameters. In each box the estimated $\hat{\sigma}^2$ value is reported. Focusing on bottom panels, the filter sufficiently smoothes the noisy data in all the three situations (left boxes), returning a profile which is very similar to the original one (right boxes). Only in the extreme case in which the noise variance is $\sigma^2 = 64$ mg^2/dl^2, the reconstruction results, not surprisingly, less accurate.

For sake of completion, it is necessary to comment results relative to the parameter estimation procedure used in the *burn-in interval*. In fact, e.g. looking at the numbers reported in Figures 4.5, 4.6, and 4.7, the σ^2 estimates (3.7, 14.1, and 62.2 mg^2/dl^2, respectively) are very close to original values. In addition, the three estimated values of the variance of the white process leading the a priori model of $u(t)$, $\hat{\lambda}^2$ equals to 0.37, 0.50, and 0.61 mg^2/dl^2 respectively, are very similar each other. This means that the ML-based procedure works correctly and it is able to precisely identify the true signal component even if the presence of (severely large) noise.

Furthermore, it is important to focus the attention on what happens inside the *burn-in interval*. Figure 4.8 illustrates, on the left panels, a compar-

ison between the noisy CGM simulated (blue) and the non-causal glycemic estimates $\hat{u}(t)$ (red) profiles in the first 6-hour window. The right column compares the noise-free CGM simulated (blue) and the non-casual glycemic estimates $\hat{u}(t)$ (red) time series. Top, middle and bottom panels are relative to simulated time series of Figures 4.5, 4.6, and 4.7, respectively. It is important to remind that the $\hat{u}(t)$ estimates are the result of the application of the ML-based parameter estimation procedure, which works in an non-casual way.

Looking at the results, the noise component has been correctly removed (left panels) and the estimated $\hat{u}(t)$ glycemic profile results very similar to the (unknown) original $u(t)$ in all three situations. This result is very important, because an optimal reconstruction of the unknown glycemic signal $u(t)$ implies that the ML-based procedure has been able to correctly smooth the noisy signal and, consequently, to adequately identify the noise component overlapped to it. Because of this optimal reconstruction of $u(t)$, the $\hat{\sigma}^2$ estimate results precise. Numerical results confirm this fact. In all left boxes of Figure 4.8, true and estimate σ^2 value are reported. Estimated values are very similar to the true ones.

At the end of this analysis, we can affirm that the ML-based σ^2 and λ^2 estimation procedure, combined with KF, is able to cope with inter-individual SNR variability and allows to reconstruct the original profile with an reasonable precision.

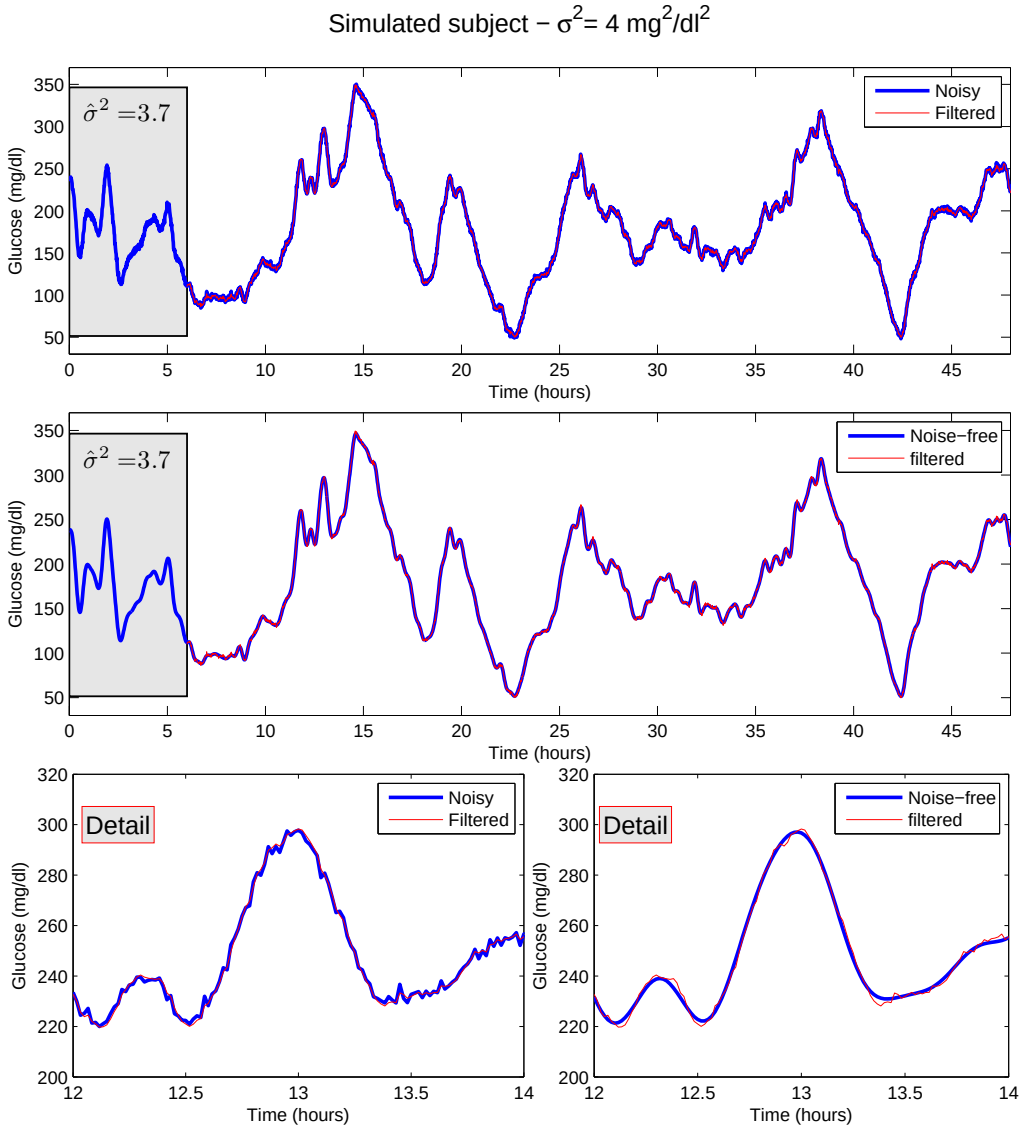

Figure 4.5: *Top: simulated CGM (blue) with* $\sigma^2 = 4\ mg^2/dl^2$ *vs KF (red) time series. The gray box is the burn-in interval, in which* $\hat{\sigma}^2 = 3.7\ mg^2/dl^2$ *has been estimated. Middle: noise-free CGM (blue) vs KF (red) time series. Bottom: details of top and middle panels (left and right boxes, respectively.*

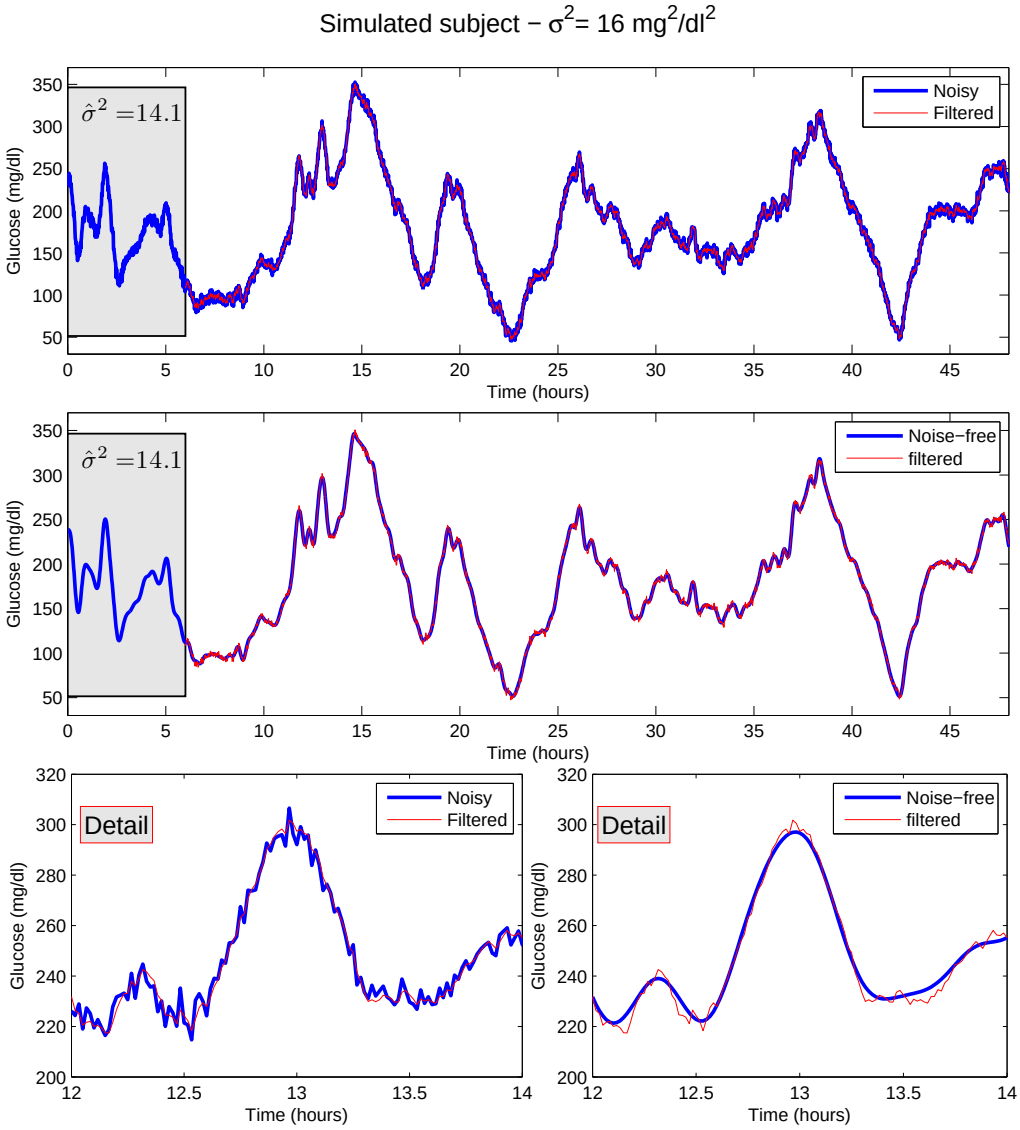

Figure 4.6: *Top: simulated CGM (blue) with* $\sigma^2 = 16\ mg^2/dl^2$ *vs KF (red) time series. The gray box is the burn-in interval, in which* $\hat{\sigma}^2 = 14.1\ mg^2/dl^2$ *has been estimated. Middle: noise-free CGM (blue) vs KF (red) time series. Bottom: details of top and middle panels (left and right boxes, respectively.*

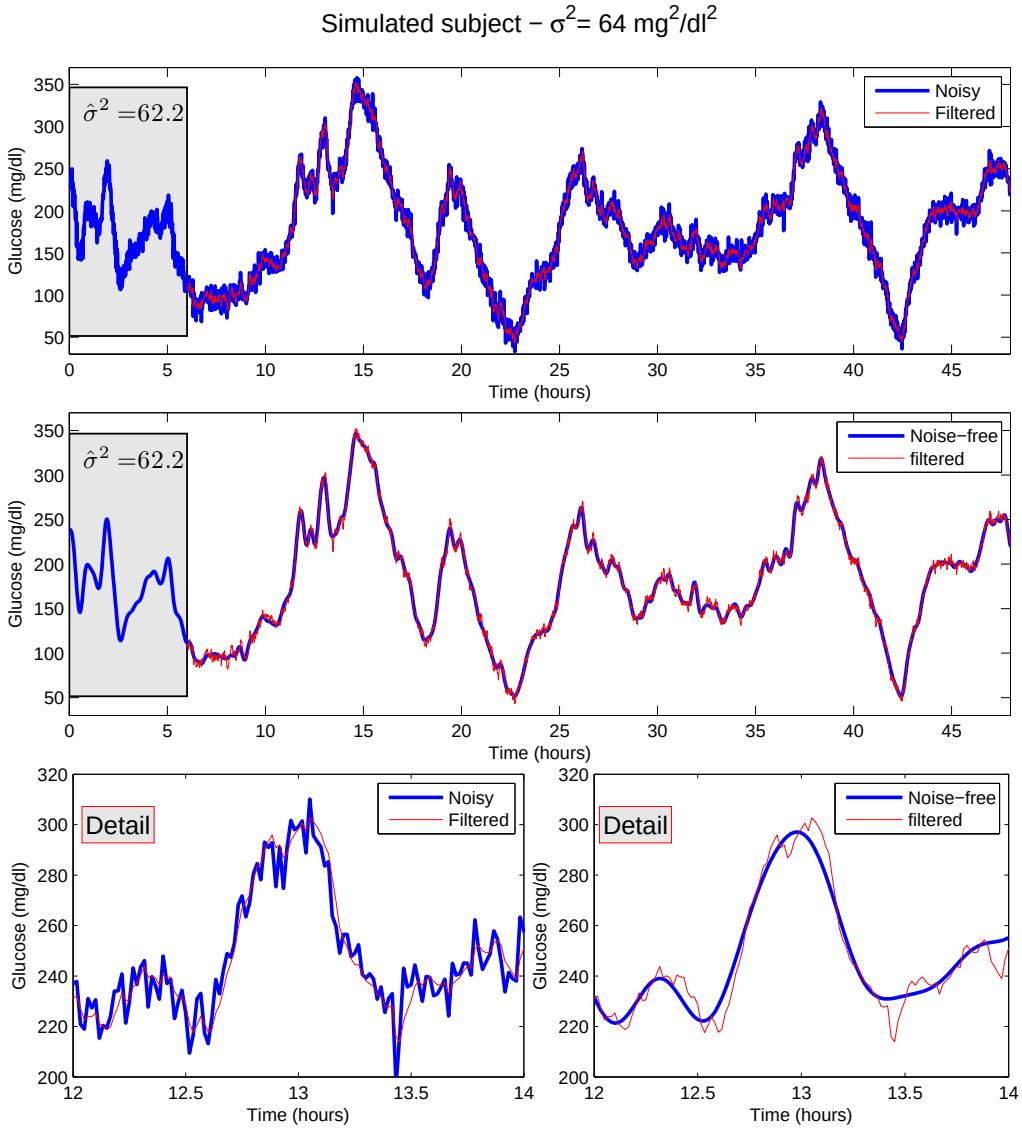

Figure 4.7: *Top: simulated CGM (blue) with* $\sigma^2 = 64$ mg^2/dl^2 *vs KF (red) time series. The gray box is the burn-in interval, in which* $\hat{\sigma}^2 = 62.2$ mg^2/dl^2 *has been estimated. Middle: noise-free CGM (blue) vs KF (red) time series. Bottom: details of top and middle panels (left and right boxes, respectively.*

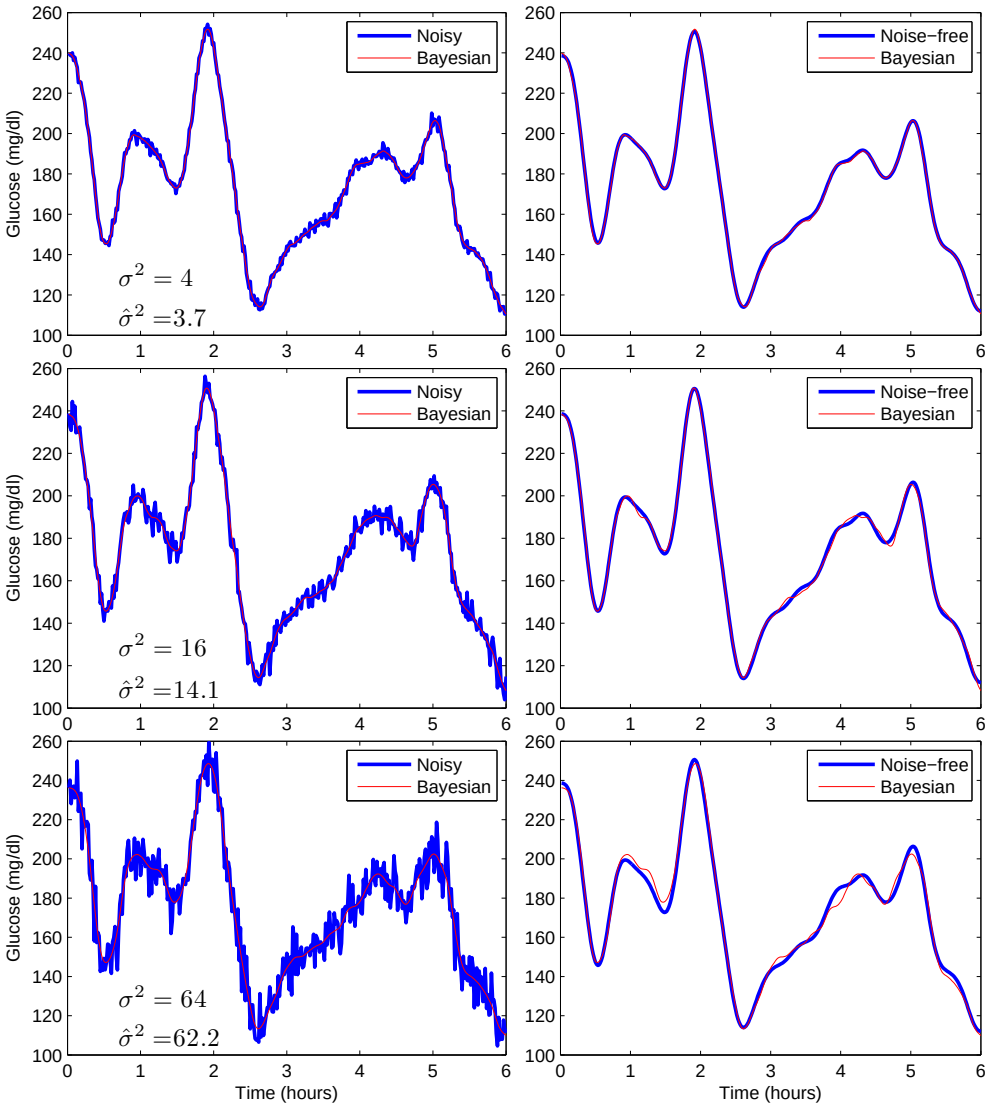

Figure 4.8: *Detail concerning the burn-in interval of the simulations of Figures 4.5-4.7. Left: noisy (blue) vs bayesian non-casual estimates $\hat{u}(t)$ (red) time series. Right: noise-free CGM (blue) vs bayesian non-causal estimates $\hat{u}(t)$ (red) profiles. Left boxes report original and estimated σ^2 values.*

4.3 Coping with Intra-Individual SNR Variability

In this section we are going to test the ability of the new stochastic filtering procedure to cope with the intra-individual SNR variability.

For this test the simulation dataset has be created as follows: three 1-minute sampled noise-free CGM profiles have been selected and a white gaussian noise $N(0, \sigma^2)$, with time-varying σ^2, has been added to them in order to create simulated CGM profiles with different characteristics. It is important to underline that the same noise realization has been used for all simulations. These three time series are visualized with a blue line on the top panels of Figures 4.9, 4.10, and 4.11, respectively. The three different time-varying σ^2 profiles (exponentially increasing from 1 to 100 mg^2/dl^2, one period of sinusoid with excursion form 1 to 64 mg^2/dl^2, and two periods of sinusoid with excursions from 1 to 16 mg^2/dl^2, respectively) used to generate the noise component are reported in the bottom panels (blue line).

Because the SNR is now time-varying, the *burn-in interval* approach filter implementation is no longer an effective working solution. Therefore, the *sliding window* approach has been used. We remind that, using this kind of approach, the KF parameter estimation procedure is applied every time a new measurement arrives.

Results of the application of the filter to the simulated dataset are reported in Figures 4.9, 4.10, and 4.11, which are all structured using the same template. The top panel shows the simulated CGM (blue) and the filtered (red) profiles, illustrating the improvement due to the action of the filter. The middle panel compares the noise-free (blue) and the filtered (red) time series, evidencing how the reconstruction of the (unknown) true signal has been performed. The bottom panel reports the time-varying σ^2 (blue line) used to generate the additive noise component and the σ^2 estimates (red line) obtained every time the parameter estimation procedure has been applied.

Results show that the noise component affecting CGM profiles has been significantly reduced in all the three situations (top panels), and noise-free CGM time series have been well matched (middle panels). It is important to observe that the *sliding window* approach allows to correctly track SNR variations in all situations. In particular, it is able to face both slow (simulation #1) and fast (simulations #2 and #3) changes of the variance of the noise component. This is quite evident looking at bottom panel of all Figures 4.9-4.11, where the σ^2 estimated profile (red line) accurately matches the true one (blue line).

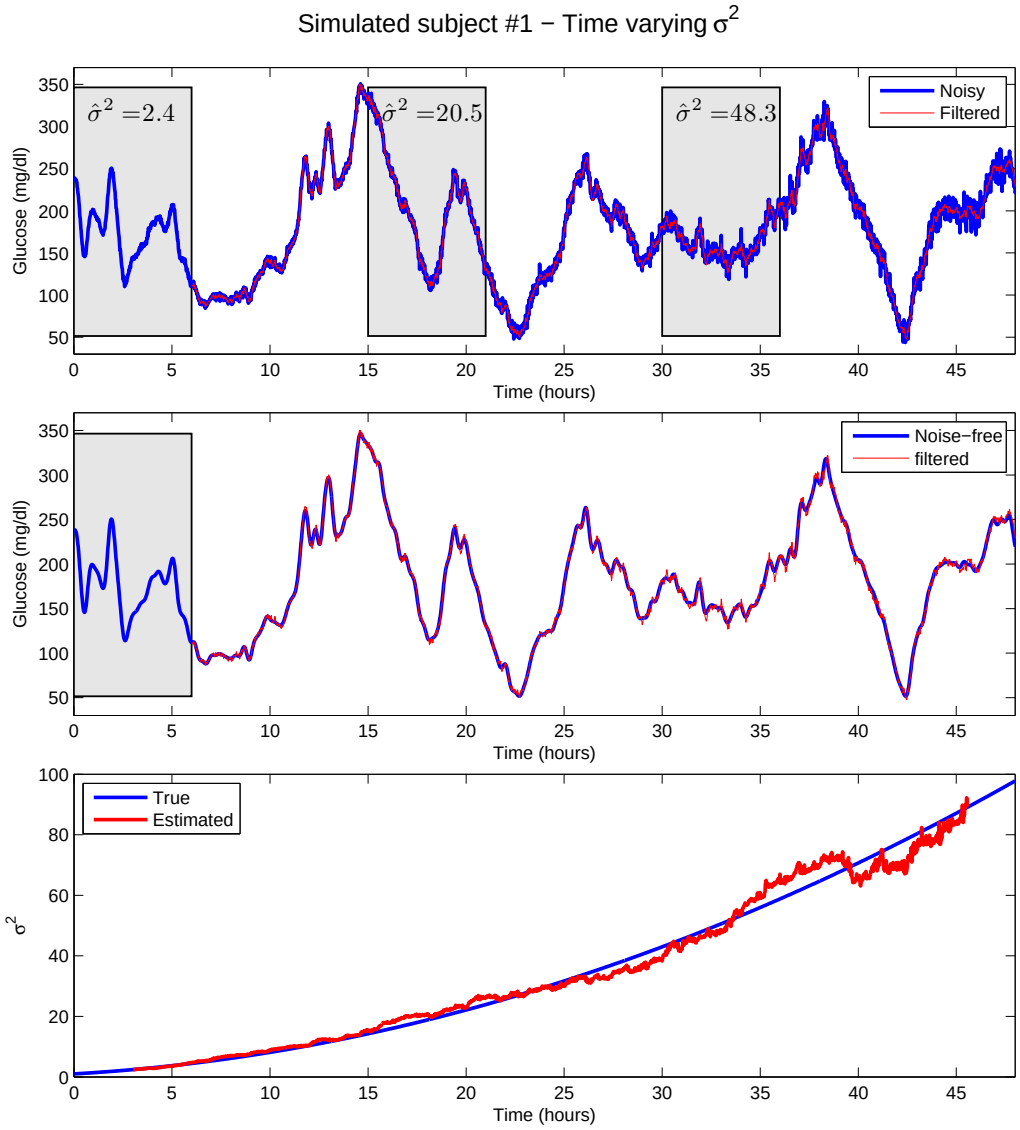

Figure 4.9: *Simulated CGM profile #1. Top: simulated CGM (blue) vs KF (red) time series. Gray boxes highlight three intervals in which σ^2 has been estimated (the estimated value is also reported). Middle: noise-free CGM (blue) vs KF (red) time series. Bottom: true (blue) vs estimated (red) measurement noise variance σ^2.*

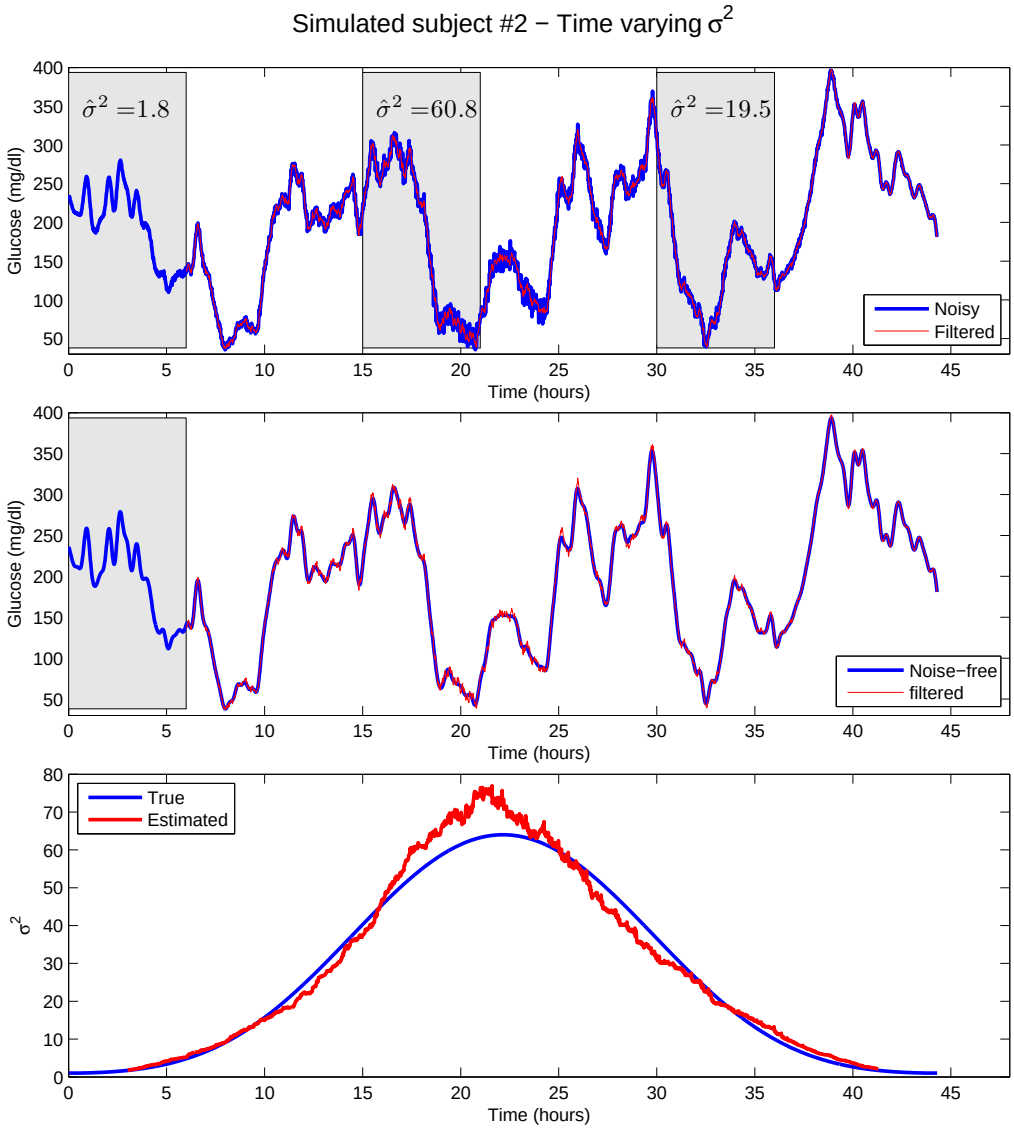

Figure 4.10: *Simulated CGM profile #2. Top: simulated CGM (blue) vs KF (red) time series. Gray boxes highlight three intervals in which σ^2 has been estimated (the estimated value is also reported). Middle: noise-free CGM (blue) vs KF (red) time series. Bottom: true (blue) vs estimated (red) measurement noise variance σ^2.*

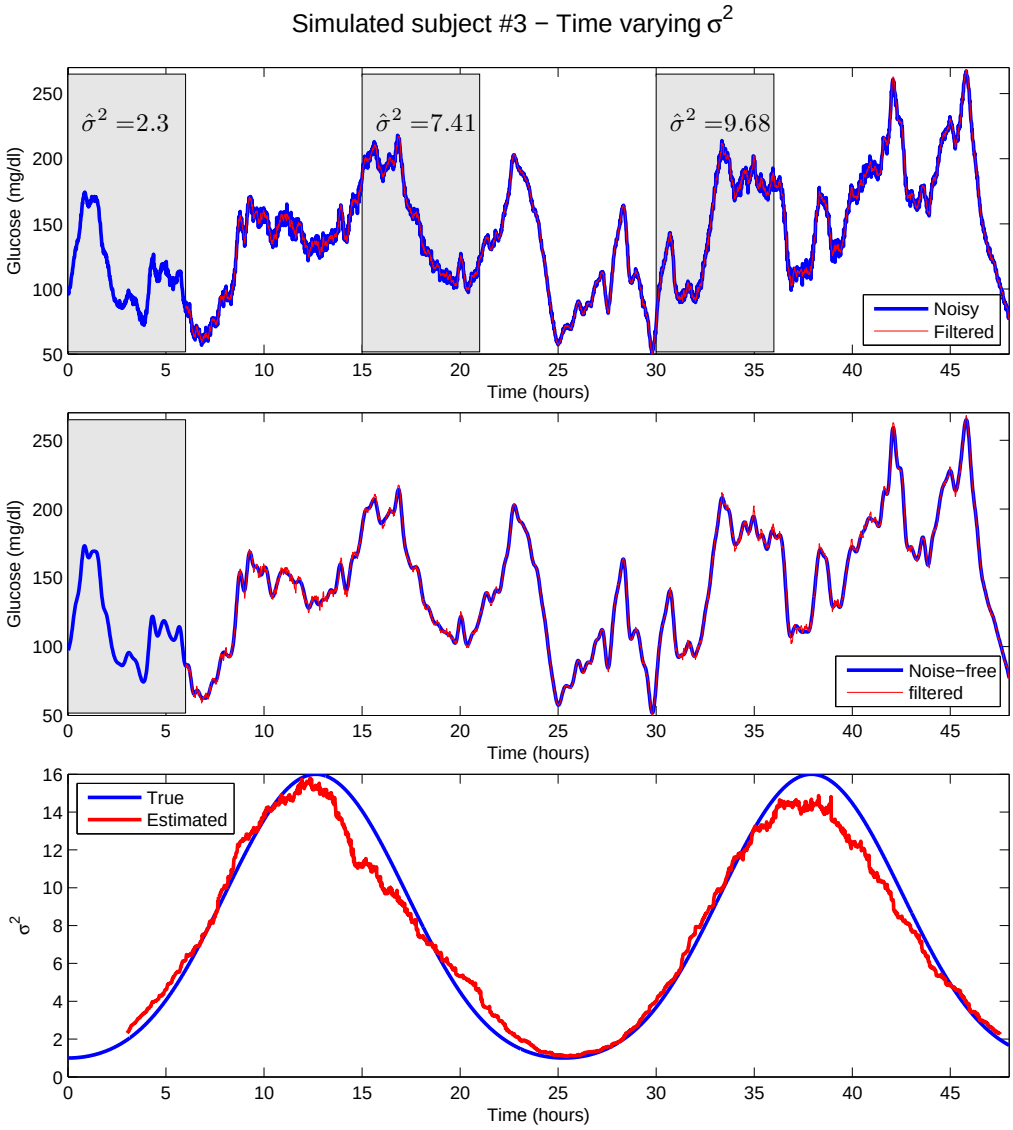

Figure 4.11: *Simulated CGM profile #3. Top: simulated CGM (blue) vs KF (red) time series. Gray boxes highlight three intervals in which σ^2 has been estimated (the estimated value is also reported). Middle: noise-free CGM (blue) vs KF (red) time series. Bottom: true (blue) vs estimated (red) measurement noise variance σ^2.*

4.4 Coping with Sensor-to-Sensor Variability

In this section we are going to show how the new stochastic filtering procedure is able to cope with sensor-to-sensor variability. The sensor-to-sensor variability does not only concern with SNR variability (see Sections 4.2 and 4.3), but it is principally related to technological aspects, whose most important is the time sampling period that characterizes CGM devices. Even if most of the CGM systems use a time sampling period of 1 minute (e.g. the Dexcom STS-7™ and the Abbott FreeStyle Navigator™), and this is the situation in which we have worked in the previous two sections, the Medtronic CGMS® System Gold™ and the Guardian® Real-Time devices still use to memorize data every 5 minutes, while the Menarini GlucoDay® every 3. Therefore, it is important to test the filter in these situations and understand if it is necessary to modify it.

In order to simulate this time sampling period variability, the dataset used in the Section 4.3, which was created with a time sampling period $T_s = 1$ *min*, has been undersampled using $T_s = 3$ and 5 *min* (i.e. operating working conditions of the Guardian® Real-Time and the GlucoDay®, respectively).

Because of the time-varying SNR of simulated data, the *sliding window* approach filter implementation has been selected. In the case with $T_s = 1$ *min* a window of 6-hour length was selected (i.e. 360 samples used for the parameter estimation). In these new situations, i.e. $T_s = 3$ and 5 *min*, the time window length is maintained the same (6 hours), in order to be able to catch all the same variations in the real glycemic profile that the procedure was able to identify in the previous situation ($T_s = 1$ *min*), but, due to the undersampling, the number of measurements is now reduced (120 and 72 points for $T_s = 3$ and 5 *min*, respectively).

Results of the application of the modified *sliding window* approach implementation to undersampled time series are reported in Figures 4.12 and 4.13, which are structured in the same way of the Figures in Section 4.3. The top panel shows the simulated CGM (blue) compared to the filtered (red) profiles, the middle compares the noise-free (blue) and the filtered (red) time series, the bottom reports the time-varying σ^2 (blue line) used to generate the additive noise component and the σ^2 estimates (red line).

In both cases, the filtering procedure produces an optimal smoothing of noisy CGM data, and this fact is confirmed observing the middle panels, in which the estimated CGM profile closely resembles the noise-free time series. In the end, looking at bottom panels, we can see that in both cases, the $\hat{\sigma}^2$ estimate accurately tracks the true one and the result is very similar to what obtained in the case of $T_s = 1$ *min* (Figure 4.11 and 4.10, respectively).

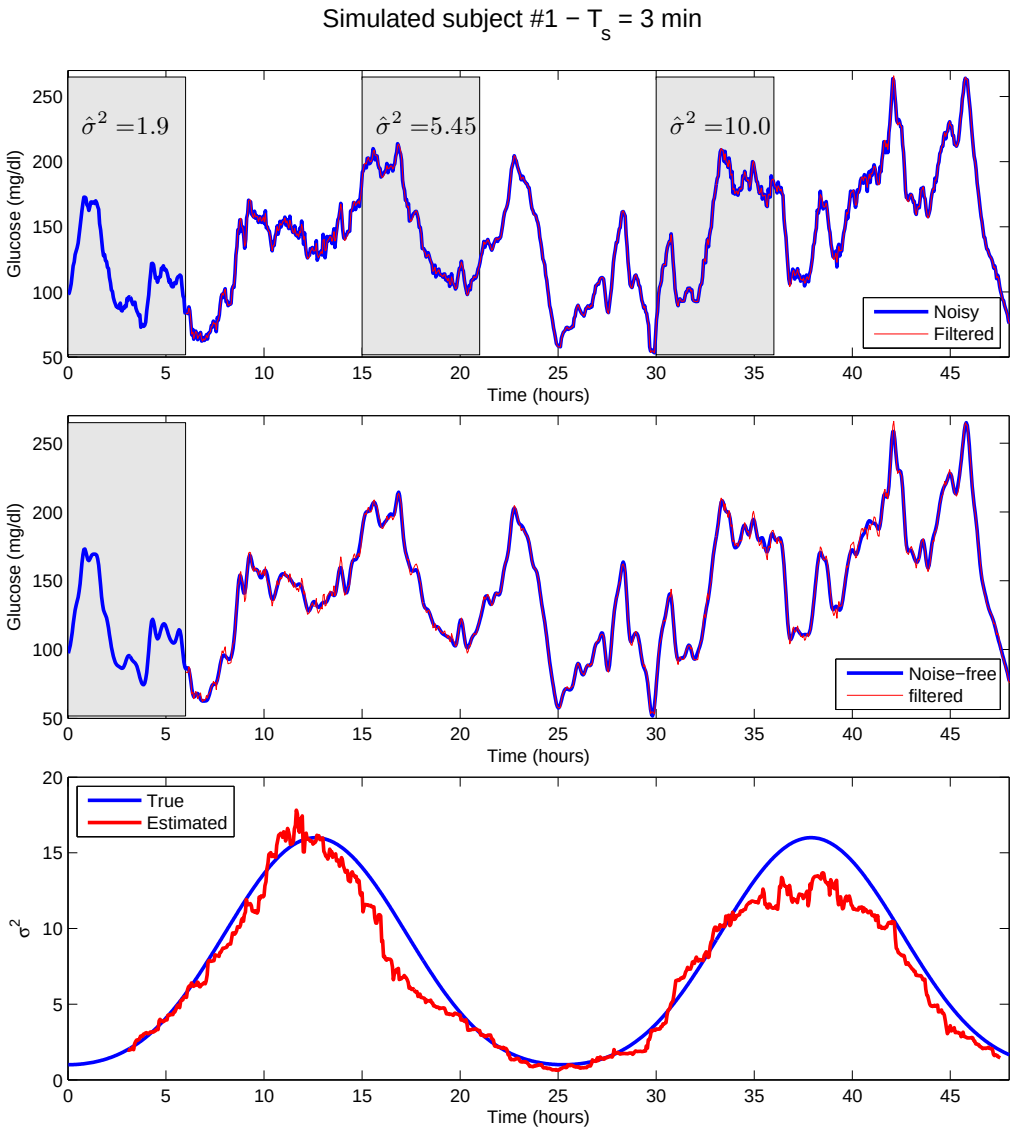

Figure 4.12: *Simulated CGM profile #3 with time sampling period* $T_s = 3$ *min. Top: simulated CGM (blue) vs KF (red) time series. Gray boxes highlight three in intervals in which* σ^2 *has been estimated (the estimated value is also reported). Middle: noise-free CGM (blue) vs KF (red) time series. Bottom: True (blue) vs estimated (red) measurement noise variance* σ^2.

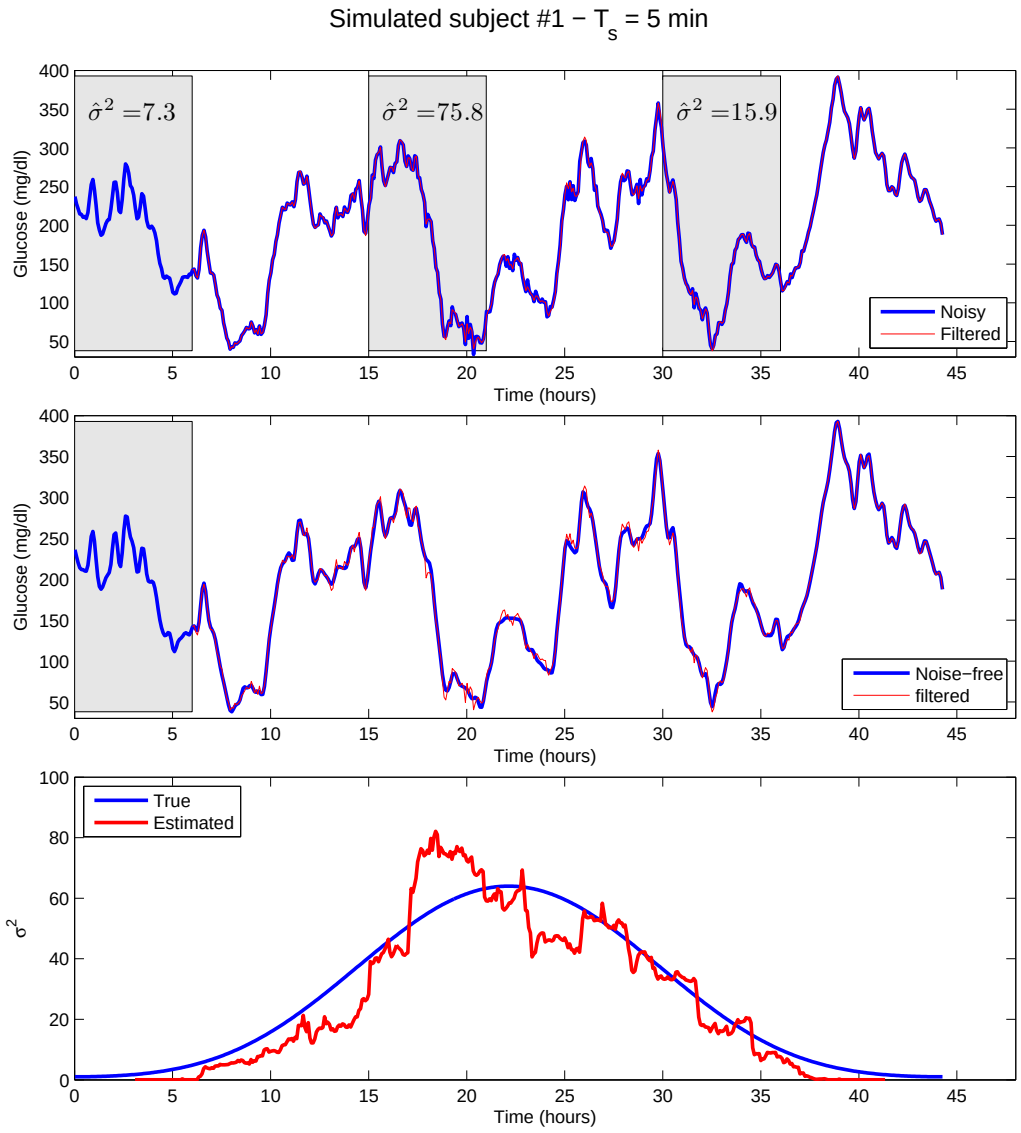

Figure 4.13: *Simulated CGM profile #2 with time sampling period $T_s = 5$ min. Top: simulated CGM (blue) vs KF (red) time series. Gray boxes highlight three in intervals in which σ^2 has been estimated (the estimated value is also reported). Middle: noise-free CGM (blue) vs KF (red) time series. Bottom: True (blue) vs estimated (red) measurement noise variance σ^2.*

4.5 Discussion

In this chapter we have used simulated datasets to show the principal advantages of the new stochastic-based filtering procedure.

A first dataset has been used to evaluate which is the optimal model to represent the real glycemic profile $u(t)$ in order to use it inside the filter. Results have shown that $u(t)$ can be correctly modeled with an integrated random walk model ($m = 2$).

Then, we have illustrated how the new filter is able to cope with both inter-individual and intra-individual SNR variability. In the first case, the new filter, implemented in *burn-in interval* modality, has been applied to simulated CGM time series with constant SNR. We have shown that the ML-based parameter estimation procedure is able to precisely identify both σ^2 and λ^2 values in the first 6-hours window, opportunely tuning the action of the filter all over the rest of the data. In the second case, the new filter, implemented in *sliding window* modality, has been applied to simulated CGM time series with time-varying SNR. Results show that, if we perform the ML-based procedure every time a new sample is received, we are able to correctly track SNR variations inside a single monitoring and, consequently, adapt the filtering smoothing.

Finally, we have proved that the new filter is able to cope with sensor-to-sensor variability, which has been simulated undersampling the time series used for the other two study cases. Results demonstrate that, maintaining the same time window length (i.e. 6-hour), the new filter is able to perform a satisfactory smoothing independently to the time sampling frequency of the CGM device.

Chapter 5

Assessment on Real Data

In this chapter we are going to apply the new stochastically-based filter on real data, i.e. a Menarini Glucoday® and a Abbott FreeStyle Navigator™ datasets consisting of 24 and 20 CGM time series, respectively. A comparison between performance of the Moving Average (MA) approach and the new filter will be presented. Criteria for the evaluation of the performance, i.e. the delay introduced by the filter and the ability of the filter to smooth the noisy signal, will be introduced for the comparison. Some representative subjects from both datasets will be selected and deeply analyzed in order to prove the ability of the new filtering procedure to optimally cope with inter- and intra-individual SNR variability.

5.1 Evaluation Criteria

As introduced in Section 2.2, one major problem in low-pass filtering is that, since signal and noise spectra normally overlap, it is not possible to remove noise $v(t)$ from the measured signal $y(t)$ without distorting the true signal $u(t)$. The distortion introduced by a filter can be principally divided in two components, i.e. the *delay* introduced by the filter and the *regularity* of the $\hat{u}(t)$ estimates. In this section we are going to define indexes to quantify these two components. These indexes will be used to compare the performance of different filters.

As far as the delay is concerned, we introduce the index T, which is defined as the temporal shift (in minutes) that has to be applied to $\hat{u}$ in order to minimize the squared norm of the difference between $\hat{u}$ and y:

$$T = \underset{T}{\operatorname{argmin}} \sum_{t} (y(t) - \hat{u}(t+T))^2 \tag{5.1}$$

The quantity denoted by T is the object to minimize. In fact, from a practical/clinical point of view, the delay introduced by the filter becomes a delay in CGM data visualization and elaboration, and therefore a delay in the possible generation of hypo and hyperglycemic alerts.

As far as signal regularity is concerned, we introduce the index named Smoothness Relative Gain (SRG), defined as:

$$SRG = \frac{ESOD(y) - ESOD(\hat{u})}{ESOD(y)} \tag{5.2}$$

where $ESOD(u)$ denotes the Energy of the Second Order Differences of a time series [44]. As it can be easily observed, SRG is an index which varies between 0 and 1, and measures the relative amount of signal regularity introduced by filtering.

5.2 The Glucoday® Dataset

5.2.1 General Overview of the Results

The first real dataset used to evaluate the performance of the new filter, hereafter simply named as NF, is the Menarini Glucoday® dataset. It consists of 24 2-day long time series taken from a larger dataset [33]. We remind that this device has a time sampling period of $T_s = 3\ min$. Figure 5.1 shows two of these time series (subjects #19 and #7, top and bottom panels, respectively).

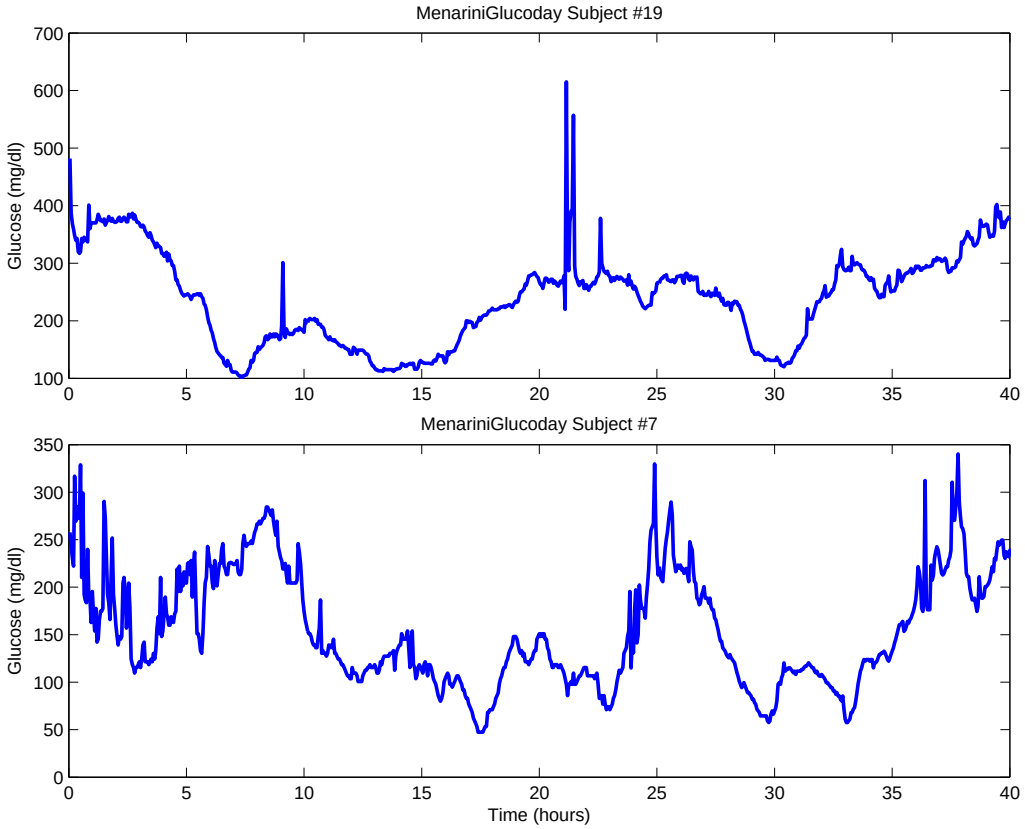

Figure 5.1: *Menarini Glucoday® time series #19 and #7 (top and bottom panels, respectively) taken from dataset used in [33].*

This dataset is characterized by presenting CGM profiles with very different SNR. It is sufficient to compare top and bottom panels of Figure 5.1 to evidence this feature. In fact, the time series in the top panel results more regular than the one on the bottom. Focusing on subject #7 (bottom panel), we can observe that the SNR varies also inside a single monitoring, e.g. we find low and high SNR in 0-6 hours and in 27-33 hours time interval, respectively. The top panel shows that some profiles of this dataset are also characterized by the presence of some large spikes (e.g. around hour 9 and 21).

From this first graphical inspection, it appears clear that an evident intra-individual SNR variability is present in almost all the profiles. Therefore, in analyzing this dataset the *sliding window* approach filter implementation has been used (Section 3.4). Once the implementation has been chosen, NF has been applied. The delay (T) and the Smoothness Relative Gain (SRG) in-

dexes, introduced in Section 5.1, have been used to evaluate the performance. A comparison with the results obtained applying the Exponential Moving Average (EMA) filter (see Section 2.4), with $N = 5$ and $\mu = 0.65$, has been also performed. Since the performance of different MA filters appears to be very similar, here only EMA has been considered. Table 5.1 reports the values of indexes T and SRG obtained in each subject for both EMA and NF. For each index, the mean value, the 10^{th} and 90^{th} percentile have been calculated.

Looking at the results relative to EMA, it appears clear that the mean value, the 10^{th} and 90^{th} percentile of both T (3.4, 3.3, and 3.5 *min*) and SRG (0.91, 0.90, and 0.92) are very close to each other. This suggests that deterministic filters, e.g. EMA, are not able to adapt their filtering action to the characteristic of the single time series, i.e. to cope with the evident inter-individual SNR variability present from one time series to another, and they threat any CGM profile in the same way, introducing very similar delays and producing the same relative smoothing.

Considering results relative to NF, instead, the mean value, the 10^{th} and 90^{th} percentile of both T (2.0, 0.43, and 3.35 *min*) and SRG (0.82, 0.66, and 0.96) are not so close each other. This is not surprising. In fact, the new stochastically-based filtering procedure has been created to face the inter-individual SNR variability and to adequately adapt the smoothing to the characteristic of the signal. Another important annotation is that the delay introduced by NF is significantly lower than EMA (2.0 vs 3.4 *min*, respectively). Subjects in which T results very close to EMA, or higher, i.e. #1, #9, #11, and #24, present, in addition, an elevated SRG, meaning that the considered CGM profile needs a more aggressive smoothing than the one performed by EMA (an example of this situation will be presented analyzing subject #9 in Section 5.2.2).

Table 5.2 reports, for each subject, the mean and the standard deviation (sd) values of $\hat{\sigma}^2$ and $\hat{\lambda}^2$ estimates, which we remind to be the parameters of the filter. These parameters allows to quantify the inter- and intra-individual SNR variability present inside a CGM dataset. In fact, concerning with the inter-individual SNR variability, we can see that the measurement noise variance $\hat{\sigma}^2$ mean value covers a very large range (from 1.4 to 32.9 mg^2/dl^2), meaning that not only some CGM profiles of this dataset are very noisy, but also that the SNR is not the same among subjects. For this reason, this variability has to be taken in consideration in filtering algorithms for improving the quality of CGM data. Another important observation regards the $\hat{\sigma}^2$ values of the estimated standard deviation, which evidence the presence of intra-individual SNR variability (the intra-individual SNR variability problem will be accurately faced in all its aspects in Section 5.2.2). In fact, $\hat{\sigma}^2$ sd values results very different from subject to subject (from 1.0 to 10.6

Table 5.1: *Menarini Glucoday® dataset: T and SRG summary results for both EMA and NF.*

	EMA		NF	
Subject	T (min)	SRG	T (min)	SRG
1	3,3	0,92	3,0	0,94
2	3,5	0,89	0,6	0,66
3	3,4	0,90	2,7	0,83
4	3,5	0,90	0,3	0,75
5	3,3	0,91	2,1	0,86
6	3,5	0,90	0,5	0,66
7	3,4	0,91	1,9	0,91
8	3,5	0,91	0,4	0,78
9	3,4	0,92	4,2	0,95
10	3,6	0,90	0,2	0,60
11	3,4	0,91	2,2	0,85
12	3,4	0,91	2,6	0,90
13	3,5	0,86	0,8	0,40
14	3,4	0,92	2,1	0,92
15	3,5	0,90	0,6	0,67
16	3,4	0,92	1,5	0,91
17	3,5	0,91	1,2	0,87
18	3,2	0,92	3,5	0,96
19	3,5	0,90	2,1	0,78
20	3,5	0,91	1,3	0,77
21	3,4	0,91	1,5	0,84
22	3,4	0,92	2,7	0,91
23	3,3	0,92	2,4	0,99
24	3,3	0,90	6,4	0,97
mean	3,4	0,91	2,0	0,82
10^{th} perc	3,3	0,90	0,43	0,66
90^{th} perc	3,5	0,92	3,35	0,96

mg^2/dl^2), highlighting the fact that the variability inside a single monitoring can not be neglected.

A last annotation on $\hat{\lambda}^2$ is needed. We remind that this parameter quantifies the variability of a glycemic profile. The larger λ^2, the higher the variability of the considered real glycemic profile. Analyzing λ^2 values of the Menarini dataset, we can observe that the regularity of the real glycemic profile $u(t)$ varies from a minimum of 1.0 to a maximum of 20.2 mg^2/dl^2.

In order to deeply show how the NF is able not only to cope with the inter-individual but also with the intra-individual SNR variability, in the next section some representative subjects (#5, #9, #13, and #14) will be extracted from the dataset and analyzed in details.

5.2.2 Representative Subjects

Figures 5.2, 5.3, 5.4, and 5.5 illustrate results of the application of both EMA and KF on the subjects #5, #9, #13, and #14 respectively. These figures are all structured in the same way. The top panel shows the original CGM (blue), the EMA (red) and NF (green) time series. The gray shaded area highlights the 6-hour burn-in window used for initialize NF parameters. Left and right boxes in the middle panel show two 6-hour details. The bottom panel reports the $\hat{\sigma}^2$ estimate obtained using the ML-based procedure, whose value is temporally updated every time a new measurement arrived.

Table 5.2: *Menarini Glucoday® dataset: $\hat{\sigma}^2$ and $\hat{\lambda}^2$ mean and standard deviation (sd) values estimated by the ML-based procedure.*

	$\hat{\sigma}^2$		$\hat{\lambda}^2$	
Subject	mean	sd	mean	sd
1	23,2	9,4	4,7	5,2
2	6,5	3,4	5,8	5,0
3	8,3	3,8	15,6	12,7
4	1,4	1,0	2,0	1,9
5	13,8	7,5	8,7	4,9
6	2,7	1,6	8,9	11,7
7	7,5	5,1	20,2	13,0
8	2,3	1,0	1,0	0,4
9	19,9	10,0	10,0	8,0
10	1,6	1,7	1,5	3,4
11	9,5	2,3	14,5	7,8
12	17,8	5,6	13,7	8,0
13	1,5	2,2	5,7	5,8
14	14,4	6,6	9,4	7,0
15	5,7	2,4	2,6	1,7
16	7,1	4,4	4,9	4,6
17	10,8	6,4	9,4	5,5
18	32,9	10,6	4,7	5,4
19	4,9	2,4	7,7	4,5
20	15,5	5,8	9,5	4,9
21	7,2	4,9	4,3	3,8
22	14,0	9,1	16,9	17,2
23	8,1	2,7	7,1	5,8
24	3,7	1,4	5,7	4,0

Subject #5

The first selected subject is #5, whose profile can be visualized in Figure 5.2. Observing the original CGM data, we can see that the noisy component overlapped to the true glycemic signal appears first to be quite elevated and second not to be the same all over the monitoring. In particular, its intensity increases in the last part (34-40 hours).

Results of $\hat{\sigma}^2$ and $\hat{\lambda}^2$ estimates relative to subject #5 (Table 5.2) show that this variability is correctly tracked by the ML-based parameter estimation procedure ($\hat{\sigma}^2 = 13.8(\pm 7.5)\ mg^2/dl^2$). In fact, not only the mean value of $\hat{\sigma}^2$ results elevated, but also its standard deviation. Looking at top panel of Figure 5.2, NF performs an optimal smoothing of the data, introducing a delay of only 2.1 *min* (which value is sensibly inferior to 3.3 *min* obtained with EMA). This optimal smoothing is rather evident also in the two boxes of the middle panel. The left box, which is relative to the time window from hour 15 to 21, shows a situation in which the SNR appears to be elevated (that corresponds to a low value of the measurement noise variance σ^2), without the need of producing an overregularized smoothing. Compared to EMA, NF performs a suitable signal enhancement introducing less delay. This reasonable way of operating of NF is due to a correct σ^2 estimation. In fact, in this time interval (i.e. 15-21 hours), the ML-based procedure correctly identify a low value of σ^2 (bottom panel of Figure 5.2) reducing the aggressiveness of the filter. On the other hand, if we focus on the right box (i.e. 34-40 hours), here the SNR appears to be significantly lower than in the previous case, calling for a more aggressive denoising. The ML-based procedure correctly identify an elevated σ^2 value (bottom panel, 34-40 hours), modifying NF parameter to perform a satisfactory smoothing also in this situation.

A last comment can be made on $\hat{\sigma}^2$ estimates reported in the bottom panel of Figure 5.2. Comparing this profile with the original CGM time series, we can see how precisely the $\hat{\sigma}^2$ estimate results in high and low values accordingly with the low and high graphically apparent SNR situations, respectively.

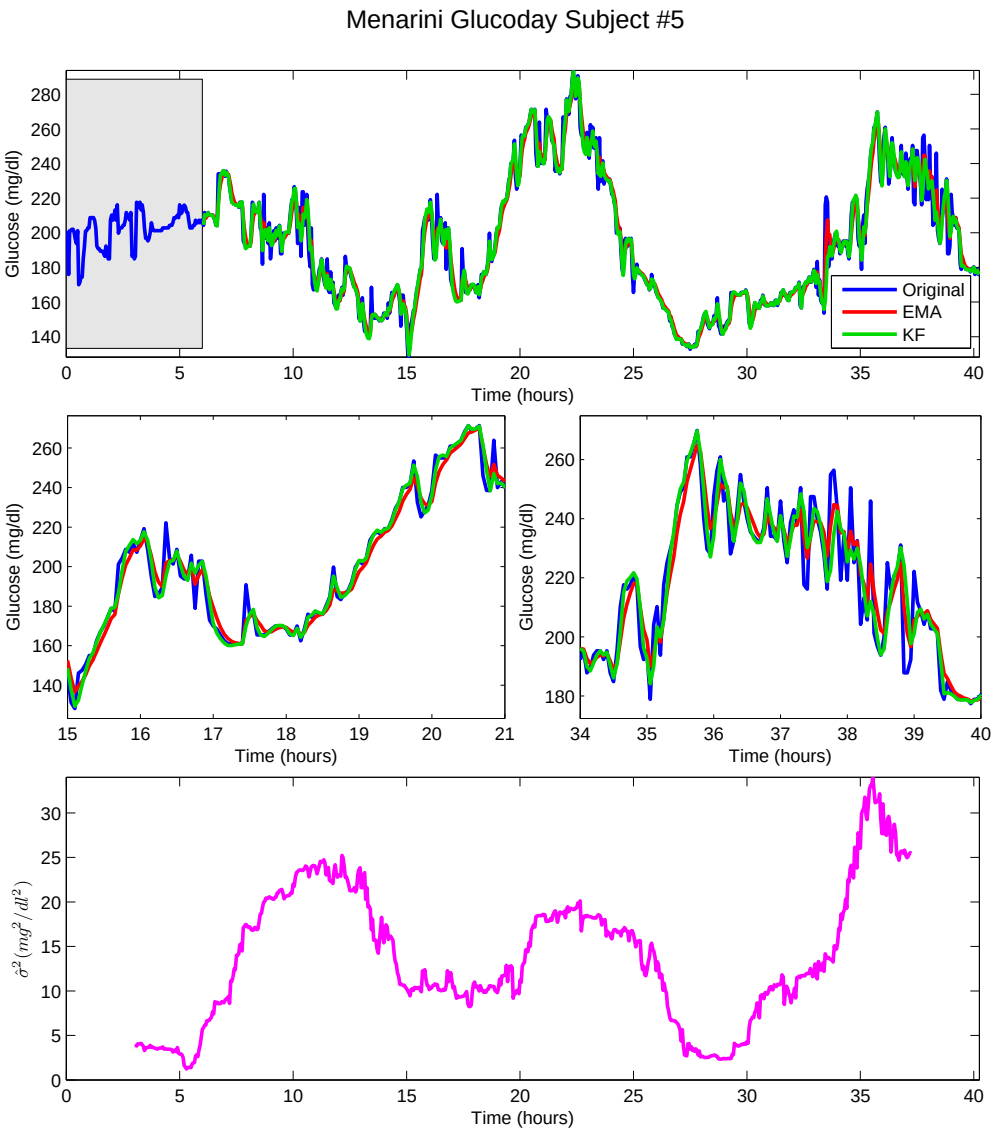

Figure 5.2: *Menarini Glucoday® subject #5. Top: original CGM (blue), the EMA (red) and NF (green) time series. The gray shaded area highlights the 6-hour burn-in window used for initialize NF parameters. Middle: two 6-hour details. Bottom: the $\hat{\sigma}^2$ estimate obtained using the ML-based procedure.*

Subject #9

This subject has been selected because is one of the only four cases in which the SRG value of NF is higher than EMA (0.95 vs 0.92, respectively), as reported in Table 5.1. Original CGM data (top panel of Figure 5.3, blue line) presents in general a low SNR, but this condition in some time intervals (e.g. between 30-36 hours) drastically rises up, highlighting an evident intra-individual SNR variability. Even if in Table 5.1 T values for NF and EMA are 4.2 and 3.4 min, this results does not mean that NF performs worse than EMA. Simply, for the major part of this CGM monitoring, EMA performs undersmoothing. The two 6-hour time window details reported in the middle panel of Figure 5.3 will allow to clarify the previous affirmation.

The left box in the middle panel reports the 15-21 hours time window, in which the SNR is very low. The filtering action of EMA is not sufficient to smooth data (undersmoothing). The ML-based parameters estimation procedure correctly identifies a low SNR situation, as $\hat{\sigma}^2$ shows in the bottom panel. The action of NF results in a more aggressive smoothing than EMA, introducing an higher delay.

The right box displays the 30-36 hours time window, in which the SNR results elevated. Original CGM data are quite smooth and the filtering action of EMA produces an overregularized profile. Also in this situation the ML-based parameters estimation procedure correctly identifies an elevated SNR situation, as $\hat{\sigma}^2$ shows in the bottom panel. The action of NF does not produce oversmoothing, minimizing the delay.

Also in this subject the satisfactory filtering action of NF has been confirmed. As reported in Table 5.2, from a general point of view, the ML-based procedure correctly identifies an elevated measurement noise variance, $\hat{\sigma}^2 = 19.9(\pm 10.0)\ mg^2/dl^2$, and also correctly tracks all SNR variations that are present in the monitoring, adapting NF parameters for a suitable smoothing in any situations.

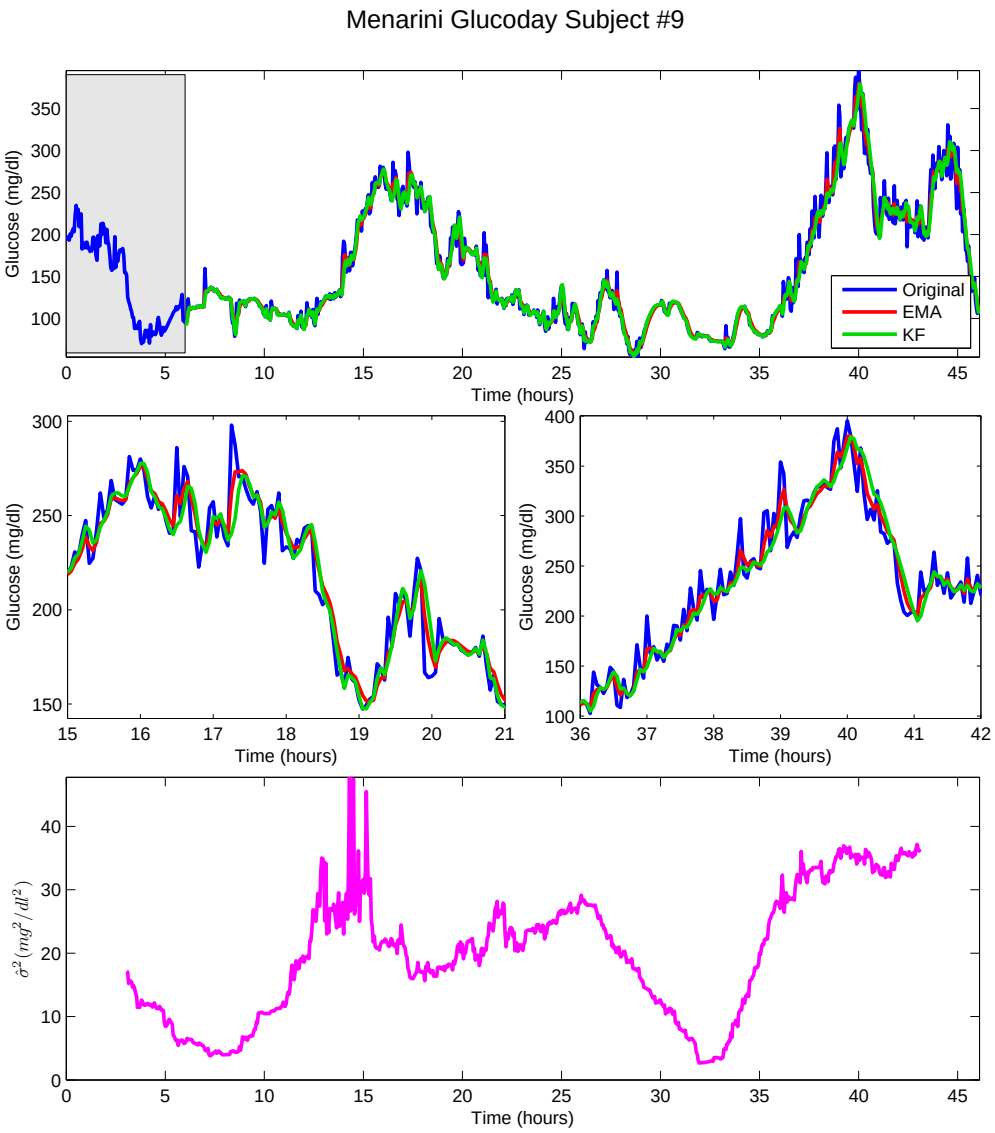

Figure 5.3: *Menarini Glucoday® subject #9. Top: original CGM (blue), the EMA (red) and NF (green) time series. The gray shaded area highlights the 6-hour burn-in window used for initialize NF parameters. Middle: two 6-hour details. Bottom: the $\hat{\sigma}^2$ estimate obtained using the ML-based procedure.*

Subject #13

Subject #13, whose profile can be visualized in Figure 5.4, has been selected as representative subject because, by graphically inspection, its CGM time series presents an elevated SNR (higher than subject #5), and also because its SNR does not seem to vary too much during the monitoring. For all these reasons, for Subject #13 we expect neither NF to perform oversmoothing (data of are quite smooth their selves) nor $\hat{\sigma}^2$ to vary too much during the monitoring.

The top panel of Figure 5.4 reports results of the application of both EMA and NF. Both graphical and numerical results (Table 5.1) show that EMA introduces a consistent delay. This consistent delay does not appear comparing original to NF data. In fact, the ML-based procedure is able to identify a high SNR condition, estimating very low values of σ^2 all over the monitoring ($\hat{\sigma}^2 = 1.5(\pm 2.2)\ mg^2/dl^2$). As expected, $\hat{\sigma}^2$ sd value is very low. The profile of the estimated σ^2 values is reported in the bottom panel of Figure 5.4. Except for the first hours, the $\hat{\sigma}^2$ value remains more or less on the same level for the rest of the monitoring.

Thanks to this ability to correctly identify SNR conditions, the original profile is not oversmoothed (SRG of 0.40 for NF vs 0.86 fro EMA) and the delay introduced by NF is sensibly less than EMA (0.8 vs 3.5 min). Details in the middle panels highlight these aspects. In both boxes it appears clear that original data presents an elevated SNR. NF performs a good smoothing everywhere is needed, with a minimum delay.

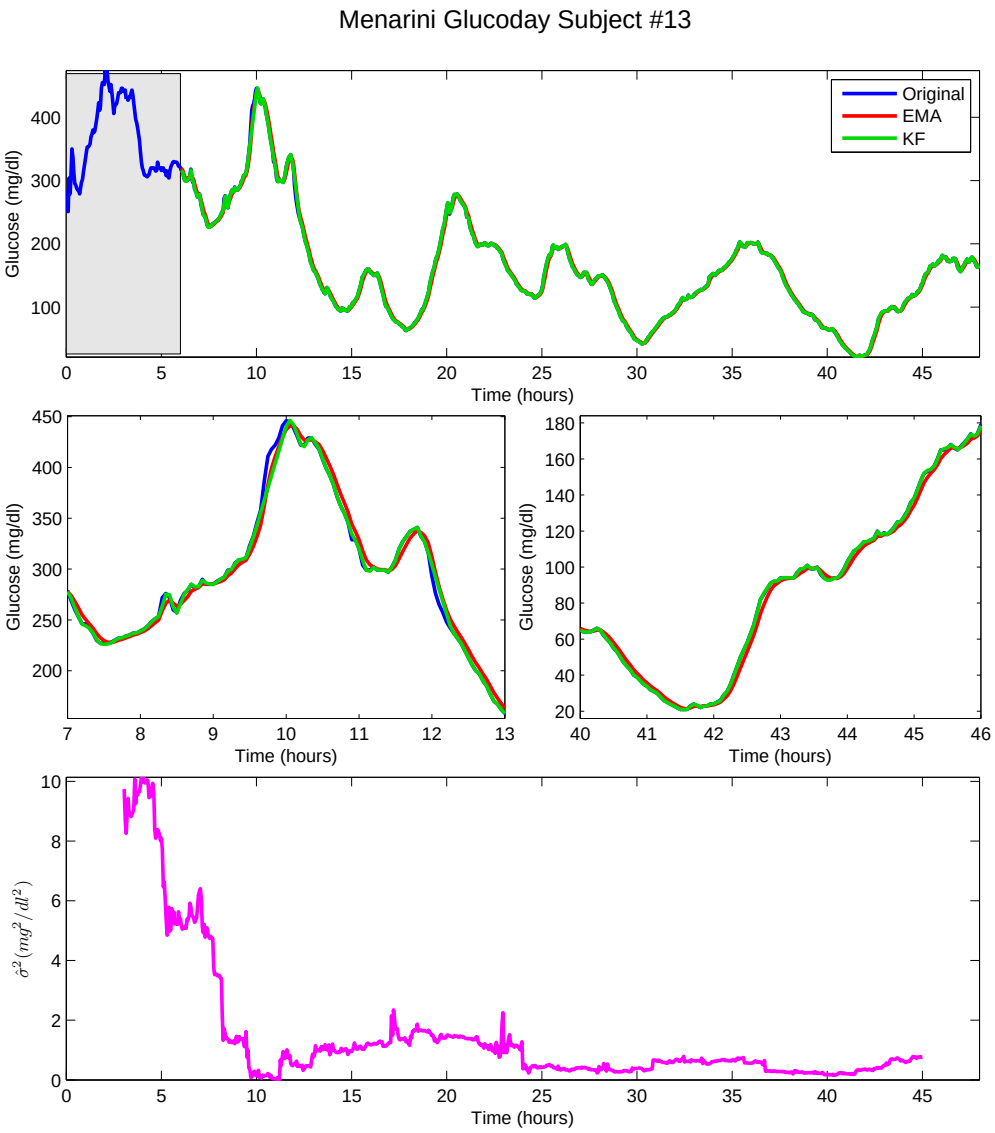

Figure 5.4: *Menarini Glucoday® subject #13. Top: original CGM (blue), the EMA (red) and NF (green) time series. The gray shaded area highlights the 6-hour burn-in window used for initialize NF parameters. Middle: two 6-hour details. Bottom: the $\hat{\sigma}^2$ estimate obtained using the ML-based procedure.*

Subject #14

Subject #14 is another example in which the intra-individual SNR variability is present, but it has been principally chosen for the presence of large spurious spikes, which are evident observing original CGM data in the top panel of Figure 5.5. The left box of the middle panel reports a detail of the time window from hours 12 to 18. It shows two spikes around hour 14 and 17, which need to be eliminated, or significantly reduced in amplitude, because their presence may cause the generation of false hypo- or hyper-alerts by CGM devices embedding some tools for alert generation. Observing the results, it appears clear that NF reduces the spike amplitude significantly more than EMA. Not only, as we have seen in the two previous examples, NF introduces less delay than EMA.

The comments reported so far are supported by numerical results. In fact, looking at the row corresponding to subject #14 in Table 5.1, we can see that NF performs the same smooth as EMA (SRG equal to 0.92), but with a T=2.1 *min*, which is significantly lower than 3.4 *min* of EMA.

Also in this case, the ML-based procedure is able to correctly identify the local SNR conditions, and this fact allows to perform an optimal smoothing all over the monitoring. From a numerical point of view, subject #14 presents a consistent SNR variability ($\hat{\sigma}^2 = 14.4(\pm 6.6)\ mg^2/dl^2$). The bottom panel of Figure 5.4 illustrates in details all the variability of the measurement noise present in this subject. The profile of the estimated values of σ^2 correctly resembles graphically apparent SNR changes in original CGM data.

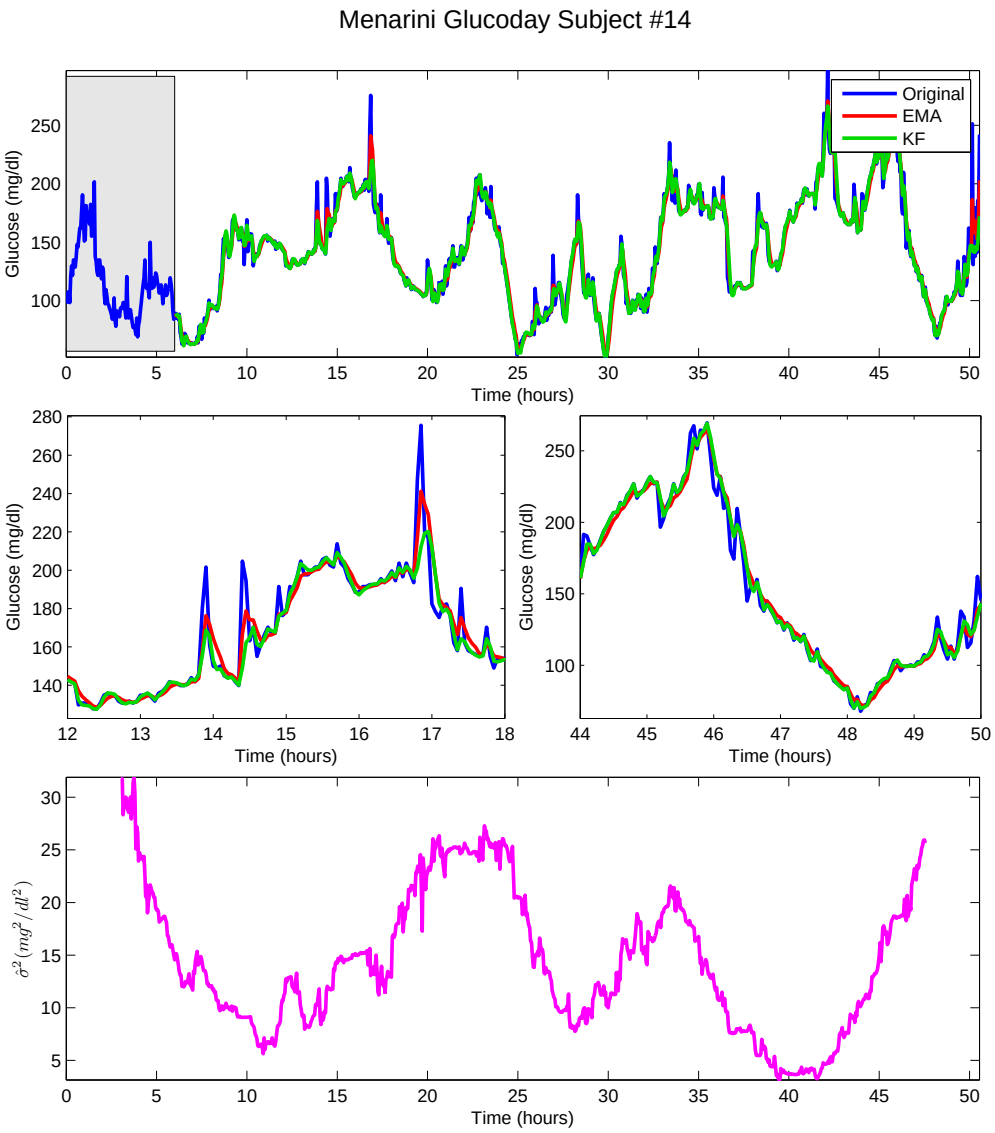

Figure 5.5: *Menarini Glucoday® subject #14. Top: original CGM (blue), the EMA (red) and NF (green) time series. The gray shaded area highlights the 6-hour burn-in window used for initialize NF parameters. Middle: two 6-hour details. Bottom: the $\hat{\sigma}^2$ estimate obtained using the ML-based procedure.*

5.3 The FreeStyle Navigator^{TM} Dataset

5.3.1 General Overview of the Results

The second dataset is the Abbott FreeStyle Navigator^{TM}. It consists of 20 time series, whose length varies from 4 to 5 days, and which are taken from a larger dataset [53]. The time sampling period of FreeStyle Navigator^{TM} is $T_s = 1\ min$. Figure 5.6 shows two representative time series (subjects #6 and #8, top and bottom panels, respectively).

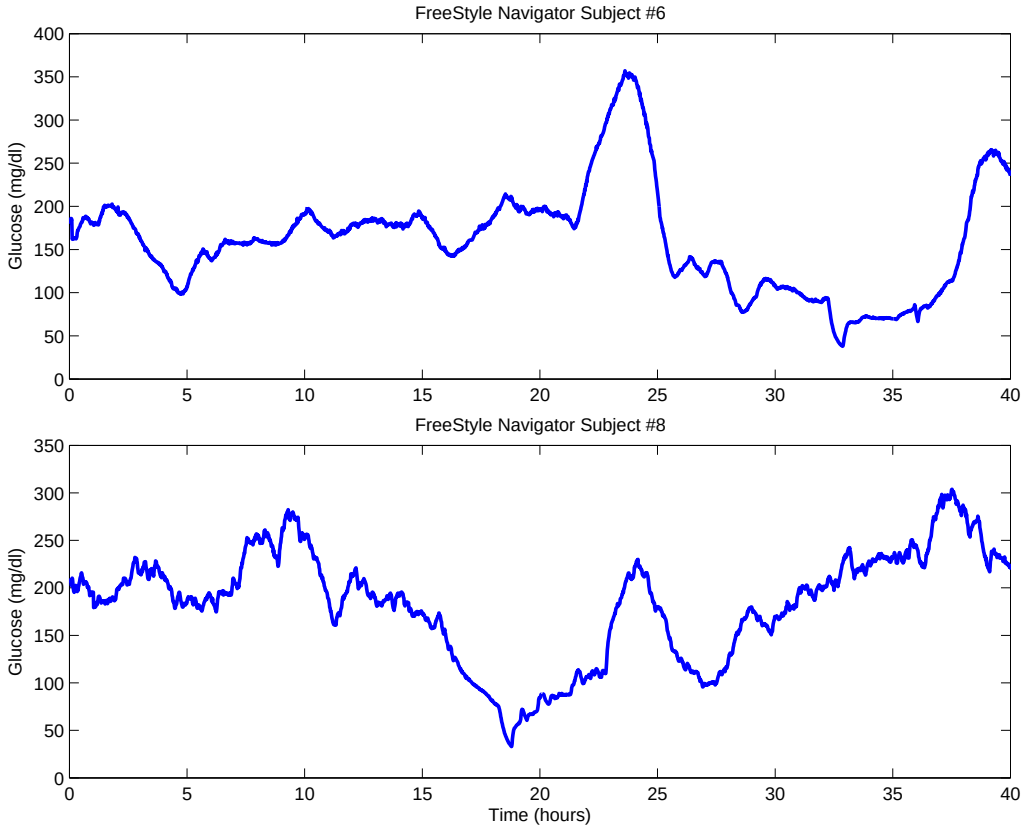

Figure 5.6: *Abbott FreeStyle Navigator^{TM} time series #6 and #8 (top and bottom panels, respectively) taken from dataset used in [53].*

As it appears comparing the two CGM time series in top and bottom panels of Figure 5.6, the inter-individual SNR variability is not so accentuated as in Menarini dataset (Section 5.2.1), even if present. In this dataset we can also observe that the SNR varies inside a single monitoring, e.g. by comparing in the bottom panel two time windows relative to 15-20 hours and 30-35 hours,

where high and low SNR (respectively) can be detected by visual inspection. No spikes have been found.

Because both inter- and intra-individual SNR variability have been detected, the *sliding window* approach filter implementation has been used (Section 3.4). Once the implementation has been chosen, NF has been applied to the dataset. The delay (T) and the Smoothness Relative Gain (SRG) indexes, introduced in Section 5.1, have been used to evaluate the performance. A comparison with the results obtained applying the Exponential Moving Average (EMA) filter (see Section 2.4), in this case used with $N = 10$ and $\mu = 0.65$, has been also performed. Table 5.3 reports the values of indexes T and SRG obtained in each subject for both EMA and NF. For each index, the mean value, the 10^{th} and 90^{th} percentile have been calculated.

As it happened for the Menarini dataset, results relative to EMA show that the mean value, the 10^{th} and 90^{th} percentile of both T (96, 92, and 100 *sec*) and SRG (0.93, 0.92, and 0.93) are very close to each other. Resembling what we already said in section 5.2.1, this suggests that deterministic filters, e.g. EMA, are not able to cope with the evident inter-individual SNR variability present from one time series to another.

Considering results relative to NF, instead, the mean value, the 10^{th} and 90^{th} percentile of both T (10, 5, and 15 *sec*) and SRG (0.74, 0.58, and 0.83) differ each other. In this case, however, T values are not so different and this is principally due to the fact that FreeStyle Navigator^{TM} time series present a lower inter-individual SNR variability than Glucoday® profiles. From a general point of view, we can observe that the delay introduced by NF is significantly lower than EMA (10 vs 96 *sec*, respectively). The second observation is relative to SRG values of NF, which result lower than EMA for each subject. Surely this means that NF does not perform oversmoothing as EMA does, but, on the other hand, it evidences that the smoothness action of EMA is excessive. This aspect will be deeply analyzed in the next section, where two representative subjects will be studied in details.

Table 5.4 reports, for each subject, the mean and the standard deviation (sd) values of $\hat{\sigma}^2$ and $\hat{\lambda}^2$ estimates. The estimated measurement noise variance $\hat{\sigma}^2$ mean value covers a very small range (from 0.7 to 3.3 mg^2/dl^2), meaning that all CGM time series are affected by very similar SNR conditions. Not only, because $\hat{\sigma}^2$ mean values are very low, the SNR of this dataset is elevated (and significantly higher than in Menarini dataset). In any case, looking at $\hat{\sigma}^2$ mean values reported in the second column of Table 5.4, the inter-individual SNR variability component is present. A second important observation regards $\hat{\sigma}^2$ sd values. Looking at the third column of Table 5.4, we can see that the $\hat{\sigma}^2$ estimated sd are significantly elevated if compared to mean values (e.g. for subject #6 we have a $\hat{\sigma}^2$ mean value of 2.1 mg^2/dl^2 and

Table 5.3: *Abbott FreeStyle Navigator^{TM} dataset: T and SRG summary results for both EMA and NF.*

	EMA		NF	
Subject	T (sec)	SRG	T (sec)	SRG
1	95	0,93	10	0,75
2	100	0,94	15	0,91
3	95	0,93	10	0,76
4	100	0,93	10	0,83
5	95	0,93	15	0,75
6	90	0,92	25	0,79
7	100	0,93	10	0,78
8	95	0,92	5	0,59
9	95	0,93	15	0,76
10	100	0,93	5	0,76
11	100	0,94	5	0,84
12	95	0,93	10	0,79
13	95	0,93	5	0,72
14	95	0,93	15	0,82
15	95	0,92	5	0,64
16	95	0,92	5	0,55
17	90	0,92	15	0,76
18	100	0,93	10	0,81
19	95	0,89	5	0,43
20	95	0,93	10	0,82
mean	96	0,93	10	0,74
10^{th} perc	92	0,92	5	0,58
90^{th} perc	100	0,93	15	0,83

a sd of 5.0 mg^2/dl^2), evidencing the presence of intra-individual SNR variability. The intra-individual SNR variability will be accurately deeply faced in Section 5.3.2. Furthermore, $\hat{\sigma}^2$ sd values result also very different from a subject to another (from 0.3 to 5.0 mg^2/dl^2), highlighting the fact that the SNR variability inside a single monitoring is not the same for all subjects.

In the end, a comment on $\hat{\lambda}^2$. Looking at the fourth column of Table 5.4 and comparing it with the same column of Table 5.2, we can note that $\hat{\lambda}^2$ mean estimated values are significantly lower than in Menarini dataset. This means that the variability of the real glycemic profile in the Abbott dataset is lower than in the Menarini. This difference could be attributed to differences in the acquisition protocol used in the two studies [33, 53]. This fact suggests that $\hat{\lambda}^2$ estimates could be a reliable parameter in quantifying the real glycemic variability of a CGM time series.

In the next paragraph representative subjects #4, and #14 will be analyzed in details.

5.3.2 Representative Subjects

Figures 5.7 and 5.8 illustrate the results of the application of both EMA and NF on subjects #4 and#14, respectively. These figures are all structured in the same way. The top panel shows the original CGM (blue), the EMA (red) and NF (green) time series. The gray shaded area highlights the 6-hour burn-in window used for initialize NF parameters. Left and right boxes in the middle panel show two 2-hour details. The bottom panel reports the $\hat{\sigma}^2$ estimate obtained using the ML-based procedure and whose value is temporally updated every time a new measurement arrived.

Table 5.4: *Abbott FreeStyle Navigator^{TM} dataset: $\hat{\sigma}^2$ and $\hat{\lambda}^2$ mean and standard deviation (sd) values estimated by the ML-based procedure.*

	$\hat{\sigma}^2$		$\hat{\lambda}^2$	
Subject	mean	sd	mean	sd
1	2,9	2,2	0,8	1,0
2	2,4	1,1	0,1	0,1
3	2,5	2,0	0,8	1,0
4	1,8	1,0	0,2	0,2
5	2,0	1,4	0,6	1,7
6	2,1	5,0	0,1	1,0
7	2,0	1,7	0,4	0,3
8	0,8	0,7	0,7	0,5
9	3,3	2,2	1,0	1,3
10	0,9	0,6	0,4	1,0
11	0,7	0,6	0,1	0,1
12	1,3	0,9	0,3	0,2
13	1,6	1,2	0,7	0,6
14	1,9	1,4	0,3	0,3
15	0,7	0,6	0,5	0,5
16	0,7	0,3	0,8	0,8
17	2,3	1,9	0,9	3,9
18	1,0	0,5	0,1	0,1
19	1,4	1,5	5,3	6,8
20	1,1	0,6	0,2	0,1

Subject #4

The first selected subject is #4, whose profile can be visualized in Figure 5.7. Observing the original profile (top panel), we can see that the noise component overlapped to the true glycemic signal is small and seems to be quite constant all over the monitoring. Results relative to subject #4 in Table 5.4 support how has been detected by graphical inspection. In fact, estimated measurement noise variance mean (and standard deviation) values resulted $\hat{\sigma}^2 = 1.8(\pm 1.0)\ mg^2/dl^2$, confirming both the high SNR in the time series and a limited intra-individual SNR variability. Because the time series is very long (more than 4 days), the action of both EMA and KF cannot be appreciated observing profiles in the top panel. For this reason, two 2-hour windows are reported in the middle panel. The left box, which is relative to the time window from hour 23 to 25, shows a situation of high SNR (that corresponds to a low value of the measurement noise variance σ^2). In this window, EMA performs oversmoothing and it introduces too much delay. On the other hand, NF performs an optimal signal enhancement, correctly reducing the noise component and introducing less delay than EMA. General results reported in Table 5.3 confirm the improvement due to NF, with a $T = 10\ sec$ (vs $T = 100\ sec$ of EMA). The right box in the middle panel (time window from hour 103 to 105) illustrates a situation in which the SNR is lower than in the left box, calling for an higher regularization of the signal. The ML-based procedure correctly identify an elevated σ^2 value (bottom panel, 103-105 hours) and induce NF to perform a suitable and satisfactory smoothing of CGM data also in this window.

A last comment can be made on $\hat{\sigma}^2$ estimates reported in the bottom panel of Figure 5.7. Comparing this profile with the original CGM time series, we can see how precisely the estimate $\hat{\sigma}^2$ results in high and low values, accordingly with low and high apparent SNR conditions, respectively.

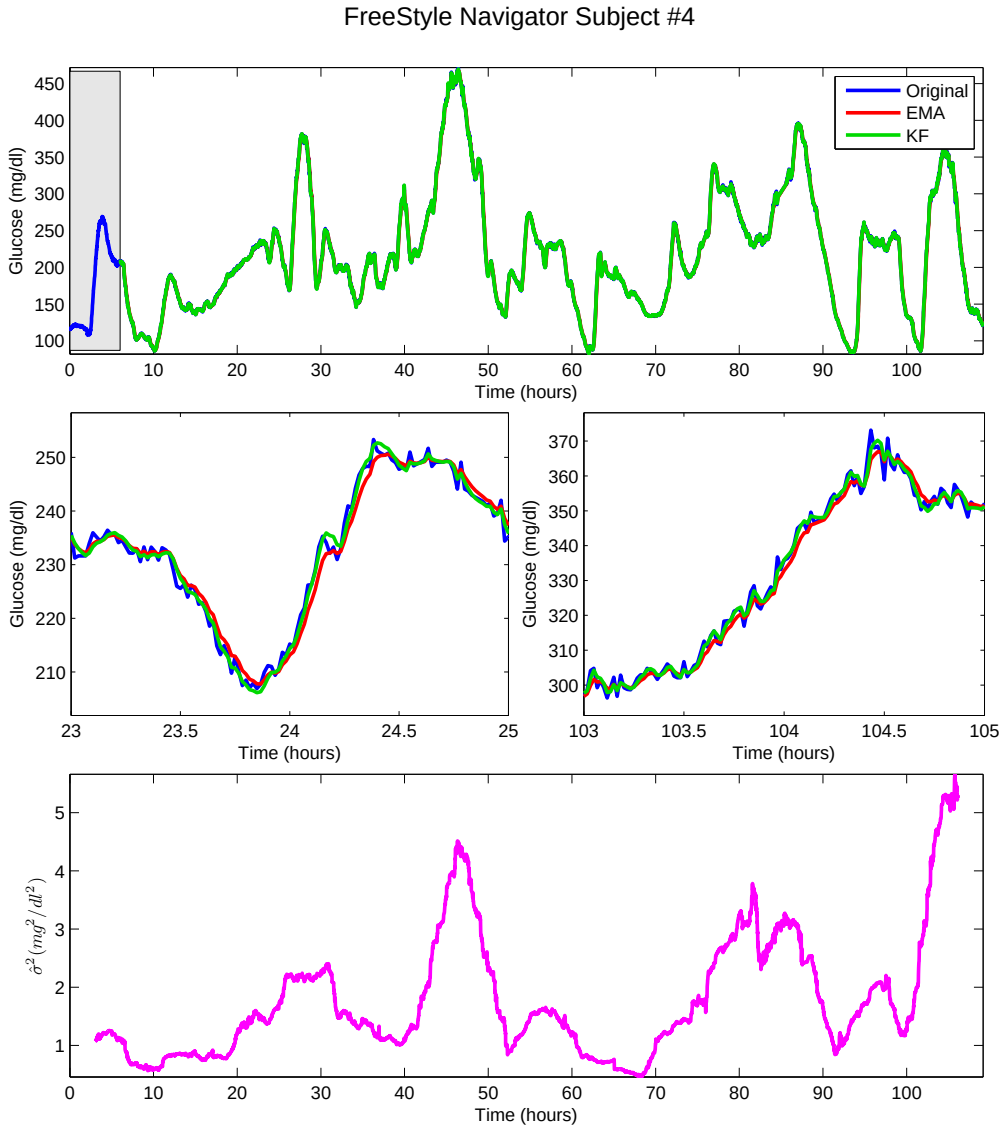

Figure 5.7: *Abbott FreeStyle Navigator^{TM} subject #4. Top: original CGM (blue), the EMA (red) and NF (green) time series. The gray shaded area highlights the 6-hour burn-in window used for initialize NF parameters. Middle: two 2-hour details. Bottom: the $\hat{\sigma}^2$ estimate obtained using the ML-based procedure.*

Subject #14

Profile of subject #14 (blue line) is visualized in the top panel of Figure 5.8, and from a preliminary graphical inspection it seems to present an elevated SNR.

Results of the application of both EMA and NF (Table 5.3) show that NF introduces lower delay than EMA ($T = 15$ *sec* vs $T = 95$ *sec*, respectively) without compromising the smoothness of the filtered time series (SRG of 0.82 for NF vs 0.93 for EMA). The reduction in SRG is principally due to the fact that, everywhere the original CGM profile presents an elevated SNR, NF does not perform oversmoothing (which means to introduce a lower time delay). This fact is evident observing the detail of the time window from hour 27 to 29 reported in the left box of the middle panel. In this time interval, the ML-based procedure is able to identify a high SNR condition, estimating very low values of σ^2 and reducing the action of the filter, minimizing the delay. On the other hand, looking at the right box in the middle panel, which is relative to the interval from hour 39 to 41, the SNR is lower than in the previous case. The parameter estimation procedure correctly identifies this condition (the bottom panel of Figure 5.8, $\hat{\sigma}^2$ estimates in 39-41 hours interval result higher that in 27-29 hours interval) and NF is opportunely tuned to perform a suitable signal enhancement.

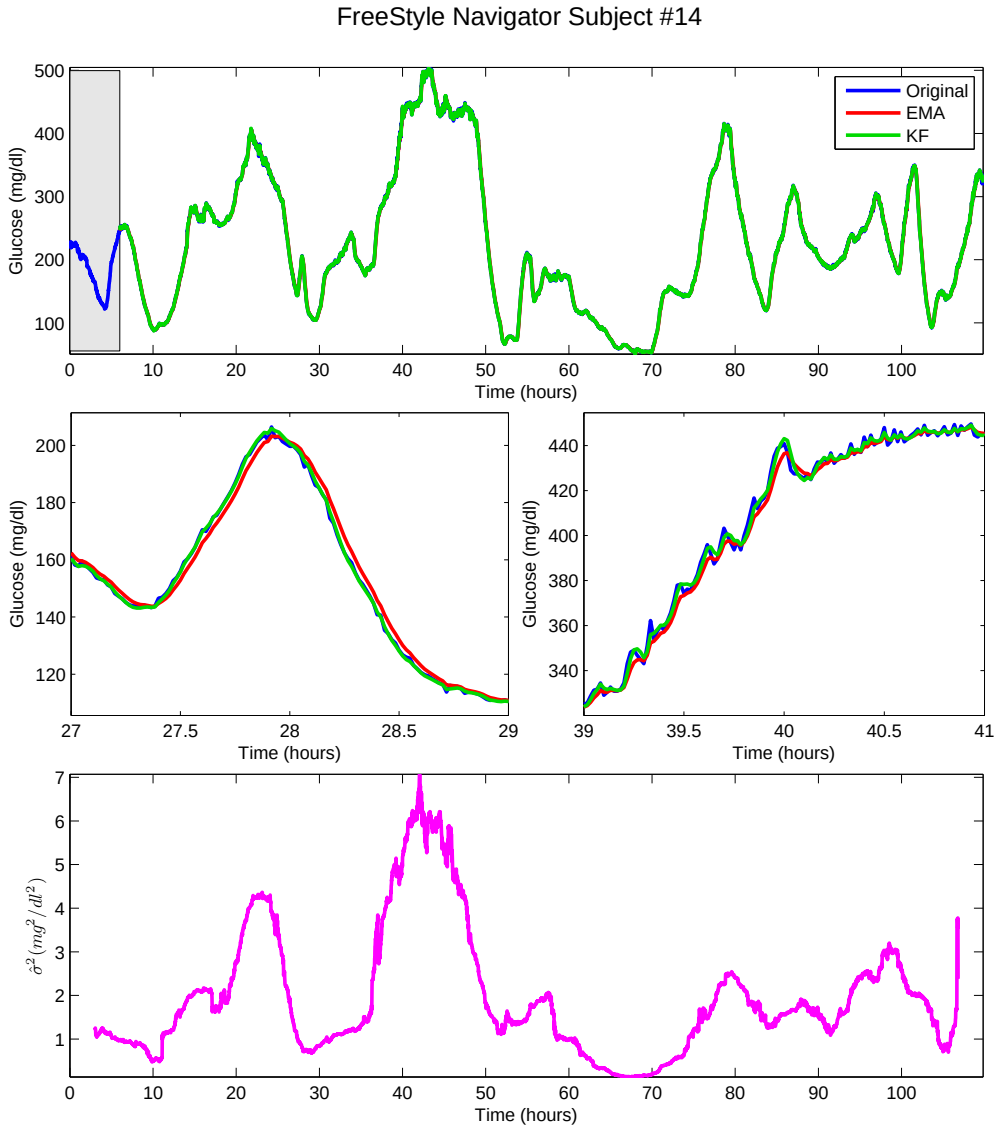

Figure 5.8: *Abbott FreeStyle Navigator^{TM} subject #14. Top: original CGM (blue), the EMA (red) and NF (green) time series. The gray shaded area highlights the 6-hour burn-in window used for initialize NF parameters. Middle: two 2-hour details. Bottom: the $\hat{\sigma}^2$ estimate obtained using the ML-based procedure.*

5.4 Discussion

In this chapter we have presented the results of the application of the new stochastic-based filtering procedure on two different real CGM datasets and compared them to results obtained applying a deterministic filter, such as EMA.

We have shown that EMA is not able to cope with neither inter-individual nor intra-individual SNR variability. Results of T and SRG indexes reported in Tables 5.1 and 5.3 illustrate quite clearly this inability. On the other hand, we have seen that the new filter, thanks to the ML-based adaptive parameter estimation procedure, optimally faces and copes with inter-individual and intra-individual SNR variability, significantly improving the quality of CGM data of both datasets and introducing a minimum delay.

Another important result is that the new filter is also able to cope with sensor-to-sensor variability. In fact, we have proved on real data that, maintaining the same time window length (i.e. 6 hours), the new filter is able to perform the same suitable signal enhancement, independently to the time sampling period, i.e. it is $T_S = 1$ and 3 min for the Abbott and Menarini datasets, respectively.

Conclusions

Continuous Glucose Monitoring (CGM) devices are potentially an efficient tool for improving the diabetes management. However, CGM data are unavoidably affected by measurement error. In order to usefully exploit all advantages they supply, the on-line enhancement of the Signal-to-Noise Ratio (SNR) of CGM profiles is needed.

Deterministic approaches for filtering, e.g. the Moving-Average (MA), which is currently the most common and diffused filter methodology embedded in CGM devices, allow to improve the quality of CGM data. However, first MA filters are not able to face SNR changes in CGM signals and second they need to be completely restructured if the time sampling varies.

In this work we proposed a new on-line stochastically-based filtering procedure to improve the quality of CGM data and the information they contain.

The new filter has several advantages over the currently state-of-art methods. First of all, it is implemented through the Kalman Filter (KF) and therefore it is recursive, i.e. it can be used to denoise CGM data in real-time. Second, it is based on Bayesian estimation, which means that the smoothing performed by the filter is "optimally" tuned accordingly to the *a priori* known statistical characteristics of both signal and noise. Third, the major advantage is that it is self-tunable, i.e. every time a new measurement is received, filter parameters can be updated in order to track the changes in both signal and noise characteristics. This feature makes the filter able to efficiently cope with inter-individual SNR, intra-individual SNR, and sensor-to-sensor variability of CGM data.

The performance of the new filter gave satisfactory results on both simulated and real data. Simulated datasets have been used to demonstrate the principal advantages of the new stochastic-based filtering procedure. The two real datasets considered for this work allowed a comparison with the performance of the MA methodology, the current standard of CGM devices. The improvement introduced by the new filter is rather evident, as shown in Chapters 4 and 5. In particular, the delay introduced by the new filter is significantly smaller than MA, and the amount of smoothing introduced is

adequate in every SNR condition, resulting in a significant and satisfactory improvement on CGM final output.

Possible developments of this work concern the use of the presented methodology in prediction and alert generation. In particular, the output of the KF is not only limited to the estimates of real glycemic value. In fact, at each step, KF also returns the estimate error covariance matrix, which contains an estimate of the error we are performing on estimating the current glucose value.

Therefore, the first natural development regards the evaluation of the error covariance matrix in order to return together to the nominal value also its confidence interval. This information could be very important in terms of hypo and hyperglycemic alerts generation. In fact, in any CGM device embedding an alert tool, the alert is generated considering only the CGM measured value [5, 23, 52]. The stochastic context introduced in this work suggests to modify the alert generation on probability basis, making it more robust e.g. against false alert generation.

The second possible development concerns the prediction of future glucose levels [14, 44, 45]. In fact, the prediction step of the KF, which does not require any new measurement, returns the optimal estimation of the next glucose value. The prediction step can be iterated as many times as the prediction horizon suggests, e.g. 30 times if the prediction horizon is 30 minutes and we are working with a 1 *min* time sampling CGM device, in order to predict the e.g. 30 minutes ahead-in-time glucose value.

The last interesting development regards the possibility to modify the KF structure in order to improve CGM sensor calibration. Theoretically, this is possible by integrating inside the KF information about the plasma-to-interstitium dynamics and exploiting a small number of SMBG measurements, which are used as references. As introduced in Section 1.5.2, in a recent simulation study of Facchinetti et al. [15] we propose a new on-line calibration method, based on the two-compartment model of [39] and implemented with the Extended Kalman Filter, which is simultaneously able to filter and recalibrate CGM data, and to reconstruct the plasma glucose concentration, exploiting only 4 SMBG samples per day. However, this new procedure has been tested only on simulated data and further investigations are required, both on simulated and real datasets.

Finally, the new filter has been inserted into the AP@HOME project submitted for the EU FP7 programme, in the part regarding the denoising, the prediction and the alarm generation of CGM time series.

An Italian Patent on the new filtering procedure proposed in this work has also been deposited (#MI2008A000837).

Bibliography

[1] Alspach D.L., *A parallel processing solution to the adaptive Kalman filtering problem with vector measurements*, Computers & Electrical Engineering, 1973 Jun;1(1):83-94

[2] Amir O., Weinstein D., Zilberman S., Less M., Perl-Treves D., Primack H., Weinstein A., Gabis E., Fikhte B., Karasik A., *Continuous Noninvasive Glucose Monitoring Technology Based on "Occlusion Spectroscopy"*, J Diabetes Sci Technol, 2007 Jul;1(4):463-9

[3] Anderson B.D.O. and Moore J.B., *Optimal filtering*, Dover Publications, 2005

[4] Ansley C.F., Kohn R., Wong C.M., *Nonparametric spline regression with prior information*, Biometrika, 1993;80:75-88

[5] Bode B., Gross K., Rikalo N., Schwartz S., Wahl T., Page C., Gross T., Mastrototaro J., *Alarms based on real-time sensor glucose values alert patients to hypo and hyperglycemia: the guardian continuous monitoring system*, Diabetes Technol Ther, 2004 Apr;6(2):105-13

[6] Breton M.D. and Kovatchev B.P., *Analysis, Modeling, and Simulation of the Accuracy of Continuous Glucose Sensors*, J Diabetes Sci Technol, 2008 Sep;2(5):853-62

[7] Buckingham B., *Hypoglycemia detection, and better yet, prevention, in pediatric patients*, Diabetes Technol Ther, 2005 Oct;7(5):792-6

[8] Chee F., Fernando T., Savkin A., Van Heernde P.V., *The Use of MiniMed CGMS in real-time glucose monitoring*, 7$^{\text{th}}$ Annual Australian and New Zeland Intelligence Information Systems Conference, Nov 2001, 18-21, Perth - Western Australia

[9] Clarke W.L. and Kovatchev B.P., *Continuous Glucose Sensors: Continuing Questions about Clinical Accuracy*, J Diabetes Sci Technol, 2007 Sep;1(5):669-75

[10] Choleau C., Dokladal P., Klein J.C., Ward W.K., Wilson G.S., Reach G., *Prevention of hypoglycemia using risk assessment with a continuous glucose monitoring system*, Diabetes, 2002 Nov;51(11):3263-73

[11] De Nicolao G., Sparacino G., Cobelli C., *Nonparametric Input Estimation in Physiological Systems: Problem, Methods, and Case Studies*, Automatica, 1997 May;33(5):851-70

[12] De Nicolao G., Ferrari-Trecate G., Sparacino G., *Fast spline smoothing via spectral factorization concepts*, Automatica, 2000 Nov;36(11):1733-9

[13] Facchinetti A., Sparacino G., Cobelli C., *Reconstruction of glucose in plasma from interstitial fluid continuous glucose monitoring data: role of sensor calibration*, J Diabetes Sci Technol, 2007 Sep;1(5):617-23.

[14] Facchinetti A., Baruzzo T., Vio E., Sparacino G., Cobelli C., *On-Line Time-Series Prediction Models for Continuous Glucose Monitoring (CGM) Data*, Proceedings of 7$^{\text{th}}$ Annual Diabetes Technology Meeting (DTM), San Francisco (CA), 2007 Oct:A36

[15] Facchinetti A., Cappellotto P., Sparacino G., Cobelli C., *A New On-Line Method for Improving Calibration of Continuous Glucose Monitoring (CGM) Sensor*, Proceedings of 8$^{\text{th}}$ Annual Diabetes Technology Meeting (DTM), Bethesda (MD), 2008 Nov:A37

[16] Feldman B., Brazg R.,Schwartz S., Weinstein R., *A Continuous Glucose Sensor Based on Wired Enzyme^{TM} Technology - Results from a 3-Day Trial in Patients with Type 1 Diabetes*, Diabetes Technol Ther, 2003 Oct;5(5):769-79

[17] Feldman B.J., McGarraugh G.V., *Method of calibrating an analyte-measurement device, and associated methods, devices and systems*, US Patent No. 7299082; 2007

[18] Gamber H.A., *Choice of an optimal shape parameter when smoothing noisy data*, Commun. Statist., 1979;A8:1425-36

[19] Gelb A., Ksper F., Nash R.A., Price C.F., Sutherland A.A., *Applied Optimal Estimation*, MIT Press, Cambridge, MA, 1974

[20] Ginsberg B.H., *The Current Environment of CGM Technologies*, J Diabetes Sci Technol, 2007 Jan;1(1):117-21

[21] Grewal M.S. and Andrews A.P., *Kalman Filtering: Theory and Practice Using MATLAB*, John Wiley & Sons, 2001

[22] Heinemann L., *Overcoming obstacles: new management options.*, Eur J Endocrinol, 2004 Oct;151 Suppl 2:T23-7; discussion T29-30

[23] Heise T., Koschinsky T., Heinemann L., Lodwig V., *Overcoming obstacles: new management options*, Diabetes Technol Ther, 2003 Aug;5(4):563-7

[24] Klonoff D.C., *Continuous Glucose Monitoring: Roadmap for 21st century diabetes therapy*, Diabetes Care, 2005 May;28(5):1231-9

[25] Klonoff D.C., *Benefits and Limitation of Self Monitoring Blood Glucose*, J Diabetes Sci Technol, 2007 Jan;1(1):130-2

[26] Knobbe E.J., Buckingham B., *The extended Kalman filter for continuous glucose monitoring*, Diabetes Technol Ther, 2005 Feb;7(1):15-27

[27] Kovatchev B.P., Gonder-Frederick L.A., Cox D.J., Clarke W.L., *Evaluating the accuracy of continuous glucose-monitoring sensors: continuous glucose-error grid analysis illustrated by TheraSense Freestyle Navigator data*, Diabetes Care, 2004 Aug;27(8):1922-8

[28] Kovatchev B.P., Anderson S., Heinemann L., Clarke W.L., *Comparison of the numerical and clinical accuracy of four continuous glucose monitors*, Diabetes Care. 2008 Jun;31(6):1160-4

[29] Kubiak T., Wörle B., Kuhr B., Nied I., Gläsner G., Hermanns N., Kulzer B., Haak T., *Microdialysis-based 48-hour continuous glucose monitoring with GlucoDay: clinical performance and patients' acceptance*, Diabetes Technol Ther, 2006 Oct;8(5):570-5

[30] Kuure-Kinsey M., Palerm C.C., Bequette B.W., *A dual-rate Kalman filter for continuous glucose monitoring*, Conf Proc IEEE Eng Med Biol Soc. 2006;1:63-6

[31] Lesperance L.M., Spektor A., McLeod K.J., *Calibration of the continuous glucose monitoring system for transient glucose monitoring*, Diabetes Technol Ther, 2007 Apr;9(2):183-90

[32] Lodwig V., Heinemann L., Glucose Monitoring Study Group, *Continuous glucose monitoring with glucose sensors: calibration and assessment criteria*, Diabetes Technol Ther, 2003;5(4):572-86

[33] Maran A., Crepaldi C., Tiengo A., Grassi G,. Vitali E., Pagano G., Bistoni S., Calabrese G., Santeusanio F., Leonetti F., Ribaudo M., Di

Mario U., Annuzzi G., Genovese S., Riccardi G., Previti M., Cucinotta D., Giorgino F. Bellomo A., Giorgino R., Poscia A., Varalli M., *Continuous subcutaneous glucose monitoring in diabetic patients: a multicenter analysis*, Diabetes Care, 2002 Feb;25(2):347-52

[34] Mastrototaro J.J., Gross T.M., Shin J.J., *Glucose monitor calibration methods*, US Patent No. 6424847; 2002

[35] Mehra R.K., *On the identification of variances and adaptive Kalman filtering*, IEEE Trans Aut Cont, 1970;AC-15:175-84

[36] Palerm C.C., Willis J.P., Desemone J., Bequette B.W., *Hypoglycemia prediction and detection using optimal estimation*, Diabetes Technol Ther, 2005 Feb;7(1):3-14

[37] Palerm C., Bequette W., *Hypoglycemia Detection and Prediction Using Continuous Glucose Monitoring-A Study on Hypoglycemic Clamp Data*, J Diabetes Sci Technol, 2007 Sep;1(5):624-9

[38] Rebrin K., Steil G.M., van Antwerp W.P., Mastrototaro J.J., *Subcutaneous glucose predicts plasma glucose independent of insulin: implications for continuous monitoring*, Am J Physiol, 1999 Sep;277(3 Pt 1):E561-71

[39] Rebrin K., Steil G.M., *Can interstitial glucose assessment replace blood glucose measurements?*, Diabetes Technol Ther, 2000 Apr;2(3):461-72

[40] Reifman J., Rajaraman S., Gribok A., Ward K.W., *Predictive Monitoring for Improved Management of Glucose Levels*, J Diabetes Sci Technol, 2007 Jul;1(4):478-86

[41] Ryan C., Anderson S.M., Breton M., Less M., Clarke W.L., Kovatchev B.P., *Modeling of Calibration Effectiveness and Blood-to-Interstitial Glucose Dynamics as Potential Confounders of the Accuracy of Continuous Glucose Sensors during Hyperinsulinemic Clamp*, J Diabetes Sci Technol, 2007 May;1(3):317-22

[42] Sparacino G. and Cobelli C., *A stochastic deconvolutio method to reconstruct insulin secretion rate after a glucose stimulus*, IEEE Trans Biomed Eng, 1996 May;43(5):512-29

[43] Sparacino G., Milani S., Arslan E., Cobelli C., *A Bayesian approach to estimate evoked potentials*, Comput Methods Programs Biomed, 2002 Jun;68(3):233-48

[44] Sparacino G., Zanderigo F., Corazza S., Maran A., Facchinetti A., Cobelli C., *Glucose concentration can be predicted ahead in time from continuous glucose monitoring sensor time-series*, IEEE Trans Biomed Eng, 2007 May;54(5):931-7

[45] Sparacino G., Facchinetti A., Maran A., Cobelli C., *Continuous glucose monitoring time series and hypo/hyperglycemia prevention: requirements, methods, open problems*, Curr Diabetes Rev, 2008 Aug;4(3):182-91

[46] Steil G.M., Rebrin K., Hariri F., Jinagonda S., Tadros S., Darwin C., Saad M.F., *Interstitial fluid glucose dynamics during insulin-induced hypoglycaemia*, Diabetologia, 2005 Sep;48(9):1833-40

[47] Tierney M.J., Tamada J.A., Potts R.O., Eastman R.C., Pitzer K., Ackerman N.R., Fermi S.J., *The GlucoWatch Biographer: a frequent, automatic and noninvasive glucose monitor*, Ann Med 2000 Dec;32(9):632-41

[48] Voskanyan G., Keenan D.B., Mastrototaro J.J., Steil G.M., *Putative delays in interstitial fluid (ISF) glucose kinetics can be attributed to the glucose sensing systems used to measure them rather than the dalay in ISF glucose itself*, J Diabetes Sci Technol, 2007 Sep;1(5):639-44

[49] Wahba G. and Wendelberger J., *Some new mathematical methods for variational objective analysis using splines and cross-validation*, Monthly Wheater Rev., 1980;108:36-57

[50] Wahba G., *Bayesian 'confidence intervals' for the cross-validated smoothing spline*, J. R. Stat. Soc. Ser. B, 1983;45(1):133-50

[51] Ward W.K., House J.L., Birck J., Anderson E.M., Jansen L.B., *A wire-based dual-analyte sensor for glucose and lactate: in vitro and in vivo evaluation*, Diabetes Technol Ther, 2004 Jun;6(3):389-401

[52] Ward W.K., *The role of new technology in the early detection of hypoglycemia*, Diabetes Technol Ther, 2004 Apr;6(2):115-7

[53] Weinstein R.L., Schwartz S.L., Brazg R.L., Bugler J.R., Peyser T.A., McGarraugh G.V., *Accuracy of the 5-day FreeStyle Navigator Continuous Glucose Monitoring System: comparison with frequent laboratory reference measurements*, Diabetes Care, 2007 May;30(5):1125-30

[54] Wentholt I.M., Vollebregt M.A., Hart A.A., Hoekstra J.B., DeVries J.H., *Comparison of a needle-type and a microdialysis continuous glucose*

monitor in type 1 diabetic patients, Diabetes Care, 2005 Dec;28(12):2871-6

[55] Weiss R., Yegorchikov Y., Shusterman A., Raz I., *Noninvasive continuous glucose monitoring using photoacoustic technology-results from the first 62 subjects*, Diabetes Technol Ther, 2007 Feb;9(1):68-74

[56] Zhou J. , Luecke R.H., *Estimation of the covariances of the process noise and measurement noise for a linear discrete dynamic system*, Computers & Chemical Engineering, 1995 Feb;19(2):187-95

[57] *http://www.abbottdiabetescare.com*

[58] *http://www.dexcom.com/*

[59] *http://www.diabetesnet.com/diabetes_technology/continuous_monitoring.php*

[60] *http://glucosecontrol.ucsd.edu*

[61] *http://www.lifescan.com/products/*

[62] *http://www.medcompare.com/details/33037/CGMS-System-Gold-Continuous-Glucose-Monitoring.html*

[63] *http://www.menarini.com*

[64] *http://www.minimed.com/products/guardian/*

[65] *http://www.who.int/diabetes/BOOKLET_HTML/en/index5.html*